INTERMITTENT ULTRASOUND-ASSISTED CERAMIC MEMBRANE FOULING CONTROL IN ULTRAFILTRATION

By

Kyu Min Lee

Bachelor of Applied Science, University of Waterloo, Waterloo, Canada, 2014

A thesis

presented to Ryerson University

in partial fulfillment

of the requirements

for the degree of

Master of Applied Science

in the program of

Chemical Engineering

.

Toronto, Ontario, Canada, 2019

AUTHOR'S DECLARATION

I hereby declare that I am the sole author of this thesis. This is a true copy of the thesis, including any required final revisions, as accepted by my examiners.

I authorize Ryerson University to lend this thesis to other institutions or individuals for the purpose of scholarly research.

I further authorize Ryerson University to reproduce this thesis by photocopying or by other means, in total or in part, at the request of other institutions or individuals for the purpose of scholarly research.

I understand that my thesis may be made electronically available to the public.

Abstract

Intermittent Ultrasound-Assisted Ceramic Membrane Fouling Control in Ultrafiltration

Kyu Min Lee

Master of Applied Science

Department of Chemical Engineering

Ryerson University, Canada, 2019

Ultrafiltration is one of the most promising membrane technologies for liquid purification due to its high economic efficiency in the industries. However, it has been faced with a critical problem, called fouling. The contaminants in feed solution tend to accumulate on the membrane surface, hindering permeate solution to pass through the porous spaces. Among the various solutions, application of ultrasound has been considered as the most popular method since it does not suffer a disadvantage of downtime and the filtration process does not need to be stopped for the removal of foulants. In this study, control of ceramic membrane fouling by an on-line intermittent ultrasound system was being investigated. The experiment focused on obtaining optimal operating ultrasonic condition. Frequency (20, 28, and 40 kHz), power intensity (1.44, 2.88, and $5.76 \mathrm{W/cm^2}$), and time interval of intermittent ultrasound (1, 1.5, and 2 minutes) were the parameters of interest. The effect of feed concentration was also analyzed at optimal ultrasonic condition. The quality and flow rate of the permeate streams were monitored for the evaluation of the process performance. The optimal condition of intermittent ultrasound was found at the frequency of 28 kHz and the power intensity of 2.88 $\mathrm{W/cm^2}$; and then, the application of intermittent ultrasound with short time interval successfully reduced the operating cost of ultrafiltration process while maintaining acceptable quality and flow rate of permeate solution. There was increase in efficiency of intermittent ultrasound at lower feed concentration.

ACKNOWLEDGEMENTS

DEDICATION

Dedicated to My Family

Table of Contents

List of Figures

List of Tables

Nomenclature

J_c convective flux $(g/(cm^2 s))$

J solvent (permeate) flux $(g/(cm^2 s))$

C feed solute concentration (g/cm^3)

C_p permeate solute concentration (g/cm^3)

D solute diffusivity (cm^2/s)

x length coordinate (cm)

C_w concentration of solute on membrane surface (g/cm^3)

C_b concentration of solute in bulk solution (g/cm^3)

C_g concentration of solute in gel layer (g/cm^3)

δ thickness of boundary layer (cm)

k mass transfer coefficient (D/δ) (cm/s)

C_M polarization modulus

MB   microbubble

f_o resonance frequency (Hz)

p_o ambient pressure (Pa)

K polytropic index

R_o radius of cavitation bubble (m)

ρ density of liquid phase (kg/m^3)

CUF   coagulation-ultrafiltration process without ultrasound

CUF-ultrasound   coagulation-ultrafiltration process with ultrasound

TMP   transmembrane pressure

SEM   scanning electron microscope

R_{total} total resistance of circuit (ohms)

R_i resistance of each ultrasonic transducer (ohms)

I_{total} total current of circuit (A)

I_i current that passes through each ultrasonic transducer (A)

V_i electric potential of each ultrasonic transducer (V)

P_i electric power at each transonic transducer $(\text{kg.}\, \text{m}^2/\text{s}^3)$

RCOOH   carboxyl group

Al_2O_3 aluminum oxide

$\gamma - AlOOH$ peptized sol of aluminum oxide

ZrO_2 zirconium dioxide

TiO_2 Titanium dioxide

$\bar{x}$ mean value

σ standard deviation

Chapter 1: Introduction

Water is one of the crucial natural resources that determine the quality of life for living organisms. In the case of humanity, water is not only needed for drinking purpose, but also for agriculture, hygiene, industry, and domestic use. The depletion of fresh water due to the increase in the human population every year is a real challenge worldwide [1]. In fact, humanity is faced with water quantity and quality issues in the twenty-first century [2, 3]. As an example, the average temperature of the earth is continually increasing due to the global warming problem, and this phenomenon accelerates the rate of evaporation, inducing the depletion of water resource. In addition, remained water is being polluted, because of the recent rapid industrial development and urbanization [4]. Therefore, water scarcity is an impending problem all over the world; and membrane technology has been developed as one of the ways to solve this problem.

The application of membrane separation technology has been widely used for liquid separation from 1960 since it produces high quality of water and high production rate with excellent economic benefit. In practice, 95% of the membrane separation application is for water purification, including desalination of seawater, drinking water production, treatment of industrial wastewater, and water reuse [5]. The membrane technology has been investigated to reduce energy consumption and environmental impact during the separation process so that the system can achieve a maximum production rate with a minimum operational cost. There are four main developmental focuses that are under research to improve membrane technology as belows [5]:

- To develop the type of membrane module which provides high efficiency with a large surface area,
- To develop advanced membrane materials that can assist to control the system during the separation of molecularly similar components, such as salts, colloids, and proteins.
- To adjust the membrane structure so that microscopic transport phenomena can be controlled.
- To create the membrane that is economical.

Among different membrane technologies, ultrafiltration has been widely used in various industries for water purification and recycling since it provides relatively the high permeate production rate with low operating cost compared to other types of membrane [6]. In practice, ultrafiltration has been used to produce drinking water due to the compactness, simple automation, high removal rate of turbidity, organic matters, Giardia, and even virus [7, 8, 9, 10]. However, a major challenge of ultrafiltration is the efficiency decrease with operational time by fouling. The fouling tends to decrease the flow rate of permeate solution, inhibiting its wider application for drinking water production [11]. Researchers have investigated on developing various methods to overcome this problem. Among them, back-flushing and chemical cleaning are widely used methods to remove foulants from the membrane. However, those methods suffer a disadvantage of downtime since the filtration process must be stopped for the removal of foulants. Thus, as an alternative method, the application of ultrasound has been suggested to reduce the resistance of the cake layer formed by foulants on the membrane surface during the filtration process in this study. Unlike other treatments, the ultrafiltration process is not interrupted by ultrasound-assisted fouling control. In this study, further research was investigated to find the optimal ultrasonic conditions that can produce the highest flow rate of permeate solution while the appropriate quality of it is maintained. Frequency and power intensity of ultrasound are the main parameters considered for the analysis. In addition, optimal operating conditions of intermittent ultrasound-assisted fouling control was also investigated in this study; and hence, the operating cost of the ultrafiltration process could be reduced.

This thesis contains 6 chapters:

Chapter 1 contains the overview and the research objectives

Chapter 2 includes the literature review on the principle of membrane separation, and introduction to previous methods for fouling reduction

Chapter 3 presents the experimental methods, characteristics of materials used, and technique used for sample analysis

Chapter 4 discusses the experimental result with respect to the collected amount, turbidity, and the average particle size distribution of permeate solution,

as well as the observation of SEM images for the membrane surface after filtration.

Chapter 5 concludes the content of thesis

Chapter 6 suggests the future work for improvement

Chapter 2: Literature Review

2.1 Modes of Membrane Filtration

The membrane is acting as a barrier between two homogeneous phases during liquid separation. There are mainly three different streams that correlate to membrane separation, which are the feed, permeate, and retentate. The feed stream is polluted solution that enters the membrane module for purification while the permeate stream is the purified product after passing through the membrane surface. Lastly, the retentate is the one that is rejected by the membrane surface during the separation process. In practice, there are mainly two modes of membrane filtration, which are dead-end and cross flow, as shown in **Figure 2.1**.
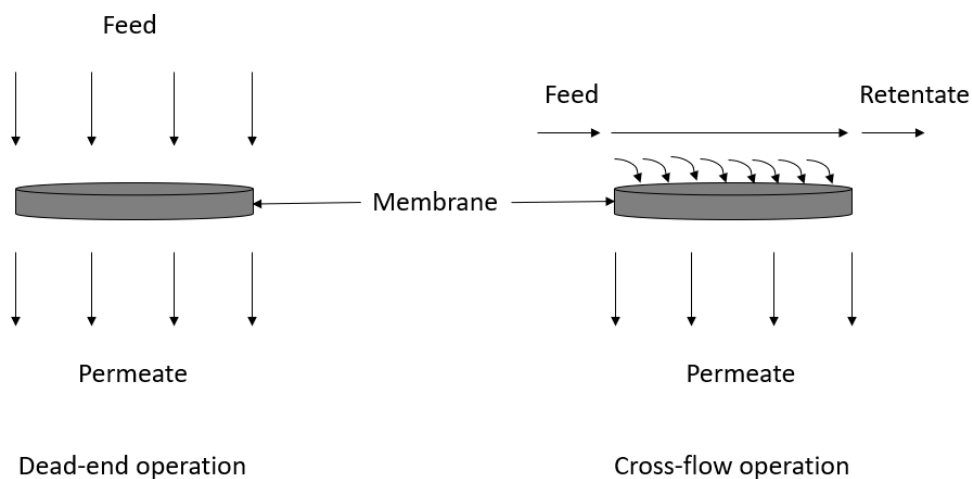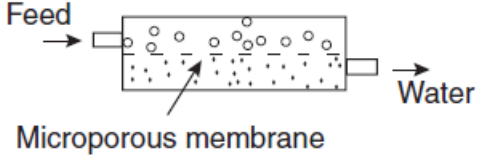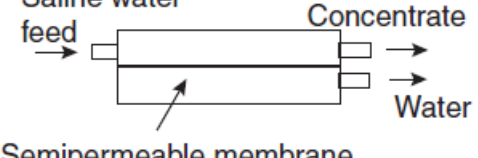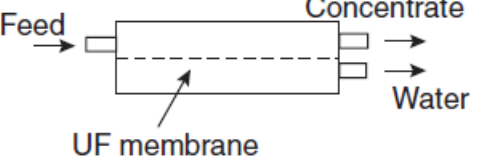
Figure 2.1 - *Mechanisms of dead-end and cross-flow modes [12]*

In case of dead-end mode, the flow direction is perpendicular to the membrane surface, and the particles larger than pore size are rejected and remained on the surface. With the application of dead-end mode, the thickness of the solid cake layer tends to increase rapidly since all the rejected particles directly accumulate on the membrane surface. For this reason, the much higher applied pressure and increasing pressure is required to maintain the constant flow rate of permeate solution. In other words, this mode requires enormous operating cost, providing low economic efficiency. As an alternative process, the cross-flow mode was developed to overcome this problem. As **Figure 2.1** illustrates, the separation is occurred by pressure driving force in cross-flow mode. The clean solvent passes through the porous spaces of the membrane

while the rest of the retentate solution is rejected and keeps flowing parallel to the membrane surface. In fact, cross-flow mode requires much less energy consumption compared to the dead-end mode to maintain equal production rate of the permeate solution due to the much lower rate of particle accumulation on the membrane surface [12]. Thus, cross-flow is widely used in industries to maximize the efficiency of the separation process.

2.2 Types of Membrane

There are different types of membrane technology depending on the purpose of separation and component of feed solutions. As **Figure 2.2** shows, three general types of membranes have been used for water filtration in the industries.

Process	Separation concept	Materials passed	Driving force
Micro-filtration	Feed → Microporous membrane → Water	Water and dissolved species	Pressure difference, typically 10 psi
Reverse osmosis	Saline water feed → Concentrate, Water → Semipermeable membrane	Water	Pressure difference, typically 100–800 psi
Ultra-filtration	Feed → Concentrate, Water → UF membrane	Water and salts	Pressure difference, typically 10–100 psi

Figure 2.2 - Types of membrane and conditions of separation process [13]

The dashed lines in the figure represent the membrane surface that allows the particles smaller than the pore size to pass through it. On the other hand, the solid line indicating the surface of the reverse osmosis membrane allows the solvents to pass through it while all the solutes are rejected to produce highly purified drinking water.

5

Other than those three types of the membrane, nanofiltration membrane has been developed during the last 20 years [5]. The pore size of nanofiltration is between ultrafiltration and reverse osmosis. **Figure 2.3** shows the range of pore size for each type of the membrane in detail.

Membrane process | Size (nm) | Region | Examples

Microfiltration

Ultrafiltration

Nanofiltration

Reverse osmosis

| Size (nm) |
| 10,000 |
| 5000 |
| 1000 |
| 500 |
| 100 |
| 50 |
| 10 |
| 5 |
| 1 |
| 0.5 |
| 0.2 |
| 0.1 |

Microparticle

Colloidal

Ion and low molecular weight

Examples
- Erythrocyte
- Cancer cell
- *Saccharomyces* (beer ferment)
- *Staphylococcus*
- Tetanus
- Shigeila
- Latex emulsion
- Oil emulsion
- Colloidal silica
- Japanese encephalitis virus
- Polio virus
- Hemoglobin
- Pepsin
- Vitamin B12
- Sucrose
- Zn^{2+}
- $Na^+ — OH^-$
- $H_2O — Cl^-$

Figure 2.3 - Membrane process designation by solute size [5]

In practice, there are two sources that must be discreetly considered to choose the appropriate types of the membrane, which are selectivity and productivity. The selectivity is the ability of the membrane to separate the particle from the solution to reach high purification while productivity presents the production rate of permeate solution from the separation process. Selectivity and productivity have the anti-proportional relationship, meaning they cannot be satisfied simultaneously. In other words, they should be balanced prudently depending on the purpose of the membrane separation [14]. For example, the solution should be purified as much as possible to produce drinking water, since it decisively relates to the living organism's health. In this case, the selectivity of the membrane should be highly considered rather than

productivity. According to **Figure 2.3**, reverse osmosis has the smallest pore size, and produces the most purified solution by separating even extremely tiny particles, such as ions and salts from the solution. However, it requires comparatively the high magnitude of applied pressure to operate the system, inducing high energy consumption. For this reason, the reverse osmosis is not the proper type for oil emulsion process due to its low economic efficiency with low productivity.

2.3 Concentration Polarization

The pressure driving membranes, such as microfiltration, ultrafiltration, nanofiltration, and reverse osmosis are used in general for the separation of liquid phases, and particles are transferred to the membrane surface by convection. As the separation process continues for a long time, solutes in the feed stream accumulate on the membrane surface, causing concentration polarization. **Figure 2.4** shows the specific schematic diagram of concentration polarization during the membrane separation process
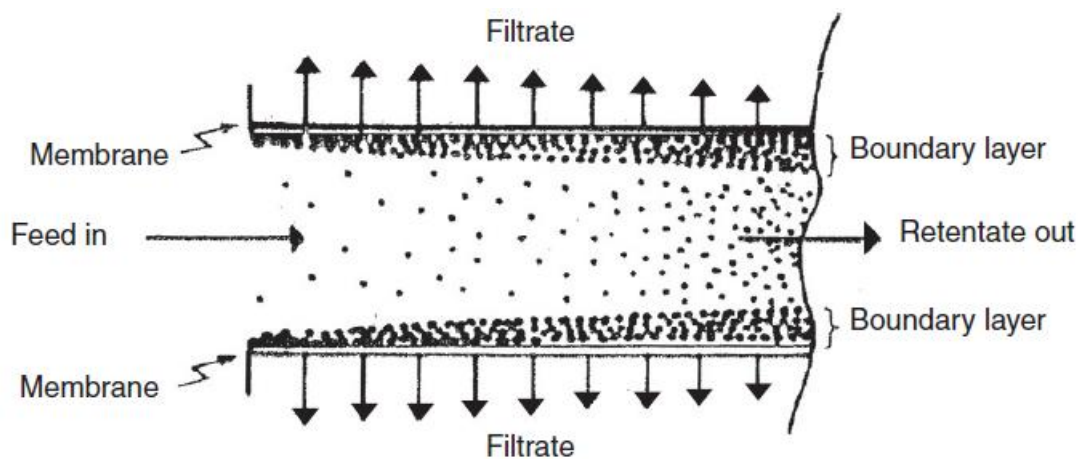
Figure 2.4 - Schematic diagram of concentration polarization during the membrane separation process [5]

While the solutes in the feed stream are flowing into the boundary layer with the convection, back-diffusion simultaneously occurs due to the concentration gradient of the solute between the cake layer on the membrane surface and the bulk solution. **Figure2.5** shows how solutes transported with convection and back-diffusion in detail.

7
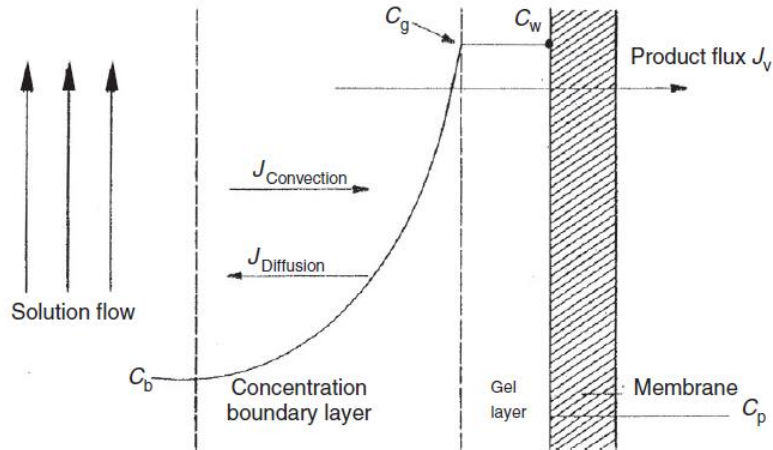
Figure 2.5 - *Concentration profile of solute during membrane process [5]*

As the membrane separation process proceeds for a long enough time to attain the steady state, the system approaches the moment when the sum of solute in the permeate flow and the back diffusive transport of the solute equals to the convective transport of the solutes. Under the steady state condition, the following equation is satisfied [15, 16].

$$J_c * C = -D * \frac{dc}{dx} + J * C_p \qquad (1)$$

where J_c is convection flux, J is solvent (permeate) flux, C is feed solute concentration, C_p is solute concentration in permeate, D dc/dx is the back diffusive flux of the solute, D is solute diffusivity, and x is length coordinate.

For most types of membranes, the system does not reach 100% solute rejection in industries, and there is still a small number of particles entering into the permeate solution after the filtration process. For this reason, the magnitude of C_p should be considered. With the boundary conditions of (x=0, $C=C_w$) and (x=δ, $C=C_b$), the integration of **Equation 1** yields **Equation 2** below.

$$J = k * \ln\left(\frac{C_w - C_p}{C_b - C_p}\right) \qquad (2)$$

Where C_w is the concentration of solute on membrane surface, C_b is the concentration of solute in bulk solution, δ is the thickness of boundary layer, and k is the mass transfer coefficient of solute back to the feed stream (D/δ)

However, the concentration of solute in permeate flow is very small compared to those in the bulk solution and on the membrane surface. For this reason, C_p value is negligible for most cases of the membrane separation process, and **Equation 2** can be simplified as,

$$J = k * \ln\left(\frac{C_w}{C_b}\right) \qquad (3)$$

By rearranging **Equation 3**, the ratio of concentration on the membrane surface and in the bulk solution can be expressed as,

$$\frac{C_w}{C_b} = \exp\left(\frac{J}{k}\right) = C_M \qquad (4)$$

In **Equation 4**, C_M is called polarization modulus. As it indicates, polarization modulus increases as the flux of solvent increases. In other words, the concentration of solute on the membrane surface increases with the higher flux of solvent. Oppositely, polarization modulus increases as the mass transfer coefficient, k decreases. Since the mass transfer coefficient is proportional to solute diffusivity and anti-proportional to the thickness of the boundary layer, the magnitude of polarization modulus also depends on them. Those relationships demonstrate that any membrane technology

that provides the low concentration of solute on the membrane surface will minimize the thickness of boundary layer, inducing the increase in the magnitude of the solvent flux through the membrane.

2.4 Principle of Fouling

Among diverse phenomena, the membrane technology has been faced to the critical problem, which is called the fouling. As an example, the flux of pure water for ultrafiltration is generally $1\mathrm{cm}^3/\mathrm{cm}^2\mathrm{min}$ while macromolecules or colloidal solutions have the flux of $0.1\mathrm{cm}^3/\mathrm{cm}^2\mathrm{min}$. This flux difference occurs due to the deposition of macromolecules and colloidal materials on the membrane surface. Because of the deposition during the separation process, the concentration polarization occurs, and the gel layer forms. This gel layer resists solution flow through the membrane and reduces the flux. For this reason, the flux of the permeate solution highly relies on the composition of the feed solution. The geometry of the gel layer is shown in more detailed in **Figure 2.6**.
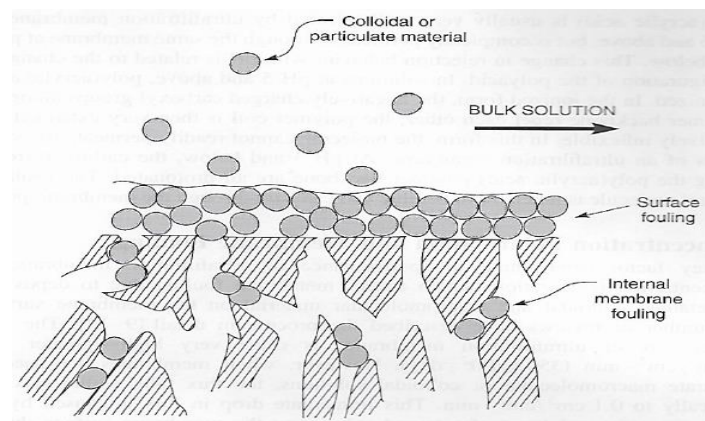
Figure 2.6 – Schematic diagram of gel layer on surface of membrane [17]

As the figure indicates, the accumulated particles on the membrane surface block the porous spaces and increase the resistance of the cake layer. As a result, the solution has less opportunity to pass through the surface, thus lower production rate of permeate solution. As an example, the change in ultrafiltration flux as the function of latex concentration in the feed stream is shown in **Figure 2.7**.
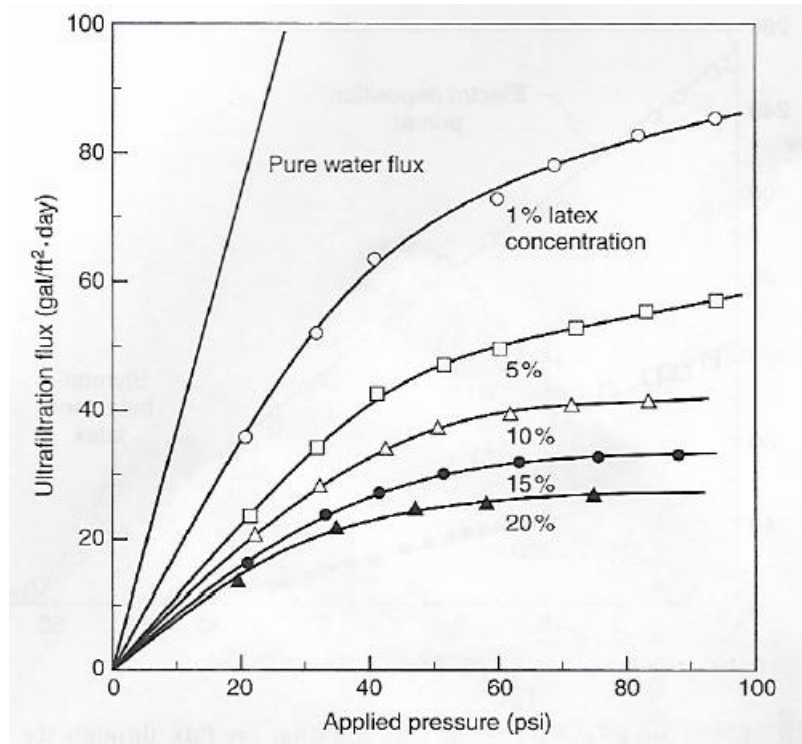
Figure 2.7 - *Change in ultrafiltration flux with respect to latex concentration in feed solution [18]*

As **Figure 2.7** shows, ultrafiltration flux decreases as latex concentration of the solution increases. This trend is expected since relatively much greater number of latex particles would accumulate on the membrane surface, resulting highly densified cake layer with high resistance.

In addition, the formation of the gel layer is related to the applied pressure of the feed solution. Based on **Equation 4**, the concentration of solute in the gel layer increases as the flux of solution increases. Therefore, higher pressure is needed to drive the permeate flow through the gel layer and the membrane. The relationship between applied pressure and membrane flux is in **Figure 2.8**.
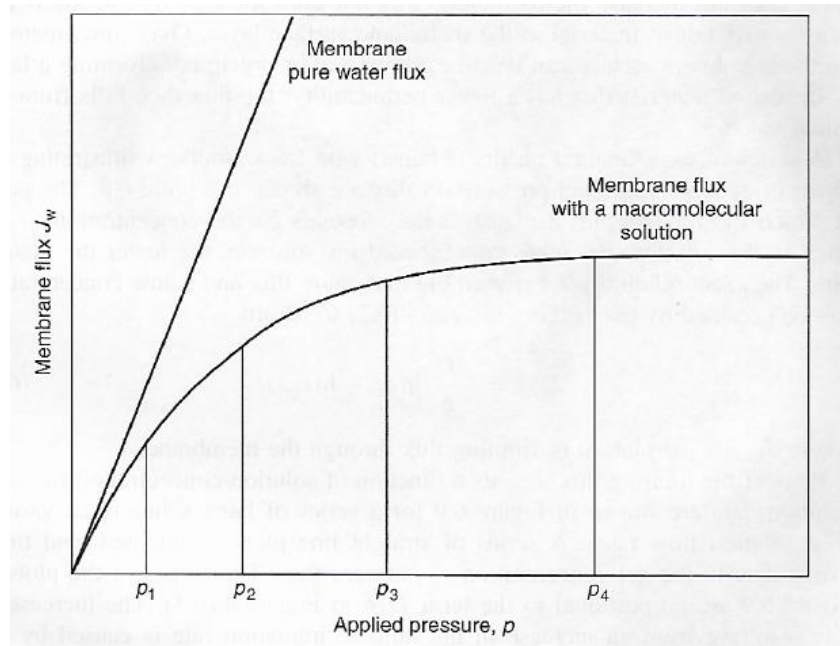
Figure 2.8 – Change in fluxes of pure water and macromolecular solution with respect to applied pressure [17]

As can be seen in **Figure 2.8**, membrane flux and applied pressure have a proportional relationship. However, higher applied pressure tends to increase the solute concentration of the gel layer, and this gel layer reduces the flux of solution. This can be illustrated by comparing the membrane fluxes of the pure water and macromolecular solution. Membrane pure water flux increases faster than the one with a macromolecular solution at higher applied pressure. There is no molecule accumulating on the membrane surface with the pure water while the macromolecular solution builds the gel layer. For this reason, the increase rate of flux with macromolecular solution becomes smaller at high applied pressure due to the increase in the resistance of the gel layer.

2.5 Factors to Control Fouling Problem

2.5.1 Rejection and Retention Coefficients

In fact, the degree of the fouling during the membrane separation process is highly related to the properties of the particles in the feed solution, such as their sizes, shapes, and electrical charges. Specifically, the particle sizes in the feed solution significantly affect the degree of fouling for porous membranes. The particles smaller than pore

sizes pass through the membrane while the rest of particles are rejected and accumulates on the membrane surface or flow away with the retentate solution. Rejection coefficient is one of the best reliable indicators to analyze the separating ability of a porous membrane, and it can be calculated from the following equation [19].

$$\%\text{Rejection} = \frac{\text{feed/bulk solute con centration} - \text{product solute concentration}}{\text{feed/bulk solute concentration}} * 100 \qquad (5)$$

In case when the particles in feed solution are perfectly filtered, the rejection coefficient of the membrane is 100%. This rejection coefficient is useful only if the membrane completely overcome the fouling problem. However, for most membrane separation in practice, the particles accumulate on the membrane surface due to the concentration polarization. Thus, the retention coefficient is considered alternatively to examine the ability of membrane to retain particles, and it can be calculated from the following equation [20].

$$\%\text{Retention} = \frac{\text{membrane surface solute concentration} - \text{permeate solute concentration}}{\text{membrane surface solute concentration}} * 100 \qquad (6)$$

2.5.2 Shape of Molecules in Feed Solution

Another critical aspect that affects the flow rate of permeate solution during membrane separation process is the shape of the molecule in the feed solution. For example, water soluble molecules, such as polydextran, polyethylene glycol, or polyvinyl pyrrolidone have the linear shape, and it is easier for them to pass through the membrane surface than globular molecules, as shown in **Figure 2.9**. Globular molecules contain strong hydrogen bonds and cannot be easily deformed to pass through membrane pores [21].
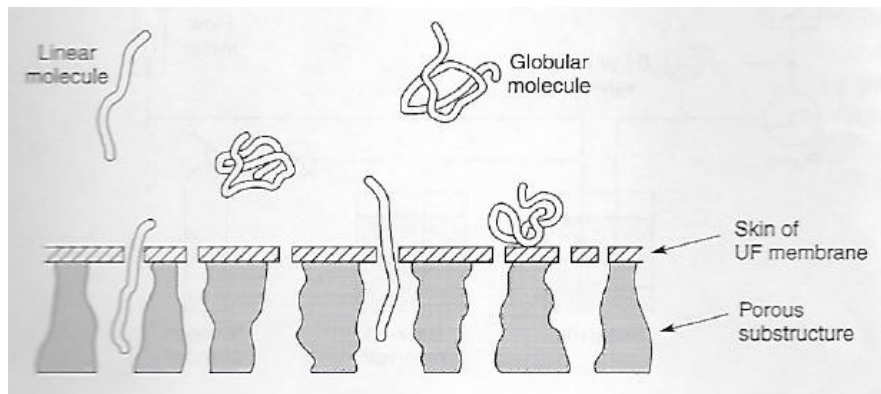
Figure 2.9 - *Porous structure of membrane and shapes of solute particles [21]*

2.5.3 Electric Charge of Membrane and Particles

Lastly, the electric charge of the membrane is another factor that affects the degree of fouling, depending on the type of the feed solution. To overcome the fouling problem, the membrane surface and feed solution should have the same charge type; i.e. both positive or negative. The membrane surface repels the materials that have the same charge, and the adhesion of the colloidal gel layer reduces. In general, carboxyl, sulfonic, and acid groups in most colloidal materials are negatively charged. For this reason, the negatively charged membrane is usually preferred. To prove this property, **Figure 2.10** shows the experimental results of the change in paint flux with respect to the charge of the membrane [18].
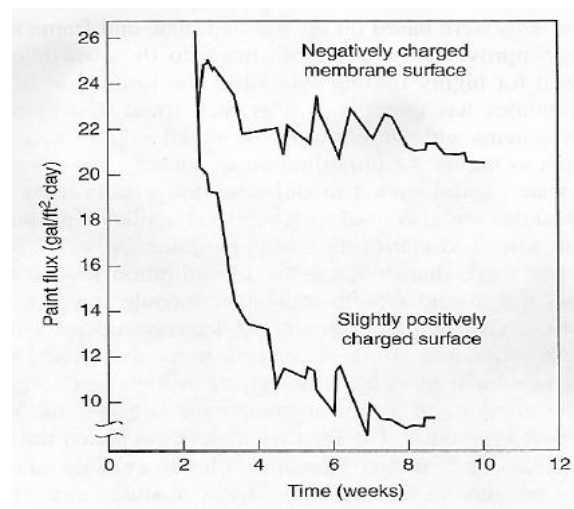
Figure 2.10 - *Change in paint flux with respect to charge of ultrafiltration membrane [18]*

14

In **Figure 2.10**, the feed solution is negatively charged electrocoat paint. It indicates that the paint flux decreases slowly over time with negatively charged membrane surface while it decreases rapidly with the positively charged one.

2.6 Methods to Overcome Fouling Problem

The previous methods investigated to alleviate the membrane fouling are chemical cleaning, air scouring, back flushing, microbubble, and ultrasound. **Table 1** shows the advantages and disadvantages of each method.

Table 1 – *Advantages and Disadvantages of Cleaning Methods for Fouling Reduction*

	Advantage	Disadvantage
Chemical cleaning	- Various types of chemical agents available.	- Limitation to recover the performance of membrane - Downtime of the filtration process to carry out the cleaning
Air scouring	- Effective removal of accumulated particles.	- Complex to control the system. - Downtime of the filtration process to carry out the cleaning
Back flushing	- Effective removal of accumulated particles.	- Requires high pressure, leading to membrane damage. - Downtime of the filtration process to carry out the cleaning
Microbubble	- Effective removal of accumulated particles. - No downtime is required for cleaning	- Additional operating cost for bubble production
Ultrasound	- Effective removal of accumulated particles. - No downtime required for cleaning	- Additional operating cost for bubble production

2.6.1 Chemical Cleaning

Chemical cleaning is the process that utilizes chemical reaction between the particles of the cake layer on the membrane surface and the chemical agent to remove the fouling on the membrane surface. In addition, it is an off-line process, meaning that the filtration needs to be stopped to clean the membrane surface. There are three main types of chemical agents that are used for cleaning, which are acid solution, alkali solution, and biocide solution [22]. The acid solution is generally used to remove accumulated inorganic particles on the membrane surface while the alkali solution controls organic particles. The biocide solution is used to remove biological substances. Since each of them has their own role, the choice of agent highly depends on the feed solution to the membrane module. In practice, feed solutions contain various components, and applying only one of the agents is not adequate. Separation of milk in the food industry can serve as a typical example. The main nutritional components in milk are water, carbohydrate, fat, protein, minerals, and minor biological proteins and enzymes. When membrane separation is performed to extract pure water from milk, more than one type of agents needs be used for the cleaning process to reduce the fouling problem. However, chemical cleaning can't remove irreversible fouling that generally happens during the membrane separation process. Thus, it is impossible to completely recover the performance of the membrane with the application of chemical cleaning.

2.6.2 Air Scouring

Air scouring is the method that enhances mass transfer of particles in feed solution to reduce the amount of accumulation on the membrane surface. In other words, the particles are forced by air to pass by the membrane surface rather than accumulate on its surface. Generally, this method is simultaneously used with rinsing, such as backwashing and forward flushing, during the filtration process to control the degree of purification of permeate water. There are, in fact, several factors that should be considered in air scouring, such as: the velocity of air, size of bubbles produced, and the frequency of air injection, so to provide an effective cleaning. For this reason, it is difficult to control the air scouring over the entire period of the membrane separation process. Moreover, reported literature on the mechanism of this method at the present

time is still limited due to its high complexity [22, 23].

2.6.3 Back Flushing

Back-flushing is the mechanical cleaning method to restore the membrane flux when chemical cleaning cannot sufficiently accomplish. In fact, back-flushing is not preferred as the first cleaning method since it requires relatively high pressure, leading to membrane damage. To avoid damage to the membrane, the allowed range of pressure for back-flushing is generally from 5 to 15 psi for ultrafiltration. **Figure 2.11** presents a schematic diagram of back flushing [17, 24].
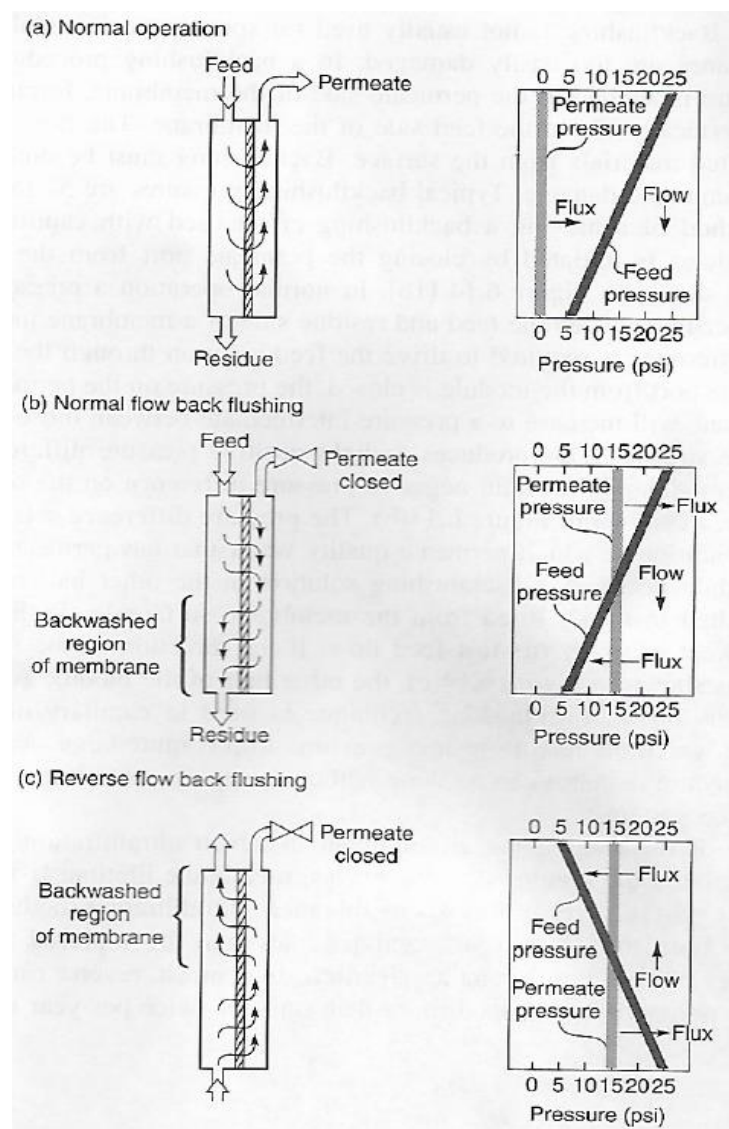
Figure 2.11 *- Schematic diagram of back flushing for membrane cleaning*

17

In general operation of the membrane, the pressure is applied to feed stream, so that solution can flow from the feed side to permeate side. However, during the application of back-flushing in **Figure 2.11** (b), permeate port is closed; and hence, over-pressure is generated in the permeate side, which force water to flow back through the membrane and remove deposited particles on the membrane surface. During this back-flushing process, the permeate side reaches a pressure intermediate between feed and residue streams. For this reason, there is the positive pressure difference at the one end of the membrane module while the other end of it has the negative pressure difference. Therefore, only half part of the module undergoes back-flushing. The Reverse flow back-washing, as depicted in **Figure 2.11** (c), can overcome this problem. The feed stream is introduced to the residue port (retentate or reject side) instead, and the other half of the membrane surface is back-flushed by water.

2.6.4 Application of Gas/air Microbubbles

Gas bubbles have been applied to clean various materials in the industries, such as metals, plastics, human skins, and biologic water treatment [25, 26, 27]. This approach can be used to remove the cake layer on the membrane surface during the separation process to overcome fouling problem. In principle, there are two types of bubbles depending on their sizes, which are macrobubbles and microbubbles, and their behaviors in water solution are different as presented in **Figure 2.12**.
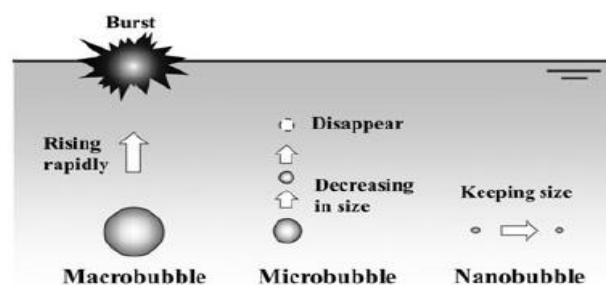
Figure 2.12 - Difference in behavior of microbubbles and macrobubbles [28]

Macrobubble rises rapidly to the water surface and burst within a short time. On the other hand, microbubble tends to stay in water for a much longer time. With this high

durability, application of microbubbles can significantly contribute to the membrane fouling remediation. It is generally defined as microbubble if the bubble diameter is 50um or less [29]. Microbubbles provide mainly four fouling control mechanisms, as shown in **Figure 2.13**.
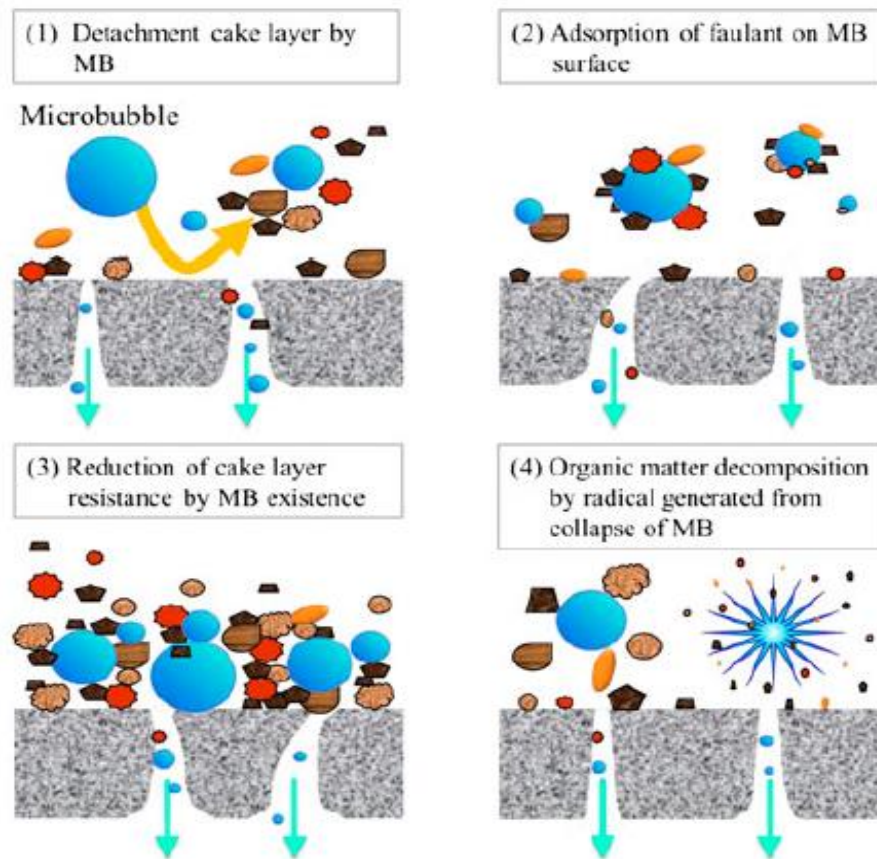
Figure 2.13 - *Mechanisms of microbubble to reduce membrane fouling [29]*

First, microbubbles could detach particles from the cake layer. As microbubbles move down to the membrane surface, the accumulated particles could be physically scoured and spread out by the bubbles. Thus, particles are detached from the cake layer and move back to the bulk fluid, resulting in the reduction of the cake layer thickness. Secondly, the accumulated particles in the cake layer are adsorbed onto the microbubble surface due to hydrophobic interaction, and this phenomenon contributes to fouling reduction. Thirdly, microbubbles can attach to the membrane surface. With the existence of microbubbles, the porosity of the cake layer increases, and it allows more solution to pass through the membrane to the permeate side. In other words, the flow rate of the permeate through the membrane increases. Lastly, the collapses of

microbubbles can create a very high temperature and pressure region, which in turn can generate radicals. As the radicals approach cake layer, the organic matters of the cake layer are decomposed; and hence, the amount of accumulated particles in the cake layer decreases [28, 29]. The cellulose acetate hollow fibre membrane was used to examine the effect of microbubbles in ultrafiltration. The raw river water from the Ibo River (Hyogo, Japan) was used as the feed solution with the inlet velocity of 0.16m/s and applied pressure of 50kPa. **Figure 2.14** shows the experimental results of the change in the permeate flux as a function of filtration time with and without microbubble.
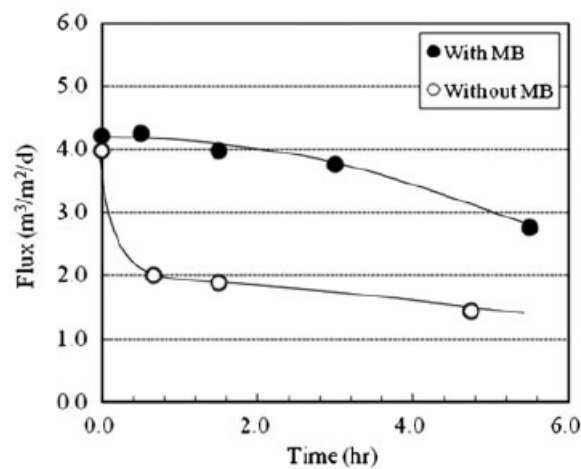
Figure 2.14 - Effect of microbubbles on filtration flux [29]

By comparing the two graphs, the result confirms that microbubbles significantly help maintaining the permeate flux while the permeate flux decreases substantially without microbubbles. In other words, the amount of foulant on the membrane surface was evidently reduced with microbubbles.

2.6.5 Application of Ultrasound

2.6.5.1 Introduction of Ultrasonic Application

Application of ultrasound as a membrane fouling control method is reviewed in detail in this section. The most critical problem for other methods is that the filtration process needs to be stopped to remove foulants, resulting in downtime for the filtration process.

The application of ultrasound is considered as a method to overcome this critical disadvantage, inducing high production rate while maintaining the high quality of permeate solution.

2.6.5.2 Mechanism of Ultrasonic Application

In order to apply the ultrasound during the filtration process, the ultrasonic transducer is installed on the external surface of the membrane apparatus. When the ultrasound propagates through the medium by activating the transducer, the solution in the membrane apparatus is subjected to a series of compression (high pressure) and rarefaction (low pressure) cycles. As the rarefaction cycle exceeds the attractive force of the liquid molecules in feed solution at sufficiently high-power intensity, cavitation bubbles are produced in liquid. In fact, cavitation bubbles have similar properties of microbubbles as described in **Section 2.6.4** [30]**.** The surfaces of them have adsorptive capability to remove accumulated particles on the membrane surface during the filtration process; and hence, the resistance of the cake layer to the permeate stream is reduced. **Figure 2.15** presents the mechanisms of the cavitation bubble in detail.
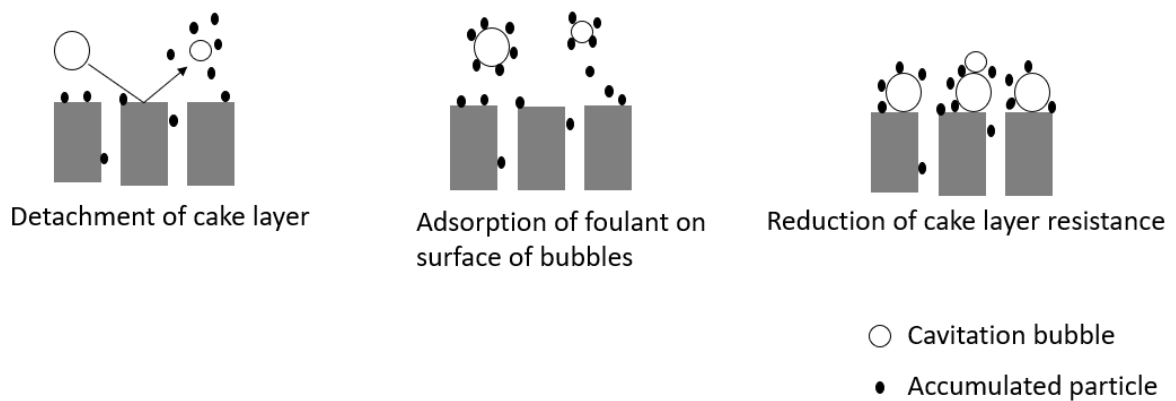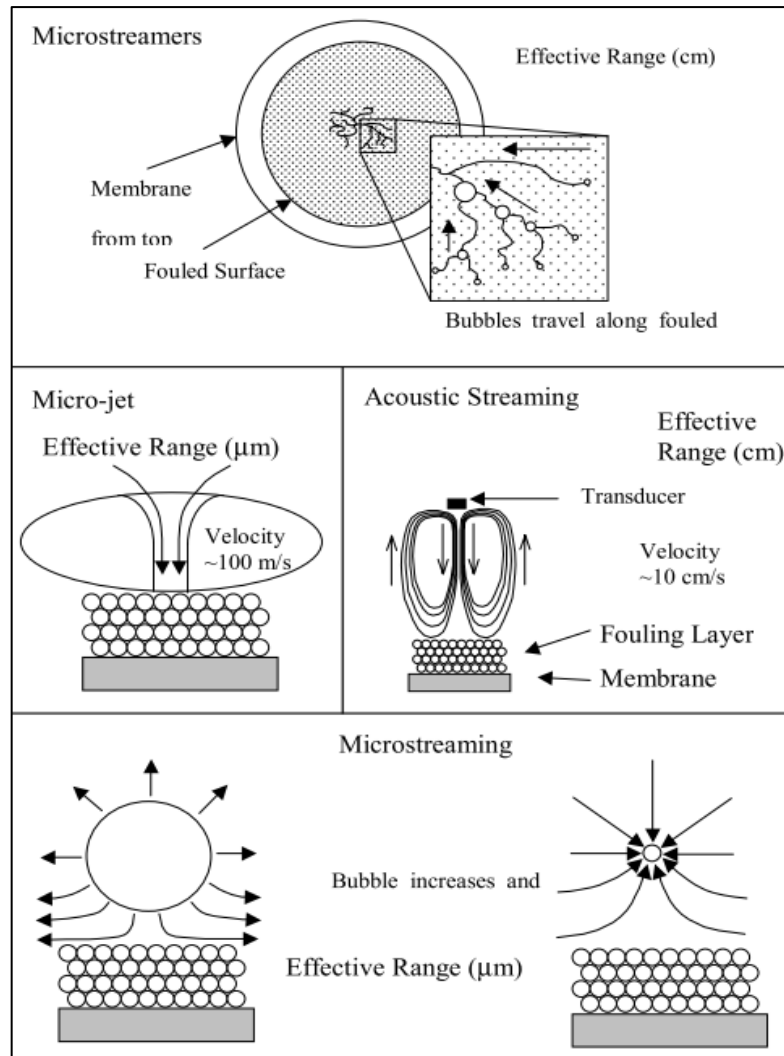
Figure 2.15 - Mechanisms of cavitation bubbles from the ultrasonic transducer [31]

As **Figures 2.13 and 2.15** indicate, microbubble and cavitation bubble have similar mechanisms to remove the foulants on the membrane surface. However, the cavitation bubble generated by ultrasound has additional mechanisms, which are

microstreamer, microjet, acoustic streaming, and microstreaming.

Microstreamers are the cavitation bubbles that form at nucleation sites within the liquid and travel toward the regions experiencing the greatest negative pressure of the acoustic wave, called antinodes. Antinodes are usually located on the fouled membrane surface during the filtration process. Microstreamers scour the accumulated particles away from the membrane surface while translating to these antinodes [32].

Secondly, fouling can be reduced by micro-jets from cavitation bubbles. Micro-jets occur when the cavitation bubbles collapse in the presence of asymmetry. The asymmetry can be the surface of another cavitation bubble or any fixed surface. When they collapse, the bubbles accelerate toward the direction opposite to the membrane surface. As a result, a jet of water strikes the cake layer with a velocity of 100 to $200\mathrm{m/s}$. The collision induces the foulants to detach from the membrane surface [32]. The effective range of micro-jets is proportional to the size of the cavitation bubble.

Thirdly, acoustic streaming is considered as another mechanism to remove foulants on the membrane surface. The acoustic streaming is described as the absorption of acoustic energy by liquid, which creates the artificial fluid flow. The flow gives a stimulus to accumulated particles. In fact, the acoustic streaming is generally efficient to remove loosely attached particles on the membrane surface due to its relatively weak strength [33]. The absorption of acoustic energy is proportional to the magnitudes of ultrasonic frequency and power intensity [34].

Lastly, microstreaming is the circulation of fluid around the surface of the cavitation bubbles that fluctuate in size, due to the oscillating sound pressure. The oscillation tends to create fluid movement to provide shear forces [35, 36]. While the cavitation bubbles stay around the cake layer, the dynamic velocity from microstreaming may exert some force on accumulated particles so to dislodge them from the surface. Like micro-jets, the effective range of microstreaming is proportional to the size of the cavitation bubble.

2.6.5.3 Physical Properties of Cavitation Bubbles

The physical properties of the cavitation bubbles are highly related to the ultrasonic

conditions, which are ultrasonic frequency and power intensity [31]. First, the size of cavitation bubbles has the anti-proportional relationship with the ultrasonic frequency as **Figure 2.16** and **Equation (7)** demonstrates [31,37].
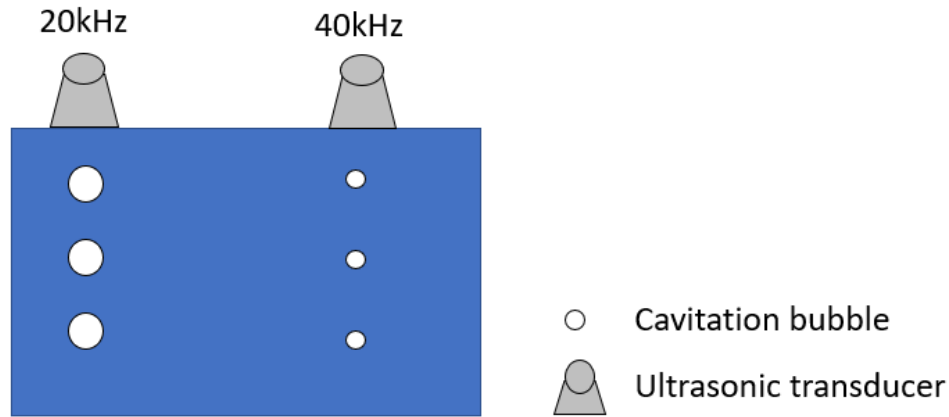
Figure 2.16 - *Relationship between the size of cavitation bubble and magnitude of ultrasonic frequency [31]*

$$f_o = \frac{1}{2\pi R_o}\sqrt{\frac{3\kappa p_o}{\rho}} \quad (7)$$

Where f_o is the resonance frequency, p_o is the ambient pressure, κ is the polytropic index, R_o is the radius of the cavitation bubble, and ρ is the density of liquid phase. In other words, the lower frequency of ultrasound produces relatively bigger cavitation bubbles, and those bubbles have larger surface area to adsorb accumulated particles on the membrane surface. Moreover, the collapse of larger cavitation bubbles leads to stronger and wider range of micro-jets to detach the foulants. They would also vibrate intensely to enhance microstreaming effect when they are present on the cake layer due to their large surface area. In addition, the magnitude of the ultrasonic frequency is anti-proportional to the production rate of the cavitation bubble. At high frequency, the rarefaction and compression cycles are extremely short, limiting the growth of the bubble into the sufficient size to disrupt liquid. The resultant cavitational effects would, therefore, be less and a smaller number of bubbles can be produced. For those reasons, there would be higher cleaning efficiency with lower ultrasonic

frequency. In principle, the ultrasonic frequency needs to be adjusted to the value between 20 and 1000kHz to facilitate the formation of cavitation bubbles [31].

Furthermore, the production rate of the cavitation bubble is proportional to the ultrasonic power intensity. The higher power intensity would create a larger size cavitating zone as the ultrasonic energy is released into the liquid phase, because of the higher pressure amplitude of the sound wave. As a result, a greater number of cavitation bubbles can be generated. Thus, more accumulated particles would be removed to reduce the resistance of the cake layer. Also, the sonochemical effects can be amplified by increasing the power intensity, leading the enhancement of acoustic streaming effect. The general range of ultrasonic power intensity for cleaning is from 0.5 to 6 W/cm^2 [38].

2.6.5.4 Previous Performance in Application of Ultrasound

The application of ultrasound has generated much interest in researchers as an alternative method to overcome the fouling problem during the membrane filtration process. Several researchers have examined the effect of it in different situations to find out the optimal condition that can provide the highest efficiency [39, 40, 41, 42]. Among them, Wenzheng Yu [39] have considered the application of continuous ultrasound for the whole period of the coagulation-ultrafiltration process (CUF) in opened system. A synthetic raw water was used as a feed solution to test the performance. Domestic sewage and 5mg/L of humic acid (International Humic Acid Substance Society, USA) were added to the local (London, United Kingdom) tap water with a volumetric ratio of 1:50 [43]. The system contained polyvinylidene fluoride (PVDF) UF membrane with a nominal pore size of $0.03\mu m$. A suction pump was adjusted to maintain constant permeate flux of $20L/(m^2h)$. **Figure 2.17** shows the change in the magnitude of transmembrane pressure with time during two different runs. One of the runs was performed with ultrasound while the other one was without ultrasound.
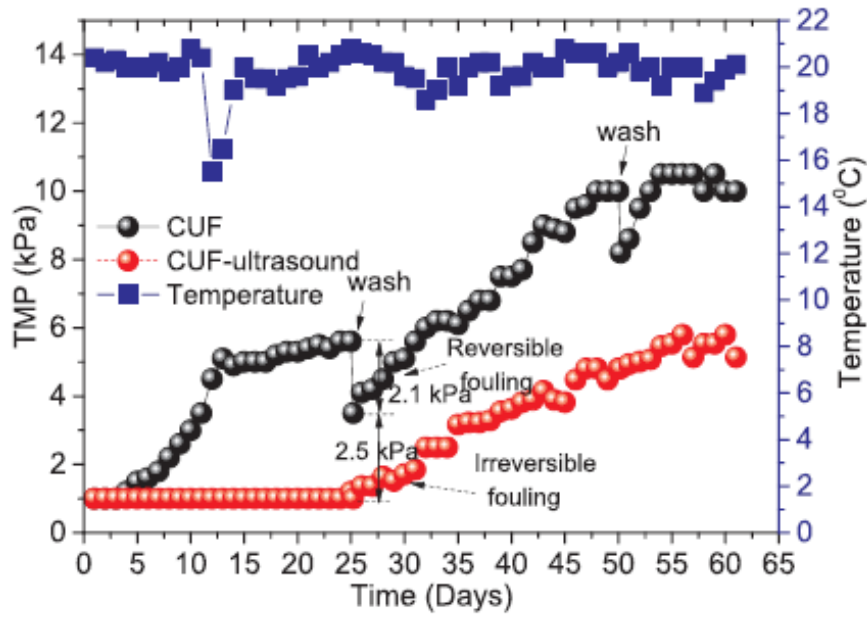
Figure 2.17 - *Temporal variation of transmembrane pressure in the two membrane systems [39]*

The CUF in the figure refers to the coagulation-ultrafiltration process without ultrasound and CUF-ultrasound is for the one with ultrasound. The transmembrane pressure is the pressure that is required to allow the feed solution to pass through the membrane to produce the permeate, and it can be calculated using the equation below.

$$\text{Transmembrane pressure (TMP)} = \text{Applied pressure} - \text{outlet pressure} \quad (8)$$

The applied pressure in **Equation 8** is the pressure at the entrance of the feed solution while the outlet pressure is generally the atmospheric pressure. **Figure 2.17** demonstrates that much lower transmembrane pressure is required to maintain the equal production rate of permeate solution with the application of ultrasound, compared to the one without the ultrasound. In fact, the CUF system without ultrasound required even higher transmembrane pressure although it was continually washed by high pressure tap water once every 25 days.

Moreover, the scanning electron microscope (SEM) image was performed for visual

26

analysis of the membrane surface after the filtration process for both the CUF and CUF-ultrasound system, and presented in **Figure 2.18**.

a)   b)
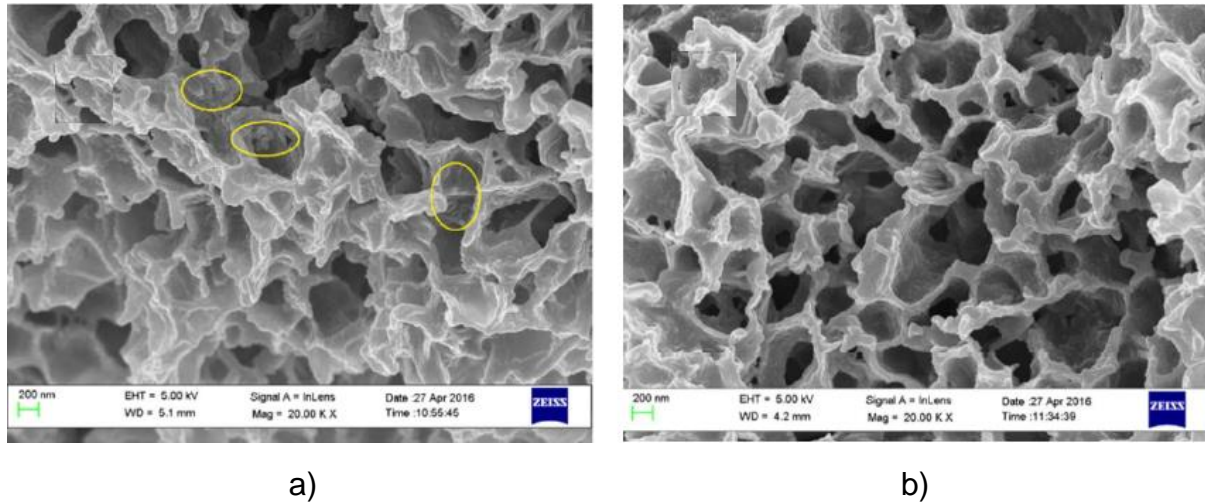
Figure 2.18 - *Scanning electron microscope (SEM) images of the membrane surface after the filtration process; a) Membrane surface in CUF system, b) Membrane surface in CUF-ultrasound system [39]*

By comparing images (a) and (b) in **Figure 2.18**, a lot of particles accumulated and blocked membrane pores in CUF system while mostly no particles can be seen in CUF-ultrasound system. Thus, the visual analysis from SEM demonstrates again that ultrasound successfully reduces fouling problem.

2.6.5.5 Problem Statements from Past Literature

In reported literature, the filtration system was adjusted to keep constant permeate flux; and changes in the magnitude of trans-membrane pressure were observed to examine the effect of ultrasound [39]. However, the membrane system was generally operated under constant transmembrane pressure in the industries; hence, the permeate flux decreased with time due to fouling. For this reason, there was a limitation in applying past experimental results to improvement in real membrane filtration plants.

Furthermore, the physical properties of the cavitation bubbles rely on the conditions of

ultrasound, such as ultrasonic frequency and power intensity [32]. It is expected that change in their properties will critically affect the degree of resistance of cake layer, leading to change in flux of permeate solution. However, the past study used a single ultrasonic condition (38kHz, 85W) [39], and compared the results between the systems with and without ultrasound.

From the previous experimental work, researchers have worked on the application of ultrasound during the filtration process with the membrane apparatus in the opened system [44]. In other words, the flow of the solution is exposed to the external environment as shown in Figure 2.19.
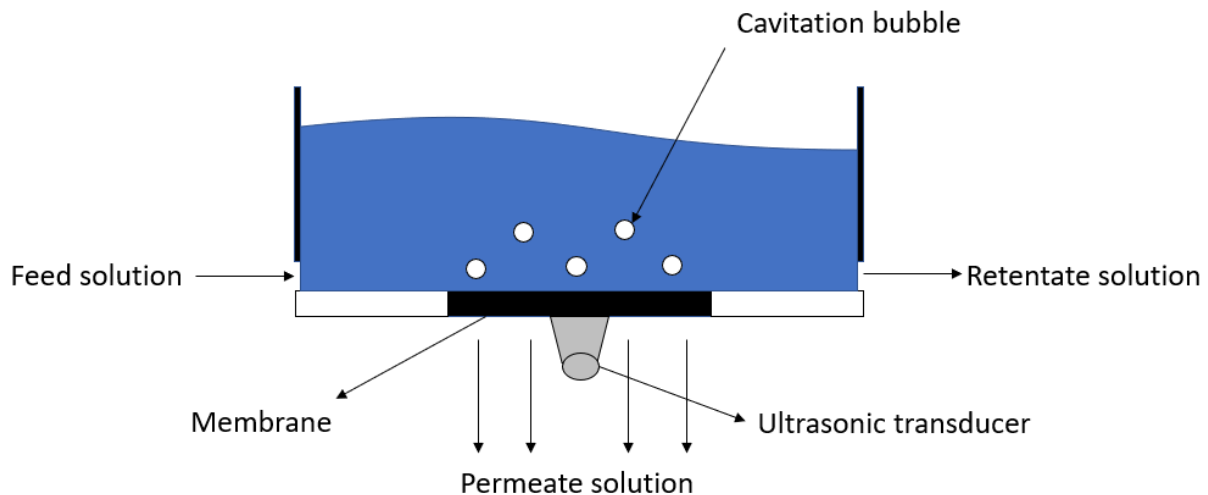
Figure 2.19 - *Diagram of membrane filtration with application of ultrasound in the opened system*

As the figure indicates, the solution is exposed to the atmosphere, and the cavitation bubbles are produced only from one flat surface of the apparatus at the bottom. This application is useful for simple membrane sheet with the flat surface. However, the most popular membrane apparatus designs in the real industries are spiral wound and hollow fine fibre. They have relatively high membrane surface area compared to the volume of the module and provides high permeate flux, meaning high economic efficiency. However, the critical problem is that they are highly susceptible to fouling. For this reason, engineers are focusing on the research to develop the methods to overcome fouling to maximize efficiency. In fact, those apparatuses are designed as

the closed system, and there is a limitation to rely on the results in the past literature since they are all based on the opened membrane system such as the one in **Figure 2.19**. Also, the membrane apparatus was submerged in a solution bath, and ultrasound was applied to the wall of the bath, not directly on the membrane unit.

2.6.5.6 Objectives of Research

This study contains 5 objectives:

1. To observe the change in cumulative mass and flux of permeate solution under constant transmembrane pressure and inlet flow rate for better application in real industries.

2. To test the wide range of ultrasonic condition to find out the optimal point, providing the highest production rate of permeate solution while maintaining the acceptable quality of it.

3. To consider intermittent ultrasound as an alternative method instead of continuous ultrasound to reduce the operating cost.

4. To analyze the change in thickness and structure of the cake layer with respect to different ultrasonic conditions to understand the mechanism of particle transport.

5. To consider the alternative design of membrane apparatus for practical application.

Chapter 3: Materials and Methods

3.1 Design of Membrane Apparatus

The alternative design of the membrane was considered to analyze the application of ultrasound in a closed system for this project, as shown in **Figure 3.1**.

Figure 3.1- *The closed system design of the membrane apparatus*

As **Figure 3.1** indicates, unlike the opened system, cavitation bubbles tend to be produced from the entire surface boundary layers when the ultrasonic transducer is activated on a closed system. Thus, there is the higher production rate of the bubbles.

3.2 Application of Intermittent Ultrasound

In reported literature, ultrasonic transducer was continuously activated over the entire period of the membrane filtration process. In fact, the most important reason of study on fouling reduction is to reduce the operating cost of the filtration process to increase economic efficiency. Therefore, minimizing the operating cost of ultrasound while maintaining the acceptable quantity and quality of the permeate solution by the application of the intermittent ultrasound was investigated. The cumulative mass of the

permeate solution was observed for quantity analysis. Simultaneously, turbidity and average particle size distribution were examined to test the quality. The operating condition of ultrasound can be reduced by half with the application of intermittent ultrasound. The on/off cycle is repeated for every fixed time interval until the end of the filtration process. The following figure shows the pattern of this intermittent ultrasound application in detail.

1 minutes interval

Time (min)	0	1	2	3	4	5	6	7	8	9	10	11	12	13	14	15
Ultrasound on/off		■		■		■		■		■		■		■		■

1.5 minutes interval

Time (min)	0	1.5	3	4.5	6	7.5	9	10.5	12	13.5	15
Ultrasound on/off		■		■		■		■		■	

2 minutes interval

Time (min)	0	2	4	6	8	10	12	14
Ultrasound on/off		■		■		■		■

■ = on
☐ = off

Figure 3.2 - Pattern of intermittent ultrasound

The length of filtration time was 30 minutes for each run since the membrane was completely fouled within this period. The time interval of intermittent ultrasound was considered from 1 to 2 minutes to repeat enough on/off cycle. There is a possibility of result being affected by changing the time interval randomly. However, it could not be considered due to the limitation on the capability of the timer connected to the ultrasonic generator.

3.3 Experimental Setting

The schematic diagram of the experimental set-up used in this study is presented in **Figure 3.3** below.
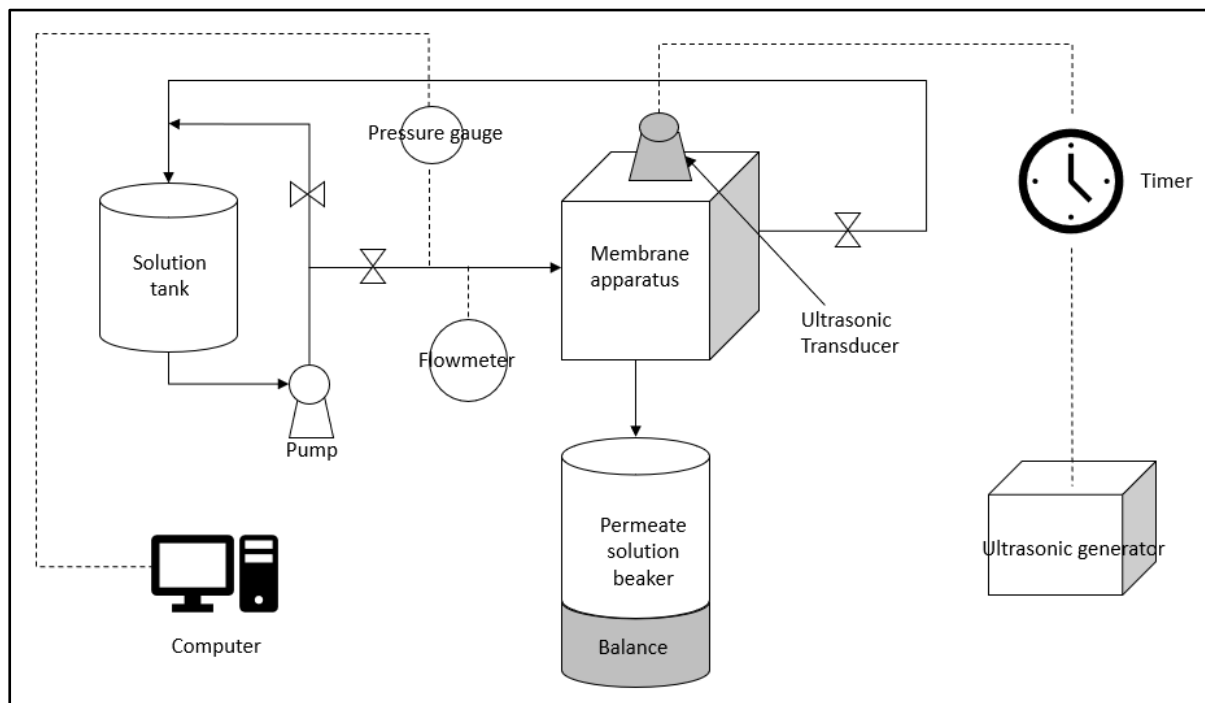
Figure 3.3 - Schematic diagram of experimental setting

The solution tank was filled with skim milk, which was used as the feed solution. The tank is connected to a magnet turbine pump (MDT-20LDB115, Iwaki Co.,LTD, Tokyo, Japan) to deliver the feed solution to the membrane apparatus. The bypass pipeline was installed to control the inlet flow rate of the feed solution. The inlet flow rate was maintained at 20 US gallons per hour and monitored using a flowmeter (FL7203, Omega Engineering Inc, Norwalk, USA). The applied pressure was set at 30psi. The applied pressure was monitored using a software program (Labview 2010, National Instruments, Austin, USA) and pressure transducer (PX303-100G5V, Omega Engineering Inc, Norwalk, USA). Those inlet flow rate and applied pressure were selected to obtain enough permeate amount at each run for accurate analysis. The ceramic membrane used in this study could withstand up to 30psi. The flowmeter could display the magnitude up to 20 US gallons per hour. Inlet flow rate and applied pressure were kept constant throughout experimental runs. The ultrasonic transducer is installed at the top of the membrane apparatus, and different ultrasonic conditions

were set for each experimental run. Three models of the ultrasonic transducers, (20kHz, 5.76W/cm^2, OURSULTRASONIC, ARS-QXHNQ20100, Guangdong, China), (28kHz, 5.76 W/cm^2, CLANGSONIC, CN2845-68LB, Zhejiang, China), and (40kHz, 5.76 W/cm^2, CLANGSONIC, CN4038-48LAP4P8, Zhejiang, China), were prepared in this project. In case of the power intensity analysis, by following the principle of the electric circuit, the transducers are connected in series to reduce the power intensity to 2.88 W/cm^2 and 1.44 W/cm^2 at each ultrasonic frequency. **Figure 3.4 and 3.5** show the circuit design of the ultrasonic transducers.
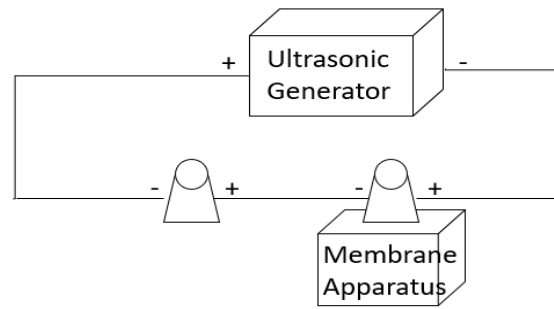
Figure 3.4 *- Circuit of two ultrasonic transducers in series*
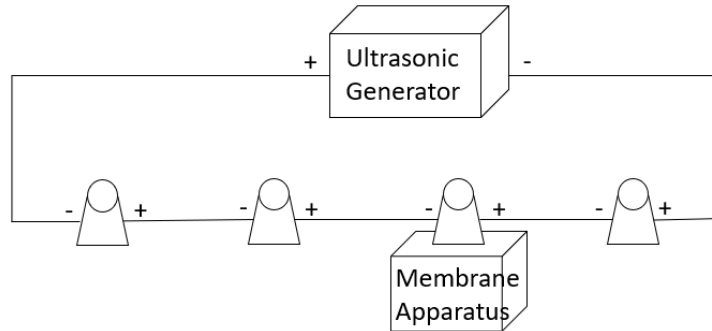
Figure 3.5 *- Circuit of four ultrasonic transducers in series*

The magnitude of the total resistance in the series circuit is the sum of the resistance of all the transducers, and the following equation can be applied to calculate it.

$$R_{total} = \sum_{i=1} R_i \qquad (9)$$

Where R_{total} is the total resistance of the circuit, and R_i is the resistance of each ultrasonic transducer. In this study, same ultrasonic transducers are connected in series at each frequency. Thus, the total resistance of the circuit expressed as below.

$$R_{total} = R_i * n \qquad (10)$$

where *n* is the number of transducers connected in series. Unlike the resistance, magnitude of the current is not affected by the circuit design in series connection and remains as a constant value. In other words, magnitudes of the current that passes through each transducer are equal as shown in **Equation 11** below.

$$I_{total} = I_1 = I_2 = I_3 = \cdots = I_i \qquad (11)$$

Where I_{total} is the total current of circuit, and I_i is the current that passes through each ultrasonic transducer. Moreover, the magnitude of the electric potential for each ultrasonic transducer in series circuit connection can be expressed by Ohm's law as in **Equation 12**.

$$V_i = I_{total} * R_i (\text{ohm's law}) \quad (12)$$

Where V_i is the electric potential (voltage) of each ultrasonic transducer. Lastly, electric power can be calculated with Joule's law:

$$P_i = I_{total} * V_i \qquad (13)$$

Where P_i is the electric power at each ultrasonic transducer.

By combining **Equations 12 and 13**, the power through a transducer can be written

as:

$$P_i = I_{total}^2 * R_i \qquad (14)$$

The total power across the circuit is:

$$P_{total} = I_{total}^2 * R_{total} = I_{total}^2 * \sum_{i=1} R_i = 100W \qquad (15)$$

With respect to the property of this connection, two of the same ultrasonic transducers were connected in series to provide the ultrasonic power intensity of 2.88 W/cm^2 while four of them were connected to provide 1.44 W/cm^2. In addition to that, only one single transducer was connected to consider the power intensity of 5.76 W/cm^2.

For the intermittent application of ultrasound, the transducer was connected to the timer (PTC-15, Omega Engineering Inc, Norwalk, USA) so that it could be automatically turned on and off at a fixed time interval. After the feed solution flows through the membrane apparatus, it was separated into two streams, which were the retentate and the permeate. The retentate solution was recycled back to the solution tank while the permeate solution flew down to a liquid collector. Thus, the feed solution in the tank would have been concentrated after the filtration. However, in the meantime, the particles in the feed solution partially accumulated on the membrane surface. Consequently, the change in the density of feed solution was found to be negligible. In fact, the solution density was measured and found to increase from 1.033 g/ml (for the original solution in the tank) to 1.05 g/ml over the experimental duration of 30 minutes. The mass of the permeate solution in the collector was measured continually every 1 minutes by an electronic balance (Scout Pro SP402, Ohaus Corporation, Pine Brook NJ, USA).

3.4 Statistical Design of Experiment

For this experimental study, Box-Behnken statistical design is considered with three

different parameters; ultrasonic power intensity, ultrasonic frequency, and time interval of intermittent ultrasound to obtain the optimal ultrasonic condition that can produce the highest cumulative mass of the permeate solution after the membrane filtration process. The advantage of Box-Behnken design is that the minimum number of the experimental run is required compared to other statistical design to obtain the optimal condition and considered in this study due to the limited number of the available ceramic membrane with the price of the material. The following table shows a three factor, three-level Box-Behnken experimental design [45, 46, 47].

Table 2 - *Box-Behnken experimental design with three factors and three levels [45, 46, 47]*

Method	Box-Behnken		
Parameters	Frequency, power intensity, interval of intermittent ultrasound		
Run	Frequency	Power intensity	Time interval of Intermittent ultrasound
1	-1	-1	0
2	-1	1	0
3	1	-1	0
4	1	1	0
5	-1	0	-1
6	-1	0	1
7	1	0	-1
8	1	0	1
9	0	-1	-1
10	0	-1	1
11	0	1	-1
12	0	1	1
13	0	0	0
14	0	0	0
15	0	0	0

Each parameter has three different values that were used in this study, as shown in **Table 3**.

Table 3 - *Three different levels of ultrasonic frequency, ultrasonic power intensity, and time interval of intermittent ultrasound*

Parameters	Range and levels		
	Low level (-1)	Centre level (0)	High level (+1)
Frequency (kHz)	20	28	40
Power intensity (W/cm^2)	1.44	2.88	5.76
Time interval of intermittent ultrasound (minute)	1	1.5	2

By applying those actual values of each parameter to Box-Behnken experimental design, the final conditions of the experimental runs can be set as shown in **Table 4**.

Table 4 - *Box-Behnken experimental design with actual values of parameters*

Method	Box-Behnken	
Parameters	Frequency, power intensity, intermittent interval	
Frequency (kHz)	Power intensity (W/cm^2)	Intermittent (min)
20	1.44	1.5
20	5.76	1.5
40	1.44	1.5
40	5.76	1.5
20	2.88	1
20	2.88	2
40	2.88	1
40	2.88	2
28	1.44	1
28	1.44	2
28	5.76	1
28	5.76	2
28	2.88	1.5
28	2.88	1.5
28	2.88	1.5

3.5 Composition of Feed Solution

The feed solution, skim milk, contains five main components including fat, protein, lactose, vitamins, and minerals [48].

3.5.1 Fat

The fat in the milk is in the form of small globules dispersed in the milk serum, and they exist as the lightest and the largest particle in the solution. The size of the particle of milk fat ranges from 0.1 to 20µm. The fat consists of various components, such as triglycerides, diglycerides, monoglycerides, fatty acids, sterols, carotenoids, and vitamins. Among them, the triglycerides are the dominating components composed of glycerol and various fatty acids [49]. Fatty acids are composed of the hydrocarbon chain and the carboxyl group (RCOOH group), and the characteristics of them highly rely on the number of the double bond in the hydrocarbon chain. The fatty acid having the double bond(s) in the hydrocarbon chain (unsaturated) has a low melting point and exists as the liquid phase at room temperature, while the fatty acid with only the single bonds in the hydrocarbon chain (saturated) remains as the solid phase. In fact, the four most abundant fatty acids in milk are myristic, palmitic, stearic, and oleic acids. Among them, myristic, palmitic, and stearic acids contain only the single bonds in the hydrocarbon chain while the oleic acid has one double bond. In other words, the oleic acid is only the one that stays as the liquid phase and considered to be separated by the membrane filtration in the industries. The following figure shows the chemical structures of myristic, palmitic, stearic, and oleic acids [48, 49, 50].
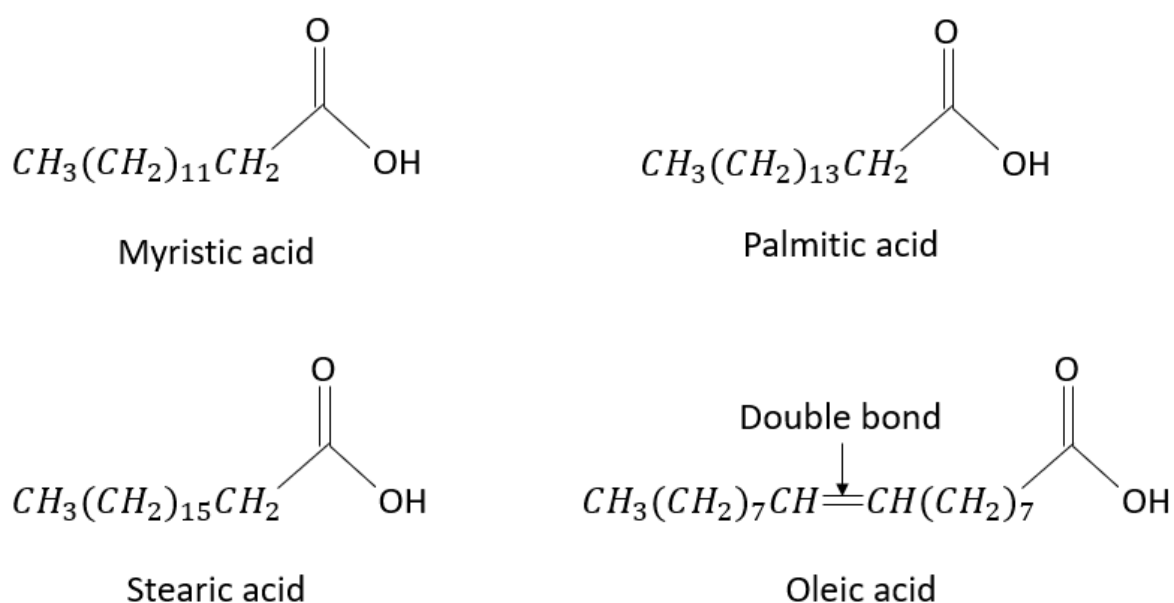
Figure 3.6 – *Chemical structures of myristic, palmitic, stearic, and oleic acids*

3.5.2 Protein

The proteins in milk are the molecules that are composed of amino acids. The amino acid is the chemical compound, which is composed of amino and the carboxyl group. Specifically, protein molecules in milk contain α amino acid, which has an amino and a carboxyl group bound to the same carbon atom as shown in **Figure 3.7**.
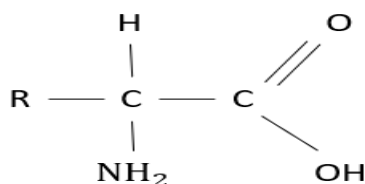
Figure 3.7 - Structure of α amino acid in protein molecule

Amino acids are linked to each other by the peptide bond between the amino and the carboxyl group to form the protein molecule. In fact, the peptide bond is formed by dehydration reaction. One of the amino acids loses hydroxyl group while the other amino acid loses hydrogen from the amino group during the reaction. Then, the nitrogen from amino group bonds to the hydroxyl group, and this peptide bond makes the linear shape of the protein molecule [51]. **Figure 3.8** shows the formation of the peptide bond between amino acids, and **Figure 3.9** presents the linear shape of the protein in accordance with the linkage of amino acids.
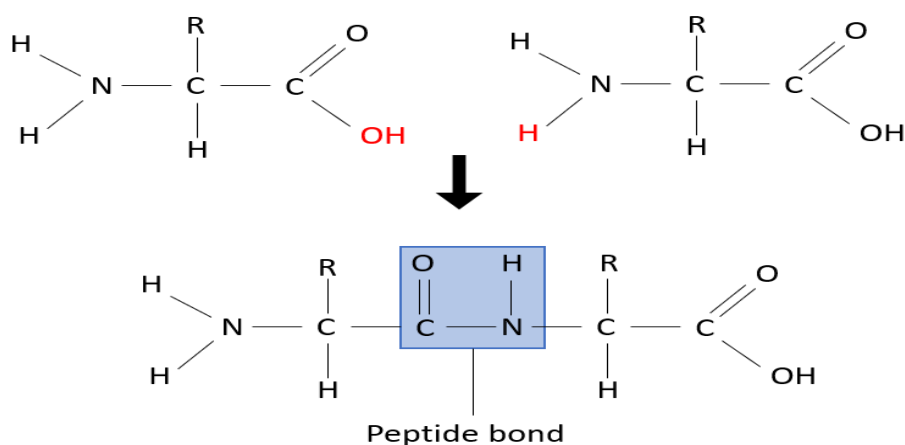
Figure 3.8 - Mechanism of peptide bond between amino acids
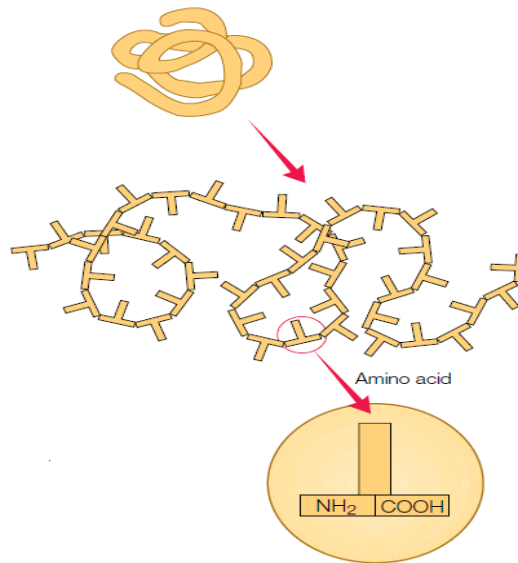
Figure 3.9 *- Formation of protein molecule with linkage of amino acids [48]*

In general, the protein molecules contain around 20 to 100 linked amino acids. In addition, as can be seen in **Figure 3.9**, part of these linear molecules forms globular shape, and they are rejected by the membrane surface during the separation process.

3.5.2.1 Casein Protein

There are mainly two different kinds of proteins in milk, and one of them is called casein. The following figure shows the casein submicelle structure in detail.
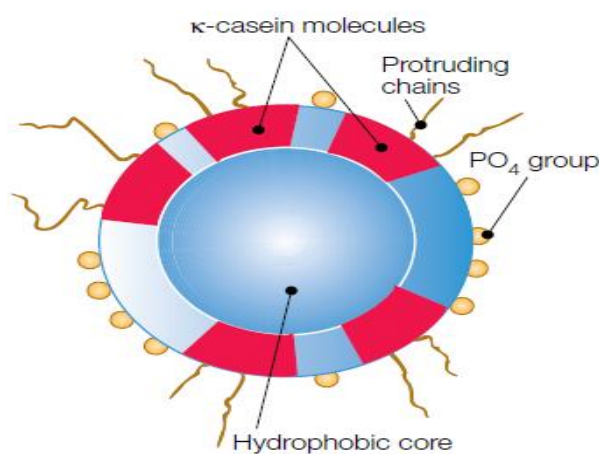
Figure 3.10 *- Structure of a casein submicelle [48]*

The hydroxyl group of amino acid in casein submicelle are esterified to phosphoric acid and binds with calcium to form bonds between and within molecules. As **Figure 3.11** shows, the calcium phosphate is acting as a bond to allow casein submicelles to hold each other to form casein micelle. Each casein submicelle is present as a particle of 10 to 15nm in size, and the bulk of casein micelle highly depends on the number of submicelles bonded. The size of casein micelle is generally up to 0.8 microns in milk.
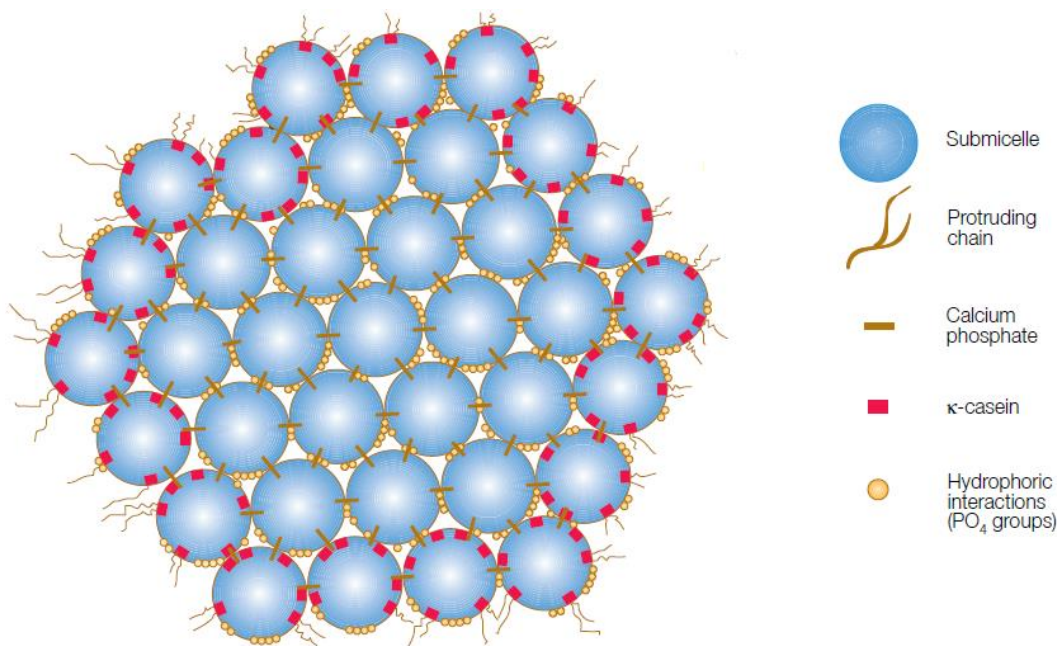
Figure 3.11 - Buildup and stabilization of casein micelle [48]

3.5.2.2 Serum Protein

The second type of protein in milk is serum, which is also called whey protein in general, and its size is ranging from 3 to 7nm [53]. In fact, serum protein has unique properties. Unlike casein micelles, serum proteins are not denatured by heat or precipitated at their isoelectric point. In addition, serum protein can be classified into two components α-lactalbumin and β-lactoglobulin. α-lactalbumin is the typical serum protein in milk from mammals in general, which is used in the synthesis of lactose. On the other hand, β-lactoglobulin is the unique component that can only be found in the milk from ungulates (large mammals) and is responsible for the flavor of milk from cow especially.

3.5.3 Lactose

Lactose is a unique type of sugar that can only be found from milk and belongs to the group of carbohydrates. In addition, lactose is one of the disaccharides which contains glucose and galactose. In fact, lactose has comparably low sweet flavor compared to other types of sugar, and the sweetness is about 30 times less than cane sugar. Lactose is highly hydrophilic; thus, it has a high solubility in water. Therefore, it generally appears as a molecular solution in milk rather than the solid particle. With this property, lactose passes through the membrane surface during the separation process in the cheese production and remains as a part of the permeate solution.

3.5.4 Vitamins

Vitamins are present as organic substance with relatively low concentration in milk. There are mainly four different types of vitamins in milk, which are A, B, C, and D. Vitamins A and D are highly soluble in the fat solvent while the others are soluble in water. Because of this solubility, vitamins appear as the solution rather than the solid particle in milk.

3.5.5 Minerals

There is a low amount of minerals in milk solution, and its total concentration is even less than 0.1%. The most representative minerals in milk are calcium, sodium, potassium, and magnesium. They exist as the molecular forms of phosphate, chlorides, and caseinate. However, due to strikingly low concentration, they do not significantly affect the membrane fouling during the membrane separation process for cheese production.

Lastly, **Table 5** shows the components of milk in overall and size of them in detail.

Table 5 - Components of skim milk [48, 52]

Component	size	Mass%*
Water	-	91.87
Fat	0.1-15um	0
Proteins in casein micelle	20-800nm	3.49
Serum proteins	3-7nm	
Carbohydrate (Lactose)	Soluble in water	4.65
Vitamins	Soluble in water and fat	-
Minerals	Negligible concentration	

*Mass percentage of each component in the skim milk from Sealtest Inc (Toronto, Canada)

In this study, the skim milk from Sealtest Inc. (Toronto, Canada), with 0% concentration of fat is used as the feed solution to examine the fouling problem during the membrane separation process. Also, lactose is presented as liquid phase due to its high solubility in water. In other words, the experiment focused on separating casein micelle from the skim milk solution using ceramic membrane pore size of 0.14 micron (47M014, Sterlitech Inc, Washington, USA).

3.6 Dilution of Feed Solution

One of the main issues for this experiment is the mass concentration of protein in skim milk. The size of the ceramic membrane used in this study is conspicuously small with 4.7cm in diameter. For this reason, the narrow surface area of the membrane tends to be completely fouled within the short period of the filtration time by highly concentrated protein particles in original skim milk. The following figure shows the cumulative mass of permeate solution during the membrane filtration process with the different mass percentage of protein particle in skim milk.
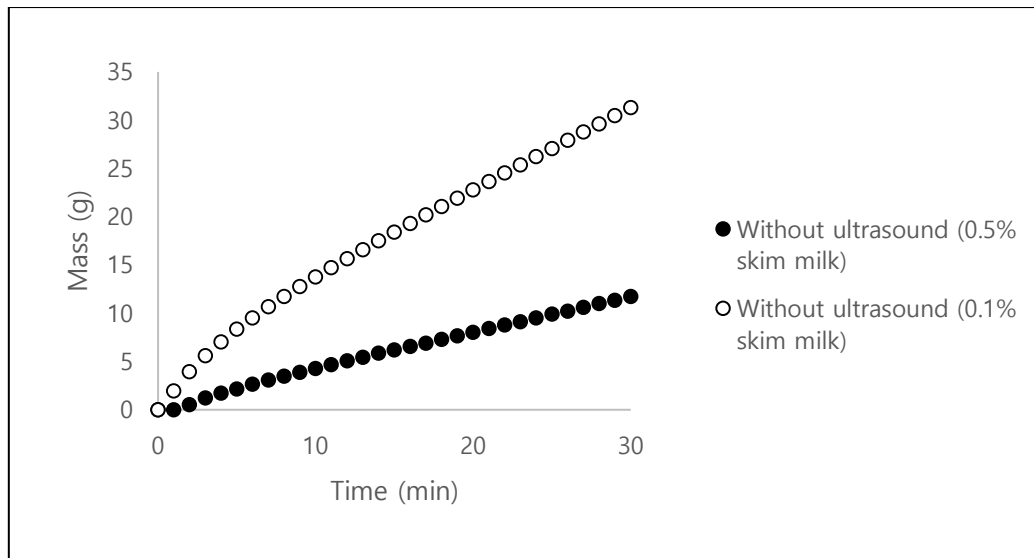
Figure 3.12 *- Cumulative mass of permeate in filtration of diluted skim milk at 0.5%*
and 0.1% mass concentration of protein

As **Figure 3.12** demonstrates, the membrane is completely fouled immediately right
after the filtration is started, even though the skim milk was diluted to 0.5% in the mass
concentration of protein. For this reason, it was difficult to observe the change in the
membrane fouling and its effect on the permeate flow rate under different operational
conditions. Therefore, the feed solution was diluted further to extend the fouling period.
For all experimental runs thereafter in the present study, skim milk was diluted to 0.1%
in the mass concentration of protein in order to observe the effect of ultrasound in
delaying and reducing the fouling during the membrane filtration process. Each 30g of
skim milk was diluted in 1 liter of distilled water to reach this concentration. As **Figure
3.13** shows, the fouling period is extended to approximately 10 minutes with 0.1% in
the mass concentration of protein particle in skim milk.
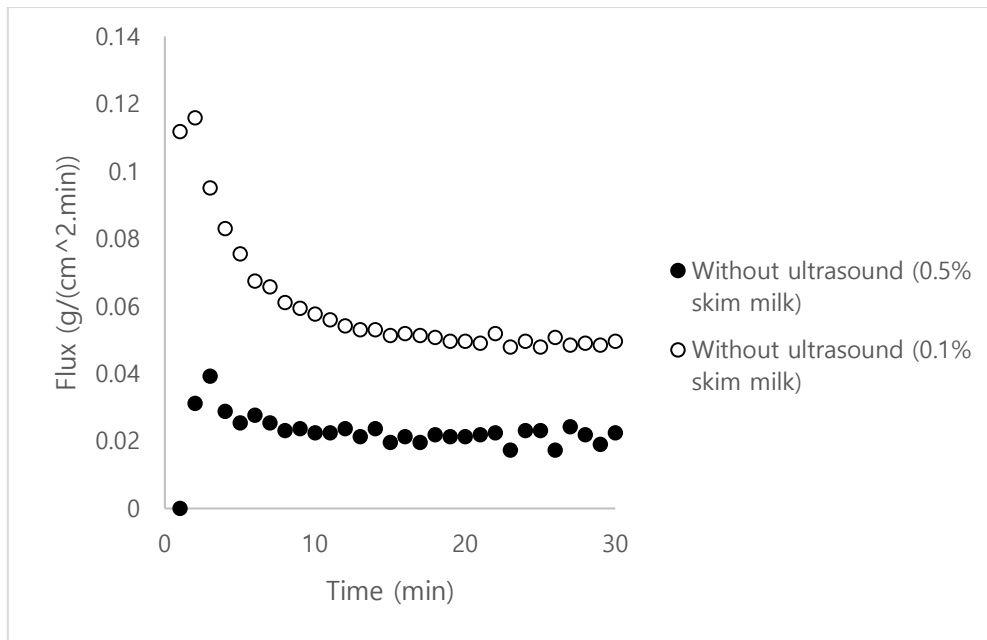
Figure 3.13*- Change in flux of permeate solution in filtration with 0.5% and 0.1% in protein mass concentration of diluted skim milk.*

3.7 Ceramic Membrane

The membrane can be separated into two different categories depending on the types of material, which are organic and inorganic. The organic membrane is generally made of the polymeric materials and used for various application in the industries. However, the polymeric materials have thermally and chemically unstable properties [53]. To overcome this problem, inorganic materials, ceramic has been developed to enhance the membrane properties. In general, the price of the ceramic membrane is higher than the polymeric one. However, the fouling is alleviated with the ceramic materials due to its high stabilities. Thus, there would be the lower power consumption of the pump to maintain the constant production rate of permeate during the filtration process; and hence, the price can be surmounted. Recently, oxide materials have been developed to manufacture ceramic membrane, and the most popular ones are the γ-aluminum oxide [54, 55, 56, 57], titanium dioxide [58, 59, 60, 61, 62], and zirconium dioxide [63, 64, 65]. Among them, γ-aluminum oxide has relatively low chemical stability compared to the other two oxide materials, and this property limits industrial application [65]. The following figure shows the difference between γ-aluminum oxide and titanium dioxide in corrosion behaviour.
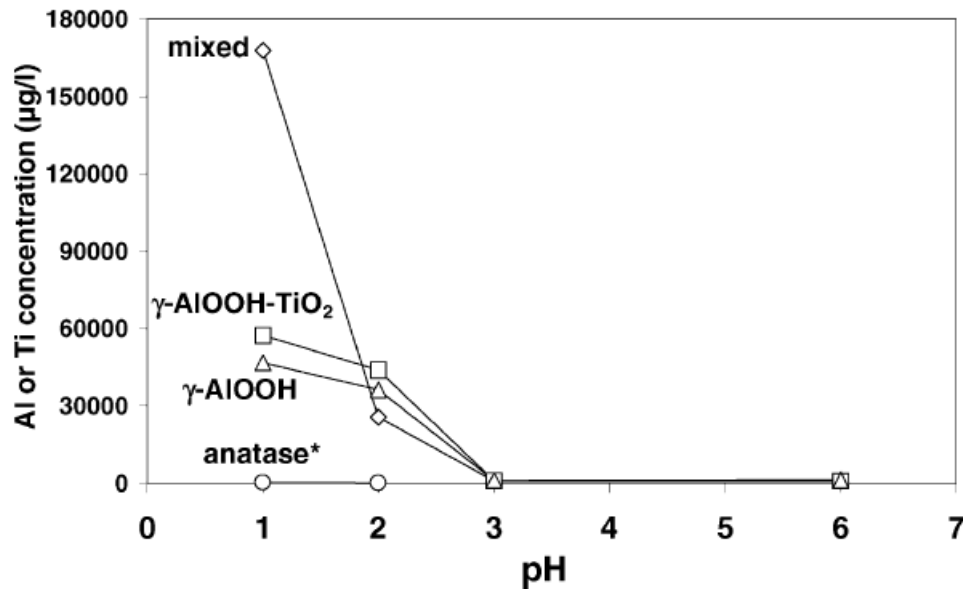
Figure 3.14 – *Corrosion behavior of $\gamma - AlOOH$, anatase, and mixed membranes [62]*

The anatase is the mineral form of titanium dioxide, $\gamma - AlOOH$ is the peptized sol of Al_2O_3, and the mixed material represents the mixture of Al_2O_3/ZrO_2. As **Figure 3.14** indicates, almost no corrosion occurs with anatase at any pH scale while other types of membranes show extreme corrosion when they are immersed to the acidic solution with the low pH scale.

Because of this chemical instability of γ-aluminum oxide, zirconium dioxide and titanium dioxide has been considered as alternative materials in the development of ceramic membrane. However, each of pure zirconium dioxide and titanium dioxide has another critical issue, which is low thermal stability [53]. The TiO_2/ZrO_2 composite was suggested as the final material of ceramic membrane instead of pure materials due to its high chemical and thermal stability. **Figure 3.15** proves the enhanced thermal stability of TiO_2/ZrO_2 composite.
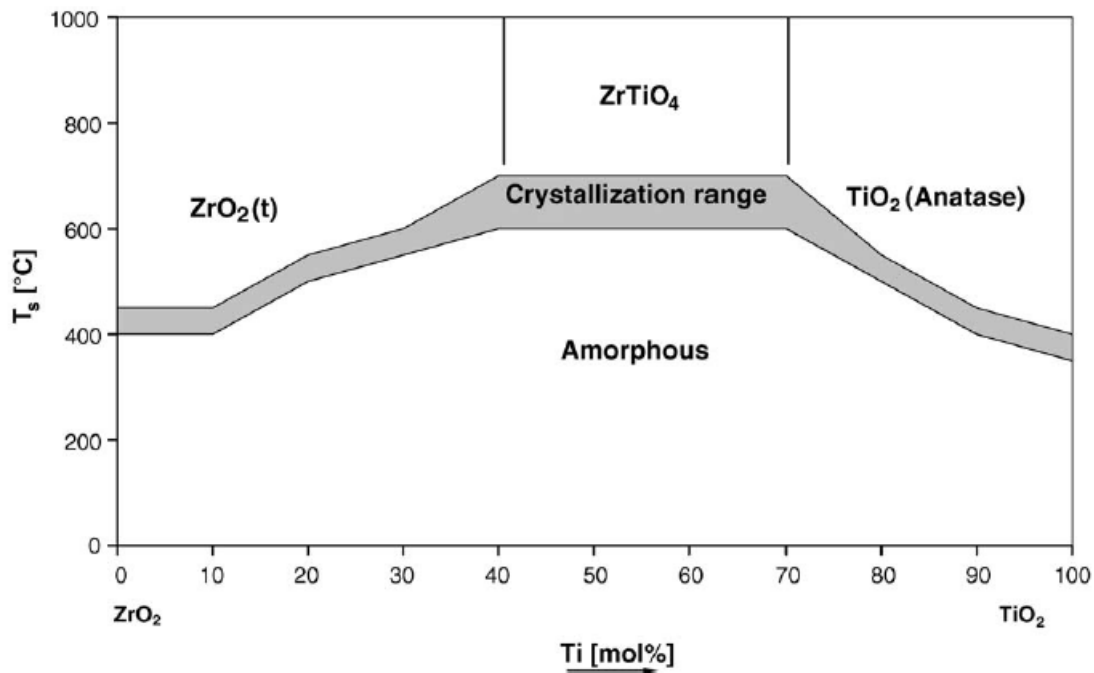
Figure 3.15 – *Crystallization behavior of TiO_2-ZrO_2 mixed-oxide membranes as a function of composition and temperature [66]*

Because of this high thermal and chemical stability, the ceramic membrane with TiO_2/ZrO_2 composite from Sterlitech Inc. (Washington, USA) was considered for this project. The membrane is the flat circular shape with 4.7cm in diameter and pore size of 0.14micron.

3.8 Turbidity Test

Not only the quantity, but also the quality of the permeate solution is the crucial factor that should be prudently examined depending on the purpose of the membrane separation. Turbidity is one of the sources that can be considered to test the quality of the permeate solution after the filtration process. In fact, turbidity is a measure of the degree to which the solution loses its transparency to the presence of suspended particles. In other words, relatively greater number of particles exist in the solution at higher turbidity, meaning low quality of the product. In this study, the turbidimeter (2020we, LaMotte, Maryland, United States) was used for the measurement. The samples were poured into a tube and inserted into the turbidity meter. The light, scattered by the particles, was detected and measured to give a turbidity reading.

47

3.9 Particle Size Distribution

The particle size distribution of the permeate solution is the crucial factor that needs to be seriously analyzed depending on the purpose of the membrane filtration. Specifically, the system requires separating even small particles, such as ion or virus to produce potable water since it critically connects to the health of the living organisms. For this reason, changes in the particle size distribution in the permeate solution with respect to conditions of ultrasound and the feed solution were analyzed and presented in this study.

The membrane fouling is generally occurred, because of the cake layer formed by the accumulated particles on the membrane surface. The structure of the layer was transformed depending on the ultrasonic condition applied during the filtration process. The different size range of particles was accumulated, generating the change in porosity of the cake layer. Thus, the different size range of particle was distributed in the permeate solution at each run. Therefore, the average particle size was considered as an additional source to examine the quality of permeate solution. The Zeta Sizer Nano Series (ZEN3690, Malven Instruments Ltd, Malvern, United Kingdom) was used for the measurement.

3.10 Scanning Electron Microscope

The visual observation of the membrane surface before and after the filtration was investigated using the image from Scanning Electron Microscope.

Scanning Electron Microscope (SEM) is a type of electron microscope, designed to observe the surface of solid objects. It is a magnification tool utilizing focused beam of electrons to obtain the images. The solid sample emits electrons, and they interact with the electron beam. Brightness of the image is determined depending on the chemical compositions in the sample. It displays brighter area as heavier elements with higher atomic number is presented. The accumulate particles and membrane surface was distinguished by this luminance. A Scanning Electron Microscope (JSM-6380 LV, JOEL Ltd, Tokyo, Japan) was used in this study.

Chapter 4: Results and Discussion

4.1 Reproductivity of Experimental Data

The experiment with the ultrasonic conditions at the centre point of the Box-Behnken design, which are 28kHz in frequency, 2.88 W/cm^2 in power intensity, and 1.5 minutes in the time interval of intermittent ultrasound, was repeated 3 times to examine the reproducibility of the experimental data. The standard deviation of the amount of permeate collected was calculated. The following table shows the final collected amount of the permeate solution for each run.

Table 6 - *Masses of collected permeate solution with intermittent ultrasonic condition of 28kHz in frequency, 2.88 W/cm^2 in power intensity, and 1.5minutes in time interval*

Run #	Mass of permeate solution (g)
1	46.61
1	45.67
2	44.33

The standard deviation from the averaged amount of permeate (45.54g after 30minutes of filtration) was 0.94, indicating an experimental error of about 2.06%. It demonstrates the high accuracy of the experimental data (**Appendix D**).

4.2 Statistical Analysis of Box Behnken Design

The statistical analysis was performed based on the Box-Behnken design in **Table 4** using the program, Minitab 18 in this study to obtain the optimal ultrasonic condition. The regression model equation includes terms up to 2-way interaction among the frequency, power intensity, and time interval of intermittent ultrasound. The significant level was set as 0.05 to surmount the experimental error of 2.06%. **Table 7** shows the result in the analysis of variance for each term of the regression model.

Table 7 *- Analysis of variance for Box Behnken design with respect to ultrasonic frequency, ultrasonic power intensity, and time interval of intermittent ultrasound*

Source	DF	Adj SS	Adj MS	F-Value	P-Value
Model	9	646.990	71.888	22.15	0.002
Linear	3	450.392	150.131	46.26	0.000
Frequency	1	164.603	164.603	50.72	0.001
Power intensity	1	220.471	220.471	67.93	0.000
Intermittent ultrasound	1	53.553	53.553	16.50	0.010
Square	3	135.200	45.067	13.89	0.007
Frequency*Frequency	1	112.521	112.521	34.67	0.002
Power intensity*Power intensity	1	19.479	19.479	6.00	0.058
Intermittent ultrasound*Intermittent ultrasound	1	3.998	3.998	1.23	0.318
2-Way Interaction	3	32.249	10.750	3.31	0.115
Frequency*Power intensity	1	27.540	27.540	8.49	0.033
Frequency*Intermittent ultrasound	1	0.502	0.502	0.15	0.710
Power intensity*Intermittent ultrasound	1	4.111	4.111	1.27	0.312
Error	5	16.227	3.245		
Lack-of-Fit	3	13.601	4.534	3.45	0.233
Pure Error	2	2.626	1.313		
Total	14	663.217			

According to **Table 7**, the p-values for power intensity*power intensity, Intermittent ultrasound*intermittent ultrasound, and all the 2-way interaction terms, except frequency*power intensity, are higher than 0.05, which exceeds the significance level. In other words, those terms accept the null hypothesis according to F-test, which indicates that those terms are not correlated to the permeate amount (dependent variable). Therefore, they are eliminated to increase the accuracy of the model. Analysis of variance is presented in **Table 8**.

Table 8 - Analysis of variance after removing insignificant terms of regression model

Source	DF	Adj SS	Adj MS	F-Value	P-Value
Model	5	617.340	123.468	24.22	0.000
Linear	3	440.832	146.944	28.83	0.000
Frequency	1	165.022	165.022	32.37	0.000
Power intensity	1	201.102	201.102	39.45	0.000
Intermittent ultrasound	1	63.225	63.225	12.40	0.006
Square	1	110.260	110.260	21.63	0.001
Frequency*Frequency	1	110.260	110.260	21.63	0.001
2-Way Interaction	1	28.332	28.332	5.56	0.043
Frequency*Power intensity	1	28.332	28.332	5.56	0.043
Error	9	45.877	5.097		
Lack-of-Fit	7	43.251	6.179	4.71	0.186
Pure Error	2	2.626	1.313		
Total	14	663.217			

As **Table 8** demonstrates, p-values of all the terms do not exceed the selected significance level of 0.05, meaning those terms reject null hypothesis and the accuracy of the model is acceptable. Based on this result, the regression model for the Box-Behnken design of the experiment could be derived into **Equation 16**.

$$\text{Mass of permeate solution} = -4.1 + 3.39 * A + 5.85 * B - 5.62 * C - 0.0571 * A * A$$
$$-0.1187 * A * B \qquad R^2 = 93.08\% \qquad (16)$$

Where A is frequency (kHz), B is power intensity (W/cm^2), C is the time interval of intermittent ultrasound (min), and R^2 is a statistical coefficient of determination. This model is valid only for the filtration process with TiO_2/ZrO_2 ceramic membrane, applied pressure of 30psi, inlet flow rate of 20 US gallons per hour, and skim milk containing 0.1% by weight of protein. R^2 is a statistical measure of how close the data are to the fitted regression model. The coefficient of determination ranges from 0 to 100%, indicating that the model explains most of the variability of response data around its mean as it closes to 100%. The R^2 value of 93.08% for the data set in this

study indicates that the regression model is moderately accurate to represent the variation of the dependent variable with the independent variables in the model equation.

Furthermore, the regression model assumes the normal distribution of raw data or residuals with the linear function between independent and dependent variables. The validity of this assumption can be examined based on the normal probability plot of residual, as shown in **Figure 4.1**.
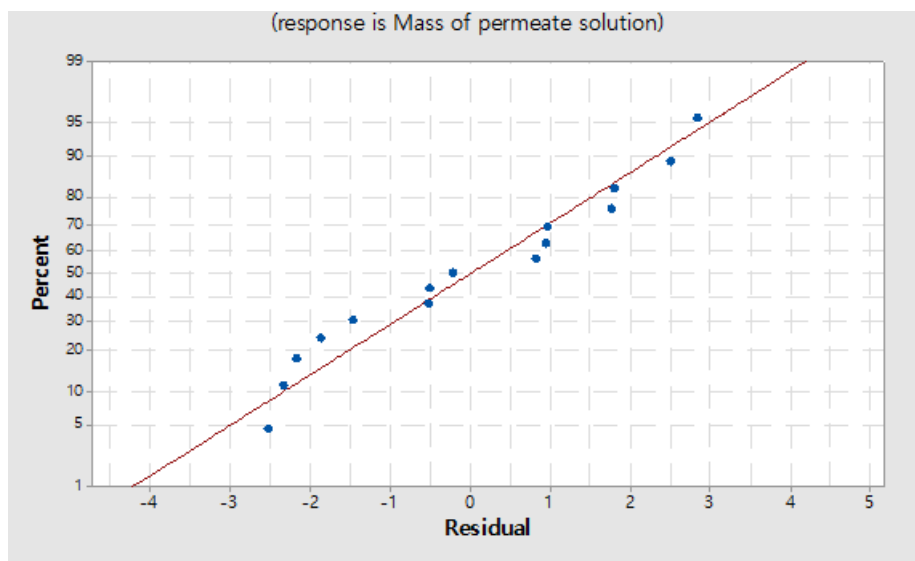
Figure 4.1 - *Normal probability plot of regression model*

The linear line on the plot represents the perfectly normal distribution of residual while the dots indicate the actual distribution obtained from the regression model. As can be seen in **Figure 4.1**, the actual residual points scatter around and close to the normal distribution line, which verifies the assumption that the residuals are normally distributed, and it proves the validity of the regression model. Another factor that can be used to check the validity of the regression model is the residual plot. **Figure 4.2** presents a residual plot of the mass of permeate solution.
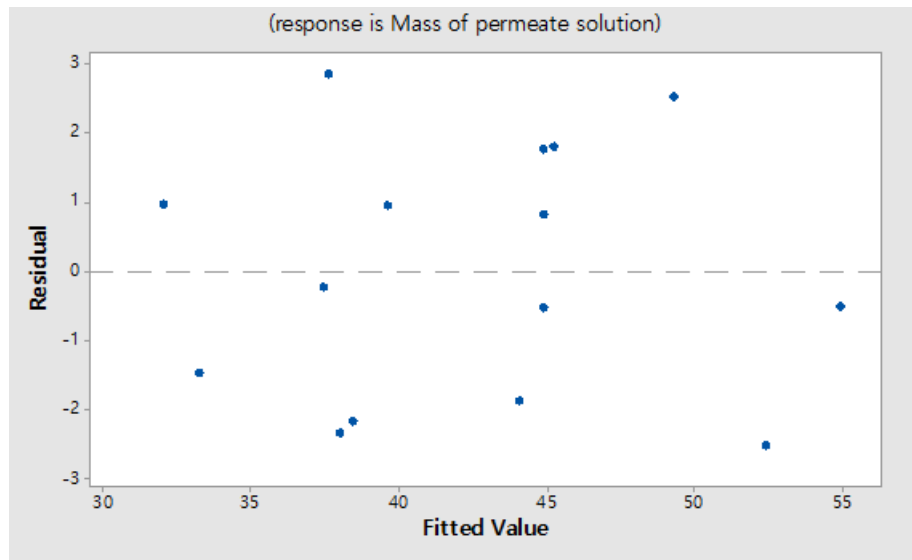
Figure 4.2 - Residual plot of the mass of permeate solution

In fact, if there are any outliers in data, the residual plot shows striking patterns which prove the inaccuracy of the predicted model. According to **Figure 4.2**, residuals are scattered randomly around the horizontal reference line at 0 without any specific pattern. This indicates that the model is good to represent experimental data.

The regression model can be used to predict the mass of permeate solution at each condition of three different parameters: frequency, power intensity, and time interval of the intermittent ultrasound. The contour plots of the permeate amount, obtained from the model prediction, are presented in **Figure 4.3**.
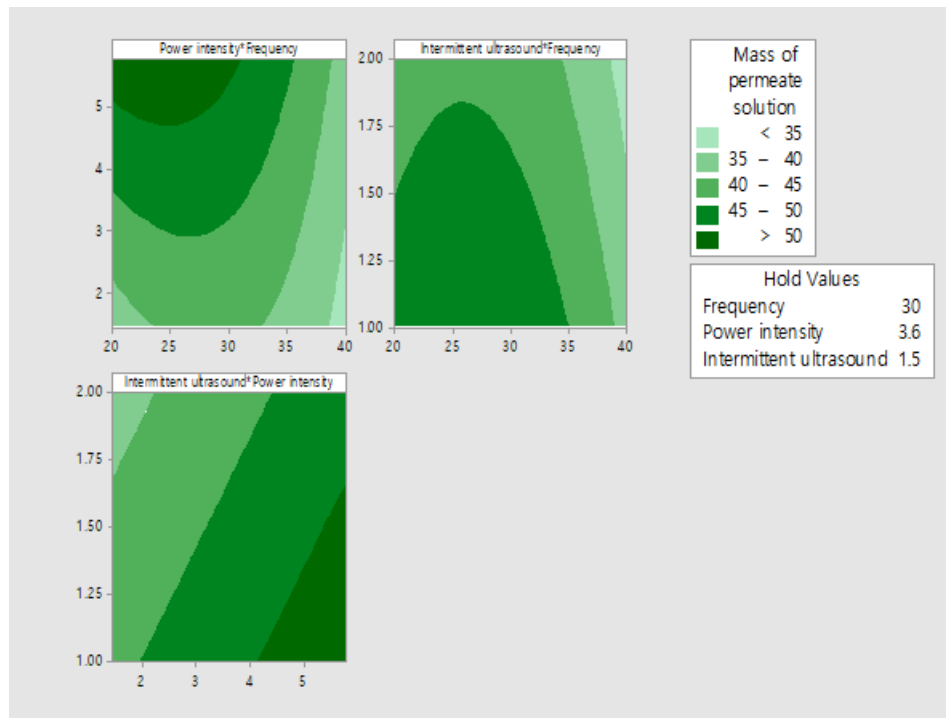
Figure 4.3 - *Contour plots of mass of permeate solution predicted by the regression model*

According to the legend in **Figure 4.3**, brightness of green colour indicates the amount of permeate solution collected at each ultrasonic condition. The darker colour represents a higher amount of permeate solution. The first graph (top left) in **Figure 4.3** shows relatively more permeate obtained at higher power intensity and the centre point of frequency (28 kHz). In addition, from the second (top right) and third graphs (bottom), the intermittent ultrasound with the shorter time interval tends to produce more permeate. These trends can also be clearly observed in the main effects plot in **Figure 4.4**.
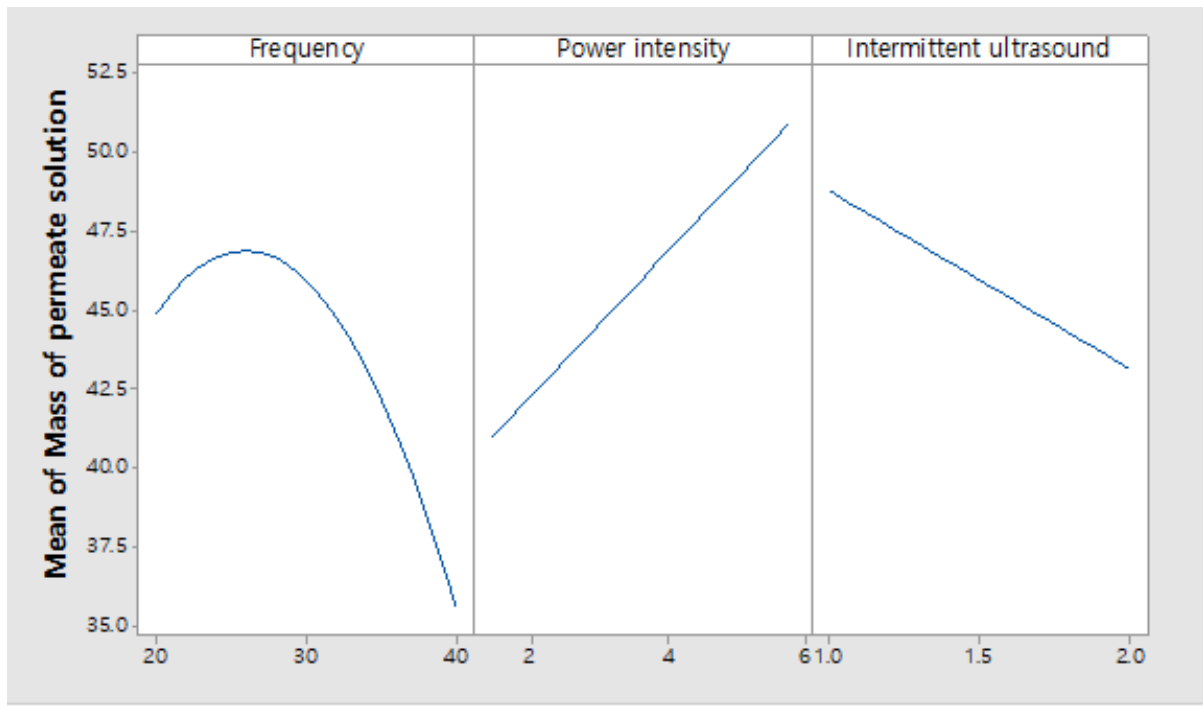
Figure 4.4 - *Main effects plot in mass of permeate solution*

The plot of frequency shows the parabolic shape and presents the optimal point at the centre (28 kHz). In contrast, there is a linear graph with the positive slope for power intensity but negative slope with the time interval of ultrasound. Overall, the statistical analysis of the data generated with the Box-Behnken experimental design shows that the optimal condition, within the operating range used in the present study, that can provide the greatest amount of permeate solution is 28kHz in frequency, 5.76 $\mathrm{W/cm^2}$ in power intensity and 1 min in the time interval of intermittent ultrasound.

4.3 Effects of Operational Variables on Collected Mass of Permeate Solution

4.3.1 Ultrasonic Power Intensity

In practice, the power intensity of ultrasound highly affects the production of cavitation bubbles which can adsorb accumulated particles on the membrane surface to provide larger porous spaces within the cake layer. **Figure 4.5** shows the cumulative mass and change in flux of the permeate solution during the membrane filtration process with application of continuous ultrasound at different power intensities while the frequency is maintained as 28kHz for all runs. Every run was operated with a constant

flow rate of 20 US gallons per hour, 0.1% in the mass concentration of protein and 30psi in applied pressure.
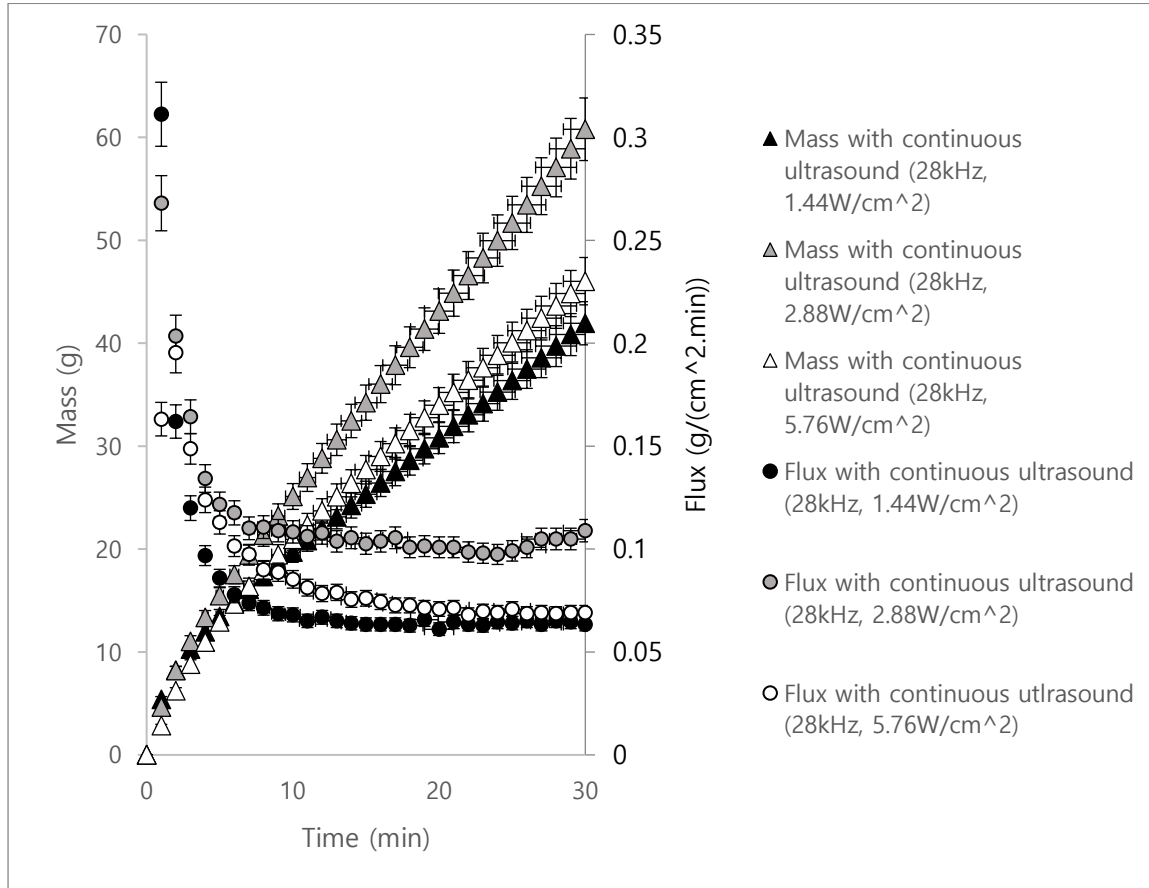
Figure 4.5 - *Comparison of cumulative mass and flux of permeate solution at different ultrasonic power intensities, ultrasonic frequency of 28kHz*

As the figure shows, a relatively greater amount of permeate was obtained by increasing the ultrasonic power intensity from 1.44 W/cm² to 2.88 W/cm². In fact, the production rate of the cavitation bubble is proportional to the magnitude of ultrasonic power intensity. In other words, a greater number of cavitation bubbles tends to be produced at 2.88 W/cm²; and hence, there would be higher total surface area of the bubbles that can participate in adsorption of the particles that are accumulated on the membrane surface, resulting in a thinner and/or more porous cake layer on the membrane surface. Consequently, the permeate solution would have more chance to pass through the membrane. In addition, a relatively higher flux of permeate solution could be maintained with 2.88 W/cm² over the entire period of the filtration process,

which means that there would be a higher production rate of the permeate solution. The same trend was also observed with the application of intermittent ultrasound, as shown in **Figure 4.3** and **Figure 4.4** in the previous analysis of the data from the Box-Behnken design.

However, the amount of the permeate solution decreases with further increase in the ultrasonic power intensity from $2.88\ \mathrm{W/cm^2}$ to $5.76\ \mathrm{W/cm^2}$. It would be relevant to note that this result does not follow the trend of the intermittent ultrasound. In fact, the effect of ultrasonic power intensity is highly related to the design of membrane apparatus. The membrane apparatus used in this experiment is a closed system, as shown in **Figure 4.6**.
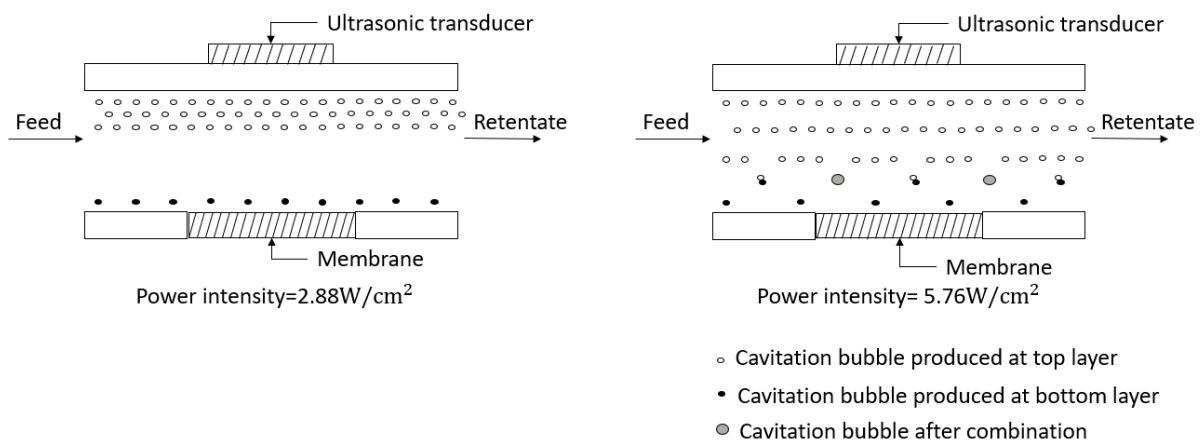
Figure 4.6 - *Behaviour of cavitation bubbles in a closed membrane apparatus*

The cavitation bubbles could be produced at both top and bottom layers while the ultrasonic transducers are activated continuously in a closed system. Furthermore, as the figure above shows, much greater number of cavitation bubbles tends to be produced at the upper boundary layer while relatively small number would be produced at the lower boundary layer. This phenomenon is related to the location of the ultrasonic transducer. As shown in **Figure 4.6**, the ultrasonic transducer was installed on top of the membrane apparatus which is closer to the upper boundary layer than the lower boundary layer. Therefore, the upper boundary layer would be vibrated at a higher degree by the transducer; and hence, this layer would produce more cavitation bubbles. In addition, as the ultrasonic power intensity was increased

to $5.76\,\mathrm{W/cm^2}$, comparatively greater number of cavitation bubbles would be produced from the upper boundary layer, and they would move down to the bottom surface. As a result, the bubbles would have more chance to contact with each other and coalesce into larger bubbles. The coalesced bubble's size increase may reach an unstable size larger than $50\,\mathrm{\mu m}$ [29], resulting in bubble collapse. Due to this phenomenon, the total number of bubbles were evidently reduced resulting much lower opportunity to adsorb the accumulated particles on the membrane surface. Thus, less amount of permeate solution can pass through the membrane surface at the ultrasonic power intensity of $5.76\,\mathrm{W/cm^2}$, as compared to the one at $2.88\,\mathrm{W/cm^2}$.

4.3.2 Effect of Ultrasonic Frequency

Ultrasonic frequency is another condition of the ultrasound that should be prudently considered to overcome the fouling problem during the membrane filtration process. As it was discussed in **Section 2.6.5.2**, the size of cavitation bubble is highly related to the ultrasonic frequency. The size of bubbles could not be estimated directly using **Equation 7** due to the unknown polytropic index value. Instead, the relationship between the bubble size and ultrasonic frequency could be expected. In this study, the effect of the magnitude of ultrasonic frequency on the amount of permeate was investigated using continuous ultrasound. **Figure 4.7** shows the results obtained with various ultrasonic frequencies.
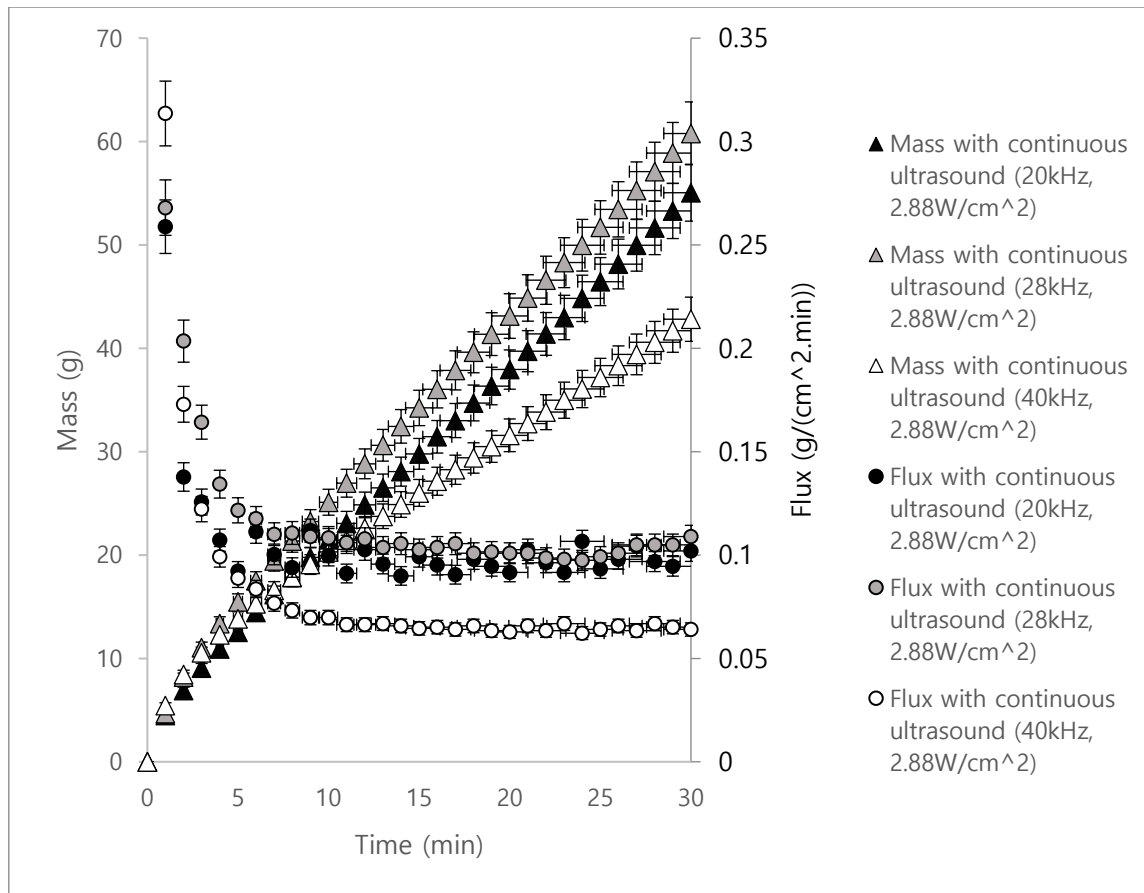
Figure 4.7 *- Comparison of cumulative mass and flux of permeate solution at different ultrasonic frequency, ultrasonic power intensity of* $2.88\,W\,/cm^2$

Since the magnitude of the ultrasonic frequency and size of the cavitation bubble are anti-proportional to each other, size of each cavitation bubble is relatively bigger at lower ultrasonic frequency as **Equation (7) in section 2.6.5.3** demonstrates. The bubbles with bigger size have larger surface area which would provide higher capacity to adsorb the accumulated particles. The higher production rate of the cavitation bubble at lower frequency even contributed to remove greater number of particles, and hence, reduce the cake layer thickness and resistance to the permeate flow. Also, there would be larger porous spaces in the cake layer that allows more amount of permeate solution to pass through the membrane. In other words, ultrasound at lower ultrasonic frequency can contribute more to the reduction of membrane fouling. **Figure 4.8** depicts the influence of cavitation bubble size on the cake layer.
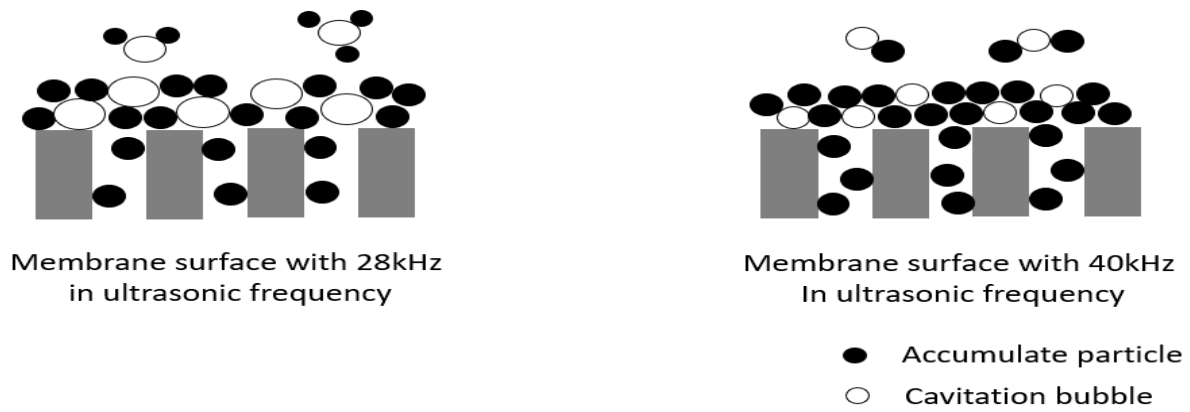
Figure 4.8 - *Effect of size of cavitation bubble on the membrane surface*

In fact, when the ultrasonic frequency was reduced from 40kHz to 28kHz, a higher amount of permeate was obtained. On the other hand, cumulative mass and flux of permeate solution decreased when the frequency was further reduced from 28kHz to 20kHz. This reverse trend might be due to the stability of the cavitation bubble generated at 20kHz. Cavitation bubbles, which were produced at the frequencies of 28kHz and 40kHz, were able to maintain their stable sizes with the diameter less than 50μm [29]. However, the bubbles generated at 20kHz might reach the unstable size with the diameter over 50 μm, and the surface tension cannot withstand the pressure difference between the inside (gas phase) and outside (liquid phase) of a bubble. Thus, some of them could collapse. This mechanism is described in **Figure 4.9** below.
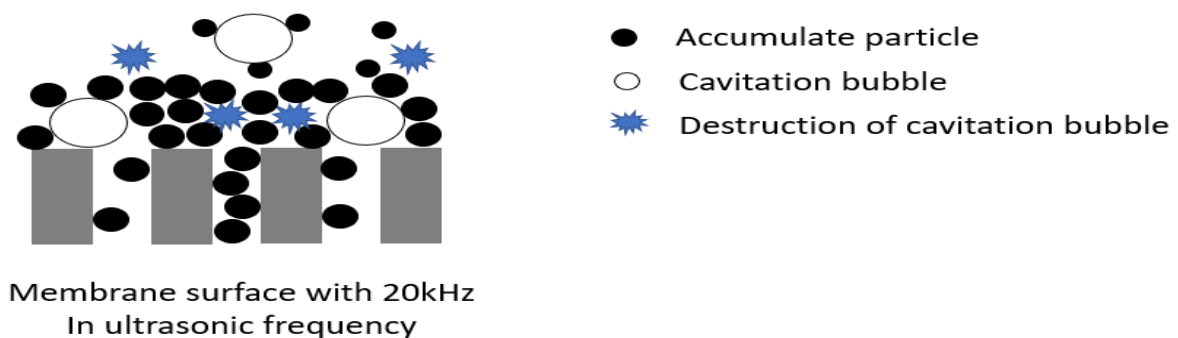
*Figure 4.9* – *Destruction of cavitation bubble at 20kHz of ultrasonic frequency*

Due to the bubble collapse, virtually smaller number of cavitation bubble would be remained, inducing a limitation on removing the accumulated particles even though the bubbles are larger. The more frequent micro-jets are expected at 20kHz with this

bubble collapse. Also, the fluid around the surface of the cavitation bubble would fluctuate more to intensify the microstreaming on impact. However, their effects were not significant enough to substitute the attenuated adsorption energy. There was relatively the smaller difference in cumulative mass and flux of permeate solution compared to the case between 20kHz and 28kHz due to the interaction between the bubble size and collapse. With respect to these analyses, 28kHz could be chosen as the optimal ultrasonic frequency to produce the highest cumulative mass and flux of permeate solution.

4.3.3 Effect of Intermittent Ultrasound

According to the analysis of the data from the Box-Behnken design, there was more improvement of membrane fouling with shorter time interval of intermittent ultrasound. In this section, the cause of this observation will be discussed in detail. In addition, the difference in the cumulative mass and flux of permeate solution obtained with continuous and intermittent ultrasound is analyzed.

In fact, the effect of intermittent ultrasound was independent of ultrasonic frequency. Thus, the optimal point, 28kHz, was considered in this session. On the other hand, the result was crucially affected by the magnitude of power intensity. The experiment was started with low power intensity, 1.44 W/cm^2. **Figure 4.10** shows the cumulative mass and flux of permeate solution with respect to different time intervals of intermittent ultrasound while the ultrasonic power intensity and frequency were maintained at 1.44 W/cm^2 and 28kHz, respectively.
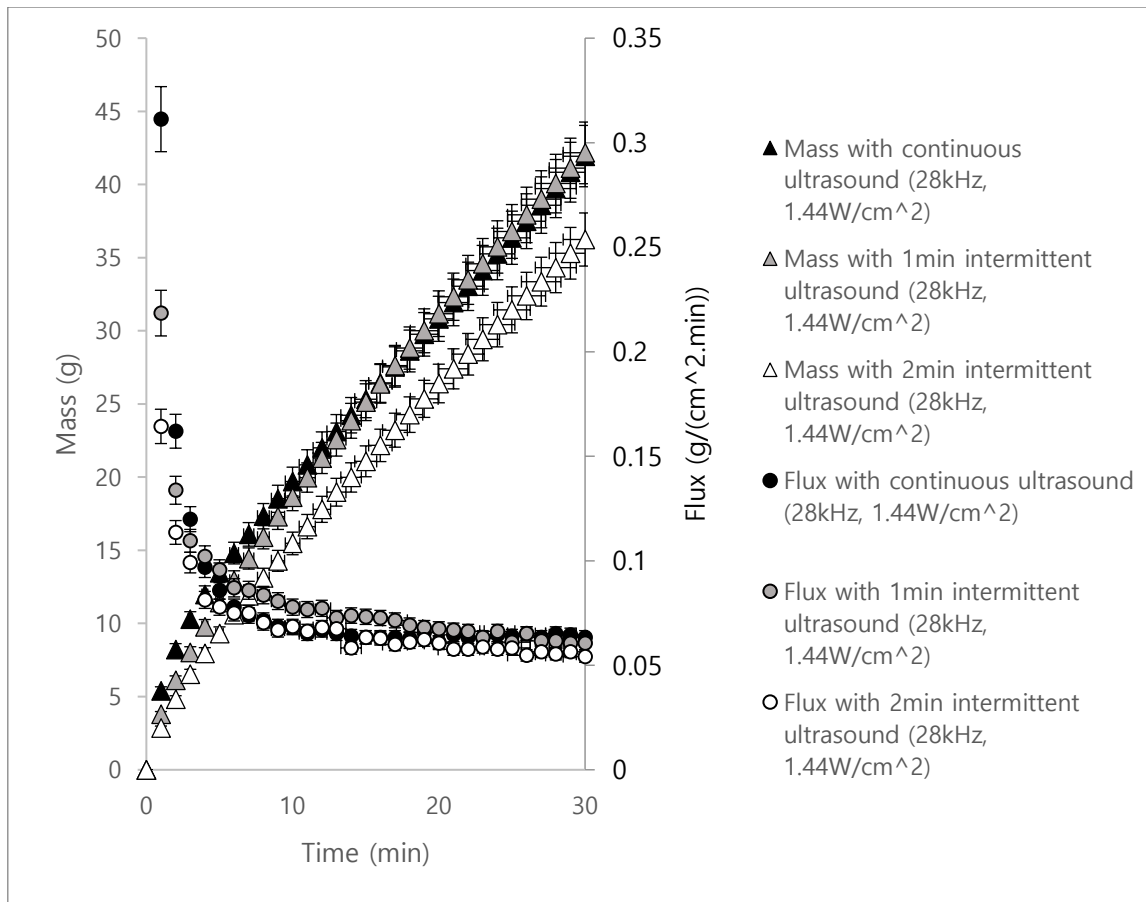
Figure 4.10 *- Comparison of cumulative mass and flux of permeate solution between continuous and intermittent ultrasound at ultrasonic frequency of 28kHz and ultrasonic power intensity of 1.44 W/cm²*

Based on **Figure 4.10**, there is no significant difference in the cumulative mass of permeate solution between the intermittent ultrasound with 1minute time interval and continuous ultrasound. At low ultrasonic power intensity, fundamentally deficient number of cavitation bubbles would be produced, even with the continuous ultrasound. Therefore, the removal of accumulated particles on the membrane surface would be negligible. This might be due to the fact that no significant difference in the number of cavitation bubbles produced between the intermittent ultrasound with 1minute time interval and the continuous ultrasound case. In other words, there is relatively low fouling control efficiency with continuous ultrasound at low ultrasonic power intensity. **Figure 4.11** illustrates this proposed phenomenon specifically.
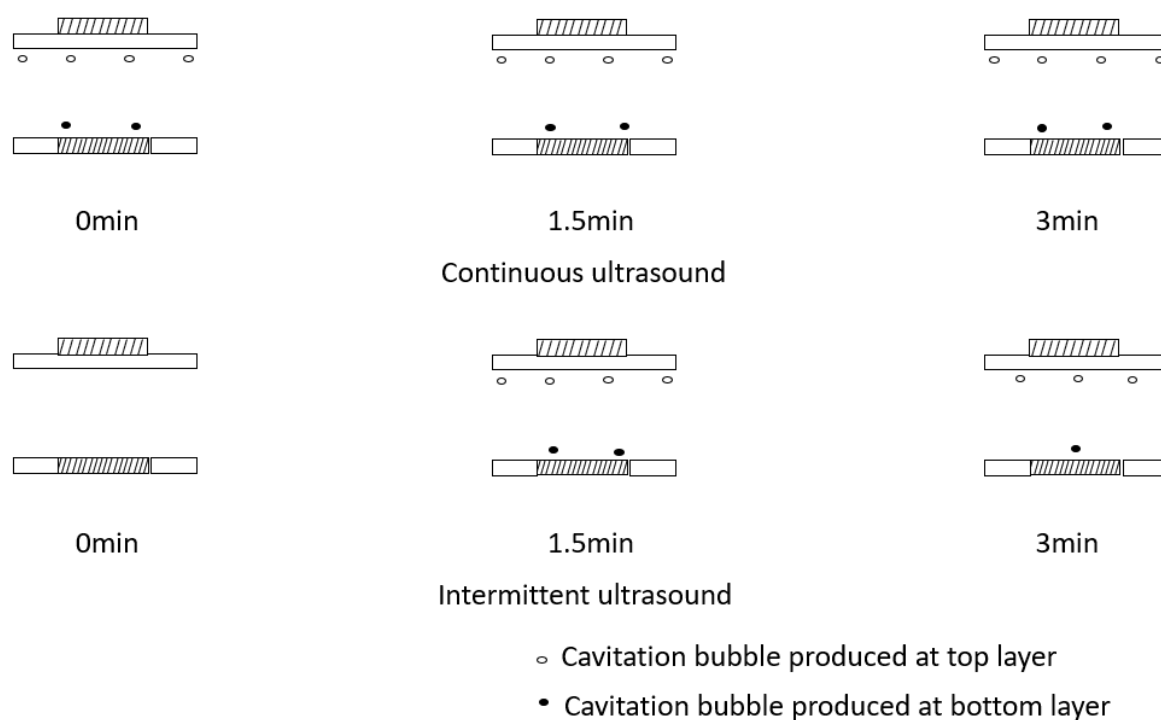
Figure 4.11 - Distribution of cavitation bubbles at the ultrasonic power intensity of 1.44 W/cm² with continuous and intermittent ultrasound

However, the intermittent ultrasound with 2 minutes time interval produced evidently lower cumulative mass and flux of the permeate solution. As the time interval of the intermittent ultrasound increased, the particles in the feed solution tended to have more opportunity to be accumulated while the ultrasonic transducer was deactivated for longer period. A thicker cake layer would thus be built on the membrane surface, resulting in a lower production rate of the permeate solution.

On the other hand, provides significant difference in cumulative mass and flux of permeate solution between intermittent and continuous ultrasound was observed at an ultrasonic power density of 2.88 W/cm², as presented in **Figure 4.12**.

Figure 4.12 *- Comparison of cumulative mass and flux of permeate solution between continuous and intermittent ultrasound at ultrasonic frequency of 28kHz and ultrasonic power intensity of 2.88 W/cm²*
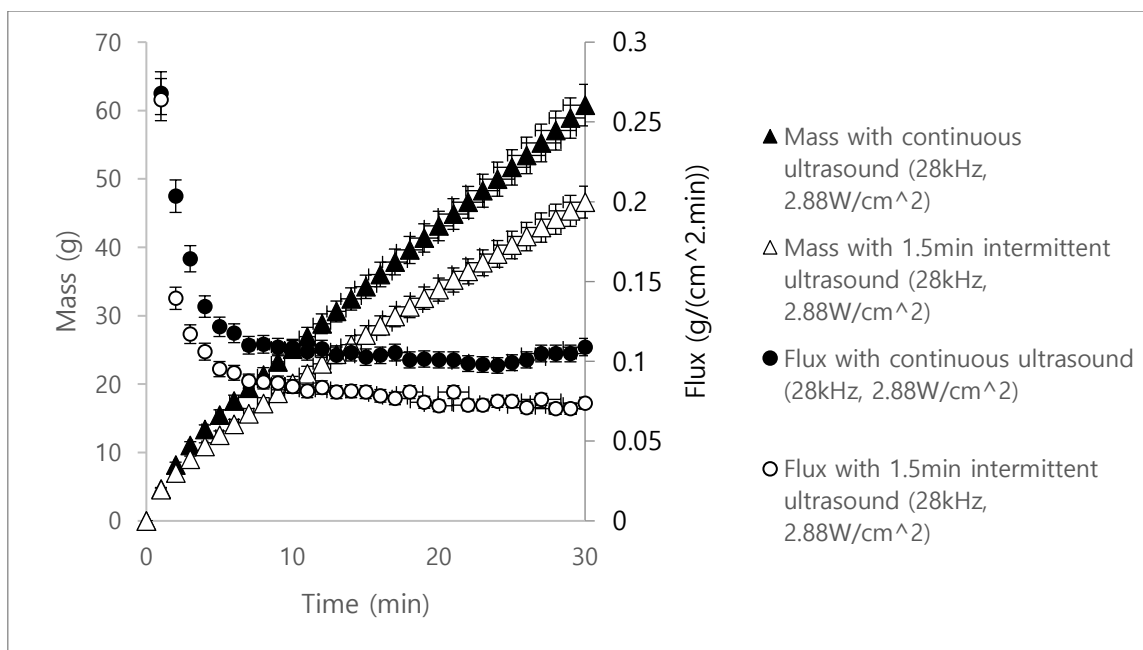
As can be seen in **Figure 4.12**, there was a distinct difference in the production rate of permeate solution between the intermittent and continuous ultrasound at an ultrasonic power intensity of 2.88 W/cm^2. In contrast with the case at the ultrasonic power intensity of 1.44 W/cm^2, relatively much greater number of cavitation bubble were probably produced by continuous ultrasound at the higher power intensity of 2.88 W/cm^2. As the power intensity was doubled, there would be a striking difference in the number of cavitation bubbles between intermittent and continuous ultrasound conditions. As illustrated in **Figure 4.13**, relatively much greater number of cavitation bubbles was produced with continuous ultrasound, as compared with intermittent ultrasound; and that would allow more permeate solution to pass through the membrane by removing a greater number of the accumulated particles on the membrane surface.

Figure 4.13 - *Distribution of cavitation bubbles at the ultrasonic power intensity of $2.88\,W/cm^2$ with continuous and intermittent ultrasound*
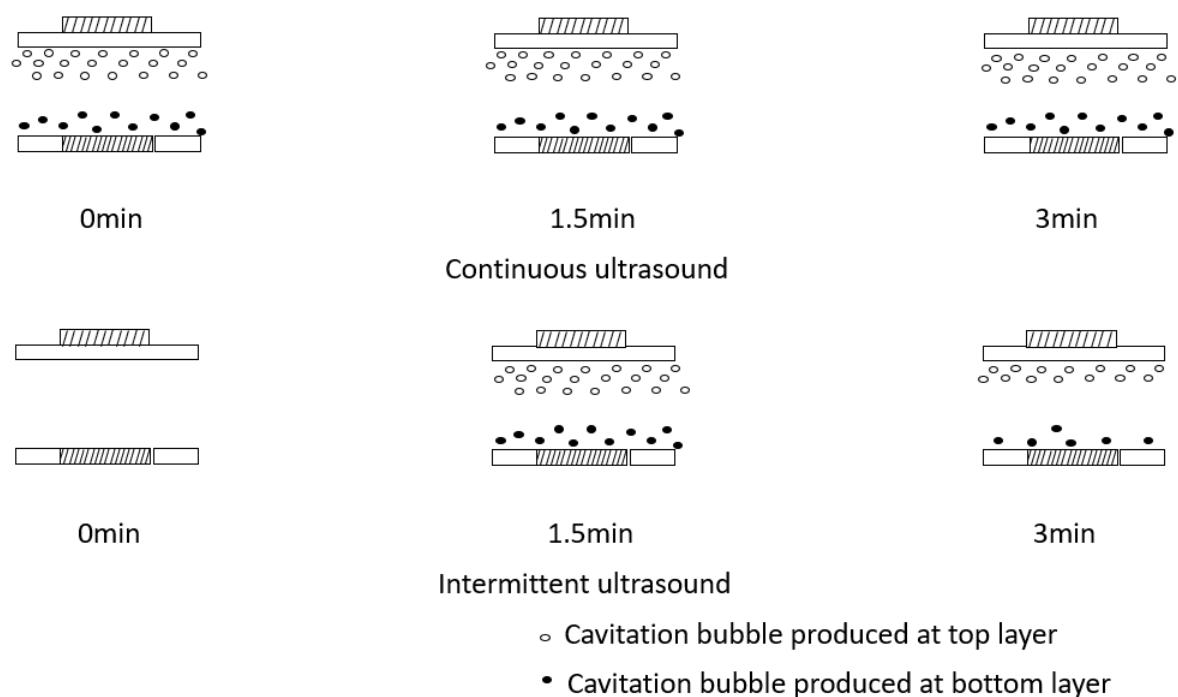
However, in contrast, unlike $1.44\ \text{W/cm}^2$ and $2.88\ \text{W/cm}^2$, a reverse trend was observed at the ultrasonic power intensity of $5.76\ \text{W/cm}^2$. a lower production rate of permeate solution was observed with the continuous ultrasound, compared to intermittent ultrasound. **Figure 4.14** shows the result of the cumulative mass and flux of permeate solution with respect to different ultrasonic conditions at 28kHz and $5.76\ \text{W/cm}^2$.
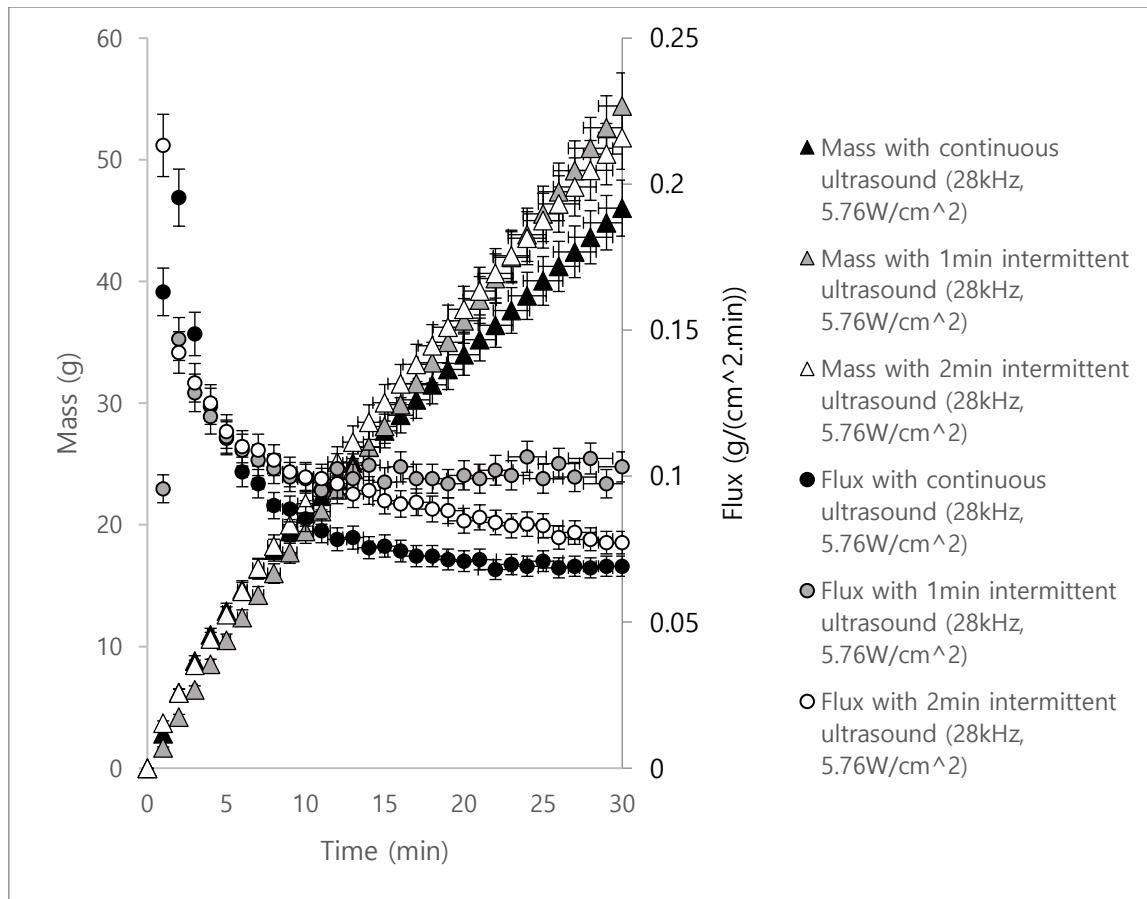
Figure 4.14 *- Comparison of cumulative mass and change in flux of permeate solution between continuous and intermittent ultrasound at ultrasonic frequency of 28kHz and ultrasonic power intensity of 5.76 W/cm²*

This result is highly associated with the design of the membrane module. As it was mentioned in **Section 4.3.1**, the module was a closed system in this study; and the cavitation bubbles would be produced at both upper and lower boundary layers, which induced bubble destruction in the membrane feed compartment with application of the continuous ultrasound. In contrast, the destruction rate of the cavitation bubbles might be effectively reduced with the application of the intermittent ultrasound, as depicted in **Figure 4.15**.

Figure 4.15 - *Distribution of cavitation bubbles at the ultrasonic power intensity of 5.76 W/cm^2 with continuous and intermittent ultrasound*
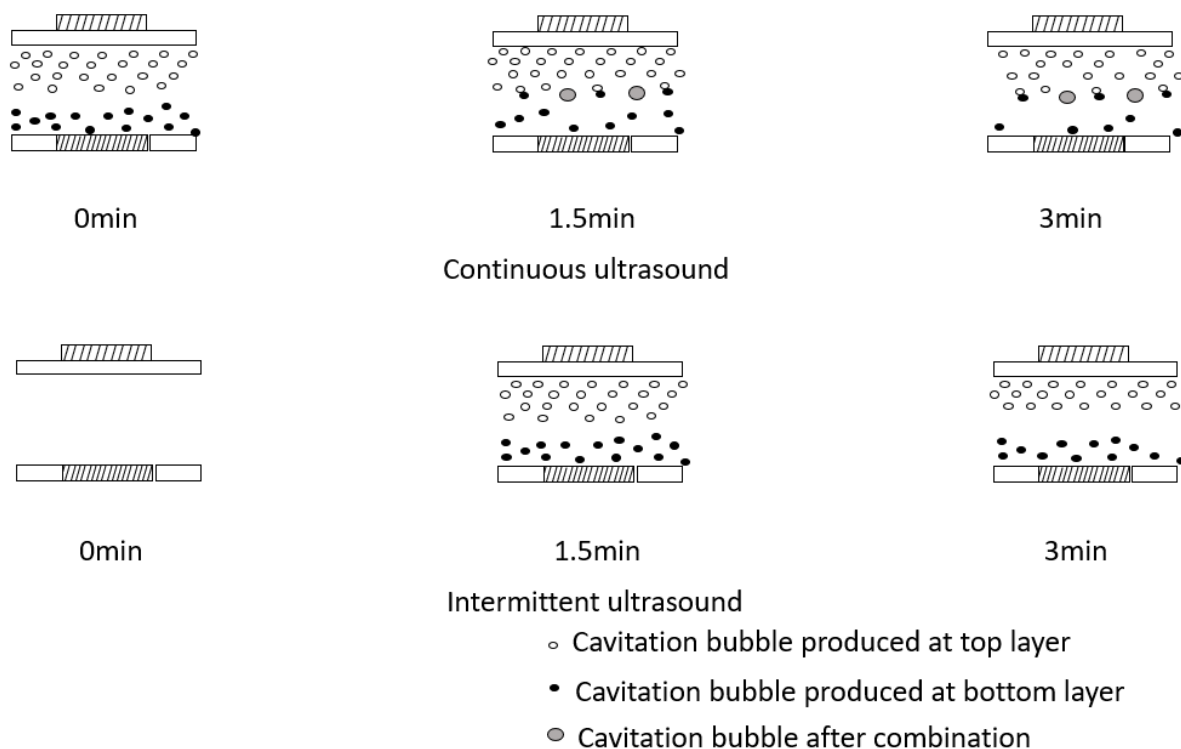
As depicted in **Figure 4.15**, no cavitation bubble would be produced at the beginning of the filtration process with the application of intermittent ultrasound since the ultrasonic transducer was deactivated; and the bubble started to be produced when the transducer was activated after 1.5 minutes. The transducer is deactivated again after 3 minutes, and it stopped producing bubbles. As a result, the number of cavitation bubbles, which were produced at the top layer and moved down to the bottom surface, might be insufficient for bubble coalescence as might be the case for continuous ultrasound. In other words, the rate of the bubble destruction was significantly reduced with the intermittent ultrasound, and relatively greater number of bubbles could be maintained on the membrane surface to remove the accumulated particles.

4.3.4 Analysis of Time Interval of Intermittent Ultrasound at Optimal Condition

With respect to the analysis of parameters in Box-Behnken design, optimal ultrasonic condition was confirmed at the frequency of 28kHz and the power intensity of 2.88 W/cm^2. The amount of permeate collected after 30 minutes of filtration without ultrasound was 31.3 g, as compared to 60.8 g for the case with continuous ultrasound

67

at 28 kHz and 2.88 W/cm^2, indicating an increase of 94%. Using this optimal condition, more diverse time intervals of the intermittent ultrasound were investigated to identify the optimal intermittent time. **Figure 4.16** shows the cumulative mass of the permeate solution with continuous and different time interval of intermittent ultrasound.
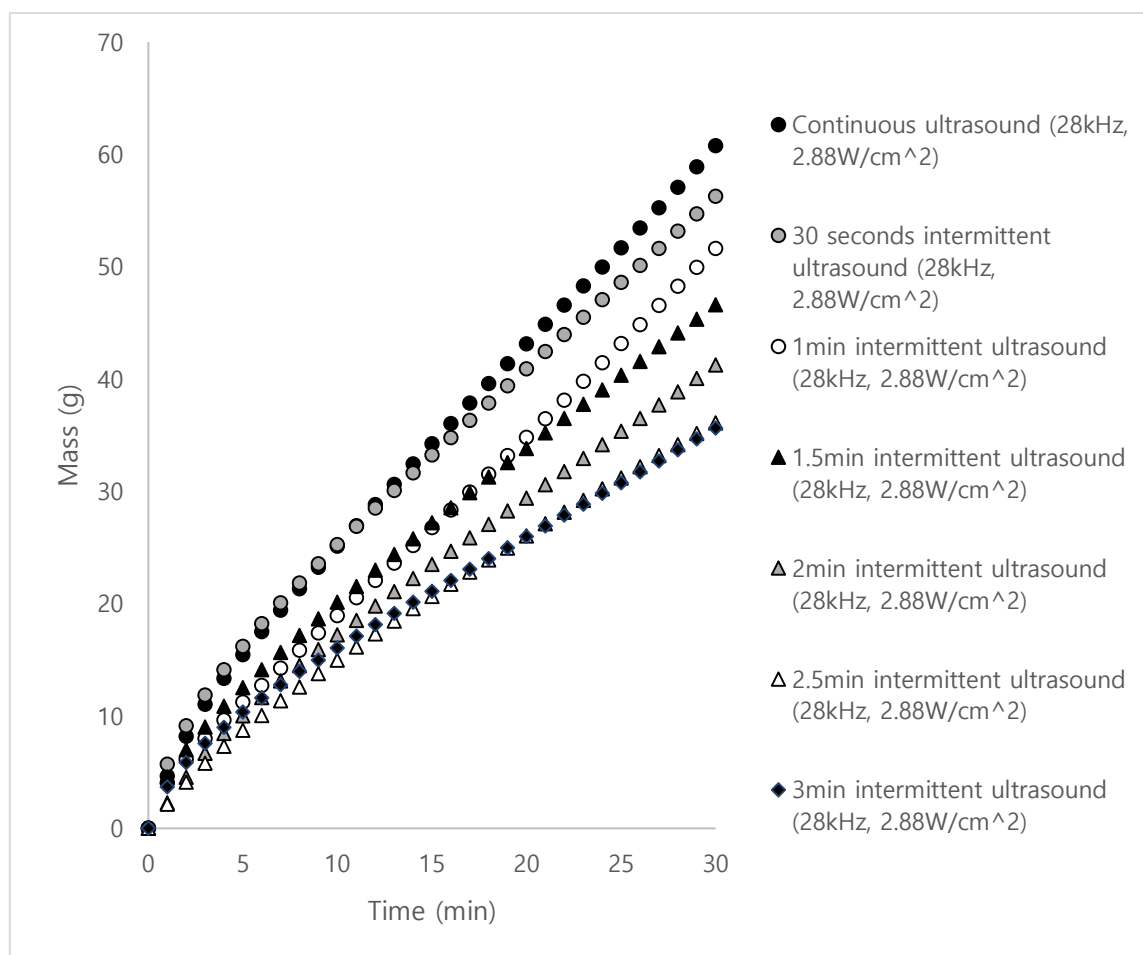
Figure 4.16 - *Comparison of cumulative mass of permeate solution among different time intervals of intermittent ultrasound at optimal ultrasonic condition (28kHz, 2.88 W/cm^2)*

Fundamentally, in contrast with the case without ultrasound, more amount of permeate could be collected at any ultrasonic condition. The figure indicates that continuous ultrasound produces the highest cumulative mass of the permeate solution at the optimal ultrasonic condition. In addition, although the intermittent ultrasound produced relatively lower mass of permeate solution, the amount approached the one from the continuous ultrasound as the time interval was adjusted to a shorter period. In other

words, the intermittent ultrasound with extremely short time interval would reach almost similar production rate of the permeate solution compared to the continuous ultrasound even though the intermittent ultrasound only operated half of the time of the continuous ultrasonic case. It is relevant to note that the permeate amount was increased by 79.8% with 30 seconds-interval intermittent ultrasound, as compared to that of the run without ultrasound. This tendency can be further illustrated in the graph of change in flux of permeate solution, as shown in **Figure 4.17** below.
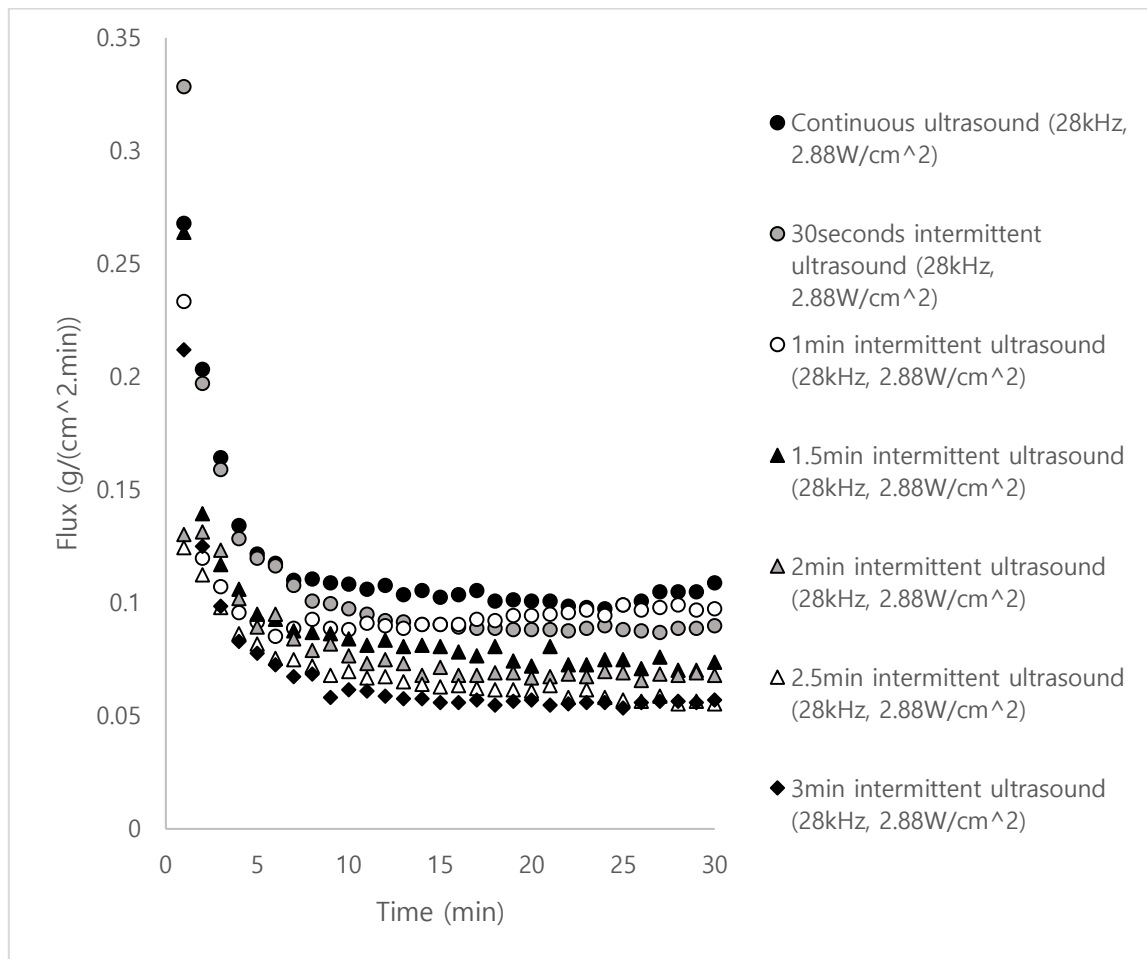
Figure 4.17 *- Comparison of flux of permeate solution among different time intervals of intermittent ultrasound at optimal ultrasonic condition (28kHz, 2.88 W/cm^2)*

The flux of the permeate solution followed a similar trend of the cumulative mass. Relatively the higher flux of permeate could be reached at any ultrasonic condition compared to the case without ultrasound. Continuous ultrasound produced the highest flux of the permeate solution while the intermittent ultrasound reached a relatively

lower flux, but it increased as time interval was reduced. The flux for 30 seconds time interval of the intermittent ultrasound approached the one for the continuous ultrasound. Thus, it can be considered that, on overall, the intermittent ultrasound facilitated higher efficiency by reducing the intermittent time interval. The reason for this phenomenon can be simply explained based on the analysis in turbidity and particle size distribution of the permeate solution, and it will be discussed more in detail in **Sections 4.4.4** and **4.5.4**.

4.3.5 Analysis of the Effect of the Protein Concentration in the Feed Solution

The property of the feed solution can be considered as another critical factor that affects the membrane fouling during the filtration process. In fact, as the concentration of the feed solution increases, greater number of particles would be accumulated on the membrane surface, resulting the increase in thickness of the cake layer. Therefore, the efficiency of the intermittent ultrasound is also analyzed with respect to the change in the protein concentration of the feed solution. **Figure 4.18** shows the results obtained with different feed solutions containing 0.05%, 0.1%, and 0.2% by weight of protein.
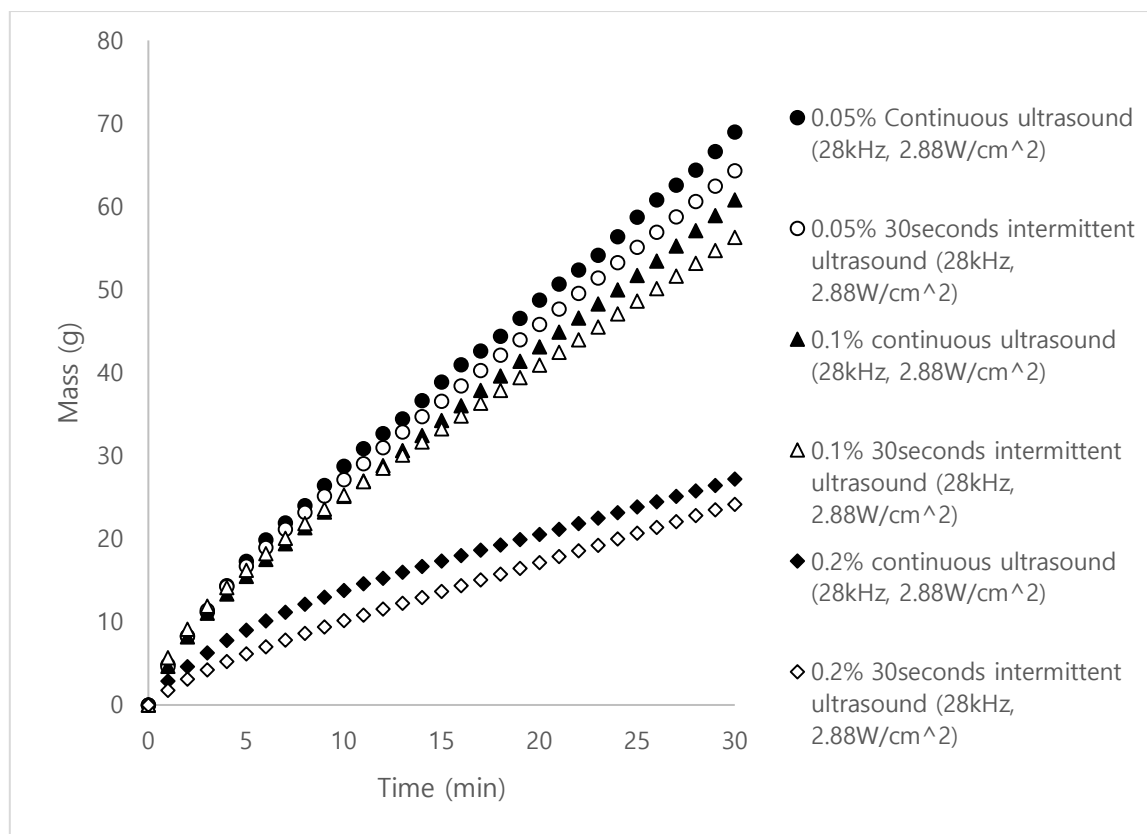
Figure 4.18 *– Comparison of cumulative mass of permeate solution between continuous and intermittent ultrasound with different mass concentrations of protein in skim milk at optimal ultrasonic condition (28kHz, 2.88 W/cm^2)*

Higher amount of the permeate solution tends to be collected with lower concentration of the protein in the feed solution, as expected. However, the degree of difference between continuous and intermittent ultrasound slightly changes depending on the protein concentration of the feed solution, as shown in **Table 9**.

Mass concentration of protein in skim milk (feed solution)	Ultrasonic condition	Final mass of permeate solution (g)	Change in final mass of permeate solution (%)
0.05%	Continuous	68.95	6.7
0.05%	30seconds intermittent	64.31	
0.10%	Continuous	60.79	7.4
0.10%	30seconds intermittent	56.27	
0.20%	Continuous	27.18	11.1
0.20%	30seconds intermittent	24.16	

According to **Table 9**, it can be observed that the percentage difference in the cumulative mass of the permeate solution between continuous and intermittent ultrasound increased slightly with the concentration of the protein in the feed solution. In other words, intermittent ultrasound provides higher efficiency at lower concentration of the feed solution. This might be due to the fact that at higher protein concentration in the feed, more protein particles were available in the solution, and hence, more particles would deposit on the membrane surface during the off-cycle of ultrasound during which the ultrasonic transducer was deactivated in the application of intermittent ultrasound. This resulted in an increase in the thickness and resistance of the cake layer to the flow of permeate through the membrane, as evidently shown in the variation of the permeate flux with filtration time for various ultrasound conditions, as shown in **Figure 4.19**.
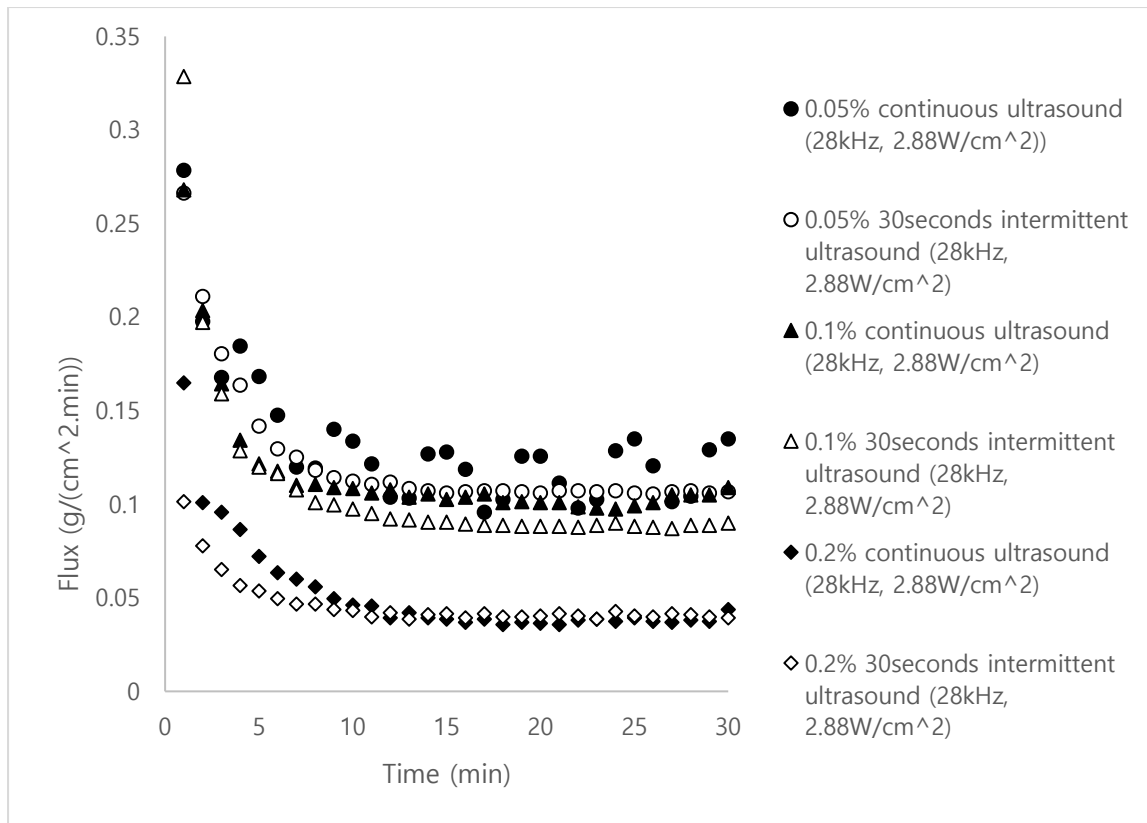
Figure 4.19 *- Comparison of change in flux of permeate solution between continuous and intermittent ultrasound with different mass concentration of protein in skim milk at optimal ultrasonic condition (28kHz, 2.88 W/cm^2)*

In general, the figure shows that relatively much lower flux of the permeate solution was obtained with 0.2% mass concentration of the protein compared to other feed solutions with lower concentrations. In addition, evidently higher flux of the permeate solution could be observed with continuous ultrasound compared to the ones with intermittent ultrasound at the beginning, but the difference decreased as time passed and became negligible at the end of the filtration process. A plausible reason for this trend was that towards the end of the filtration with highly concentrated feed solution, the thickness of the cake layer had been grown substantially to a level such that even continuous ultrasound could not sufficiently remove solid particles from the cake layer. The solid removal and deposit at the membrane surface reached a dynamic equilibrium, as indicated the by the leveling off of the flux with filtration time. Based on these results, it can be concluded that the intermittent ultrasound provides higher efficiency for longer period of the filtration with low concentration of protein in the feed solution.

4.4 Turbidity Test

In this session, turbidity of the permeate solution is measured for each run in different ultrasonic condition and compared.
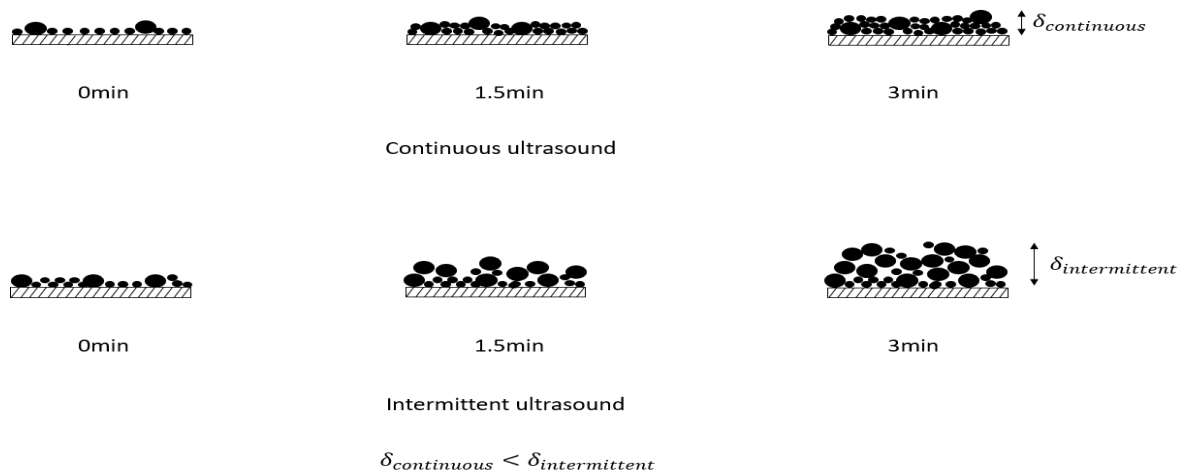
4.4.1 Condition of Intermittent Ultrasound

As the first step, the turbidities of the permeate solutions at different conditions of the continuous and intermittent ultrasound were measured, and the results are compared through **Figure 4.20**.
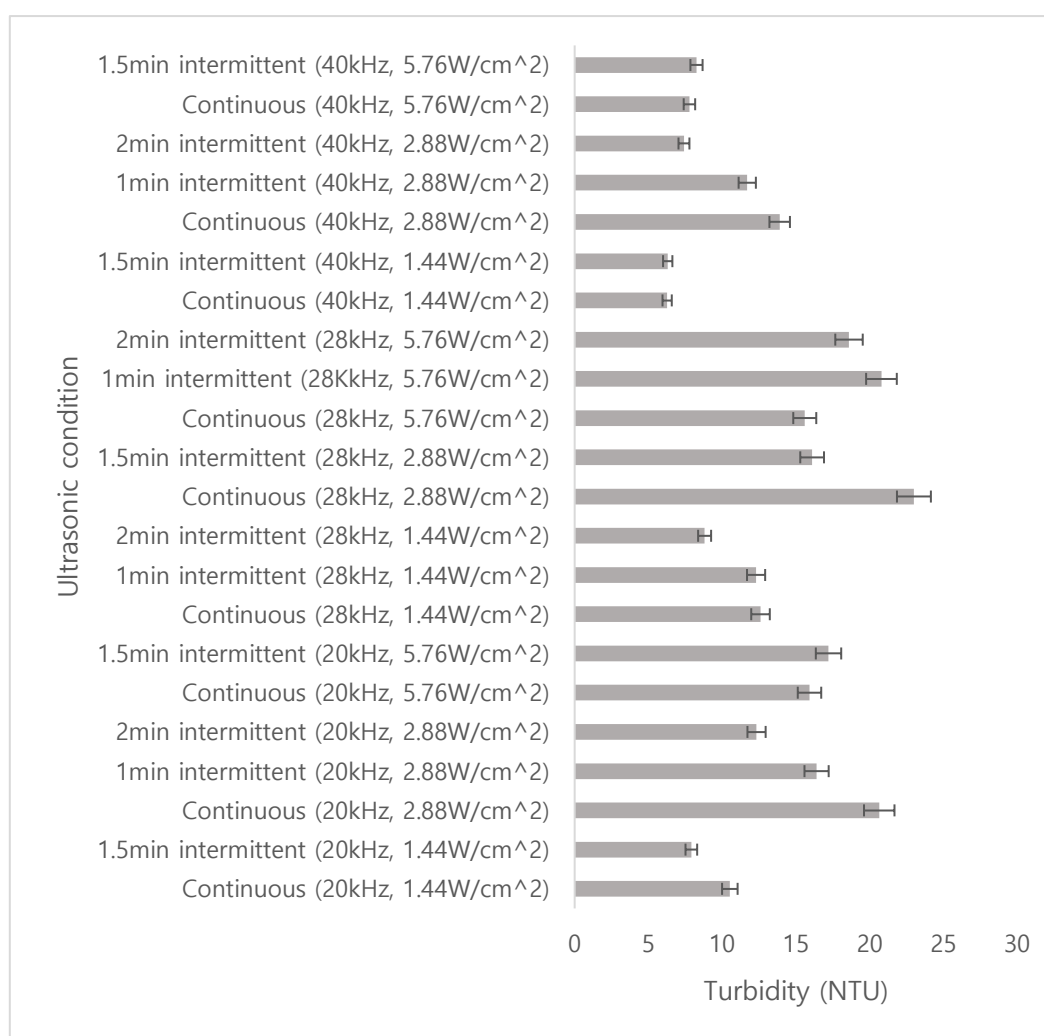
Figure 4.20 – *Turbidity of permeate solution at different conditions of continuous and intermittent ultrasound*

With respect to **Figure 4.20**, relatively lower turbidity of the permeate solution was observed with intermittent ultrasound compared to the one with continuous ultrasound at the ultrasonic power intensity of 1.44 W/cm^2 and 2.88 W/cm^2. The turbidity result is analogous to the trend in production rate of the permeate solution, which was presented in **Section 4.3.3**. In fact, the turbidity of the permeate solution is highly related to the condition of the accumulated particles on the membrane surface. **Figure 4.21** suggests the deposit process of the solid particles onto the membrane surface for the ultrasonic power intensities of 1.44 W/cm^2 and 2.88 W/cm^2 with the application of continuous and intermittent ultrasound.
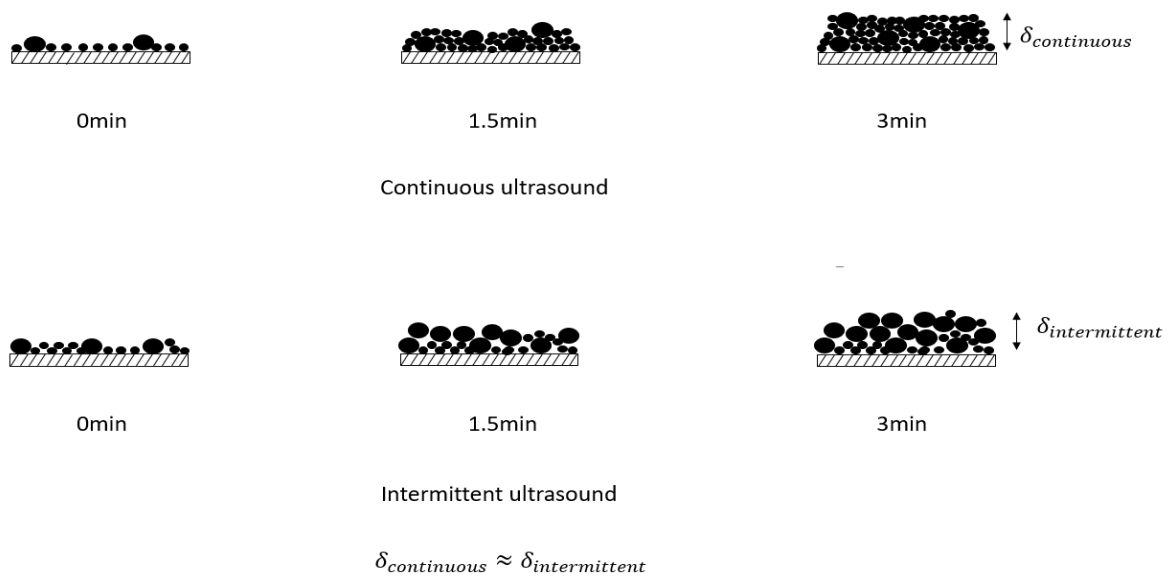

Figure 4.21 - Distribution of accumulated particles on membrane surface with continuous and intermittent ultrasound at ultrasonic power intensity of 1.44 W/cm^2 and 2.88 W/cm^2

As the figure indicates, turbidity of the permeate solution is highly connected to the size distribution of foulants on the membrane surface. The actual image of foulants on the membrane surface could not be obtained. The space inside the membrane apparatus was too narrow to inject an endoscope for visual observation. The images for the side view of the cake layer and membrane surface could not even be obtained using the Scanning Electron Microscope (SEM) after the filtration process. The ceramic membrane could not be broken down to small pieces due to its high hardness. Thus, the sample could not be injected into the SEM device. Instead, the particle size distribution on the membrane surface could be predicted based on the result of the collected permeate amount and turbidity test. It is expected that the cavitation bubble

from ultrasound can effectively remove small particles, whether they deposited on the membrane surface already or not. However, for comparatively large particles that already fouled the membrane surface, cavitation bubbles might not have enough energy to adsorb and remove them. As depicted in **Figure 4.21**, continuous ultrasound reduced a greater number of accumulated particles at the beginning of the filtration process. However, as time passed, relatively smaller size of particles deposited on the membrane surface, as compared to the case with the intermittent ultrasound. In fact, greater number of large particles would accumulate on the membrane surface during the deactivation period of the ultrasonic transducer of the intermittent ultrasound case. Thus, there the cake layer on the membrane surface would be thicker, which acted as an additional filter trapping the solid particles, resulting in a decrease in the turbidity of the permeate solution for the intermittent ultrasound.

On the other hand, the trend was reversed at the high power intensity of 5.76 W/cm^2. Similar to the trend of the cumulative mass of permeate, the turbidity of the permeate solution with the intermittent ultrasound was higher than that of the continuous ultrasound. **Figure 4.22** proposes an explanation for this reverse trend in the permeate turbidity.

0min	1.5min	3min

$\delta_{continuous}$

Continuous ultrasound

0min	1.5min	3min

$\delta_{intermittent}$

Intermittent ultrasound

$$\delta_{continuous} \approx \delta_{intermittent}$$

Figure 4.22 *- Distribution of accumulated particles on membrane surface with continuous and intermittent ultrasound at ultrasonic power intensity of 5.76 W/cm^2*

As it was discussed in **Section 4.3.3**, intermittent ultrasound tends to produce a greater number of cavitation bubbles because of the bubble destruction with continuous ultrasound at the ultrasonic power intensity of 5.76 W/cm^2. Thus, a relatively smaller number of particles would deposit on the membrane surface with intermittent ultrasound. Because of this reason, there would be no significant difference in the thickness of the cake layer between intermittent and continuous ultrasound although relatively larger particles would accumulate with the intermittent ultrasound. Overall, since there would be larger porous space among the accumulated larger particles while the same thickness of the cake layer was maintained, the particles in feed solution would have more chance to pass through the cake layer with the intermittent ultrasound, and this phenomenon produced a higher turbidity of the permeate solution.

4.4.2 Power Intensity of Ultrasound

In this section, turbidity of the permeate solution associated with the ultrasonic power intensity was analyzed based on the application of continuous ultrasound, and the results are compared in **Figure 4.23**.
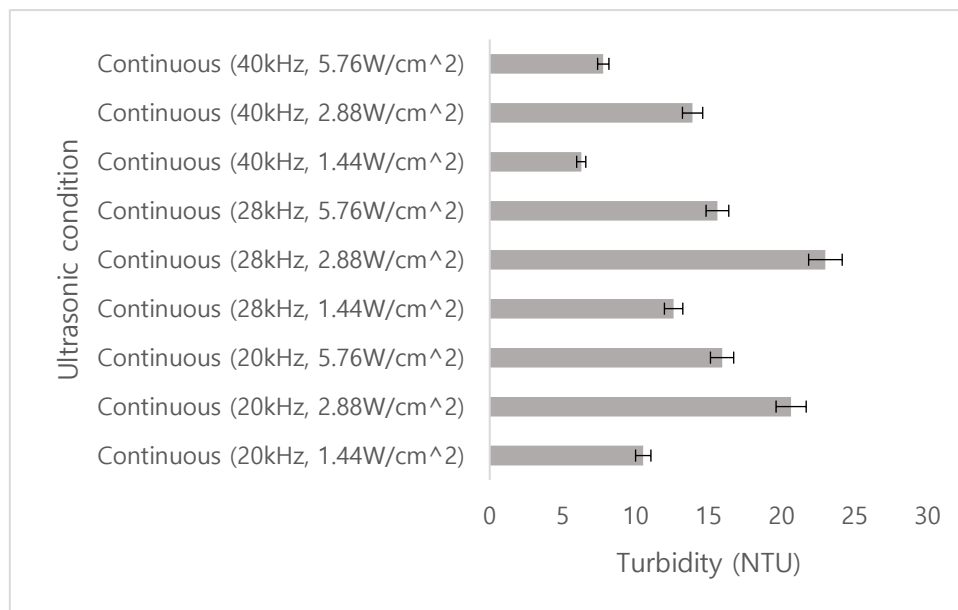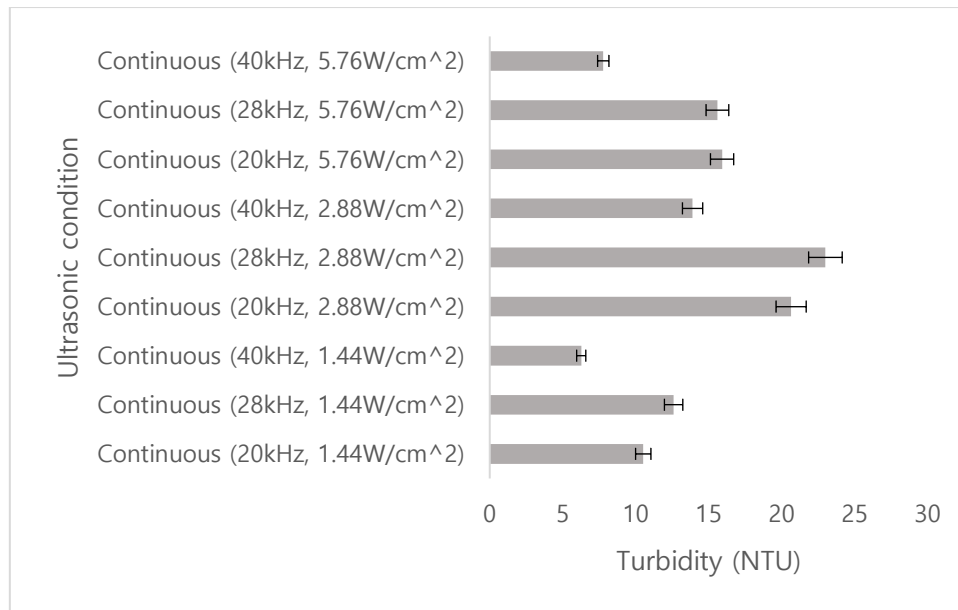

Figure 4.23 *– Comparison of turbidity of permeate solution at different ultrasonic power intensities*

Figure 4.23 shows that higher turbidity of the permeate solution was observed with increase in the ultrasonic power intensity from $1.44\,\mathrm{W/cm^2}$ to $2.88\,\mathrm{W/cm^2}$. However, the turbidity was reduced when the power intensity was increased from $2.88\,\mathrm{W/cm^2}$ to $5.76\,\mathrm{W/cm^2}$. The result of this turbidity test follows the same pattern again with the amount of permeate solution collected, as shown in **Section 4.3.1**. In other words, the turbidity of the permeate is also highly related to the amount of the permeate solution with regard to ultrasonic power intensity. Higher ultrasonic power intensity produces greater number of the cavitation bubbles, and the larger total surface area of the bubbles would contribute more to adsorption of the accumulated particles, resulting in greater porous spaces and lower thickness of the cake layer. Due to this phenomenon, there would be less resistance that affects not only the permeate flow, but also the particles in feed solution to pass through the cake layer and the membrane surface. As a result, it leads to higher turbidity of the permeate solution.

On the other hand, a relatively lower turbidity of the permeate solution was obtained with the ultrasonic power intensity of $5.76\,\mathrm{W/cm^2}$ compared to that with $2.88\,\mathrm{W/cm^2}$. This is due to the bubble coalescence and collapse, resulting in less active bubbles on fouling removal. As a result, a thicker cake layer would form, which hindered the particles to pass through the membrane to the permeate stream. This phenomenon is highly related again with design of membrane apparatus that is explained in **Section 4.3.1.**

4.4.3 Frequency of Ultrasound

Turbidity of the permeate solution was also affected by the magnitude of the ultrasonic frequency, as can be seen in **Figure 4.24**.
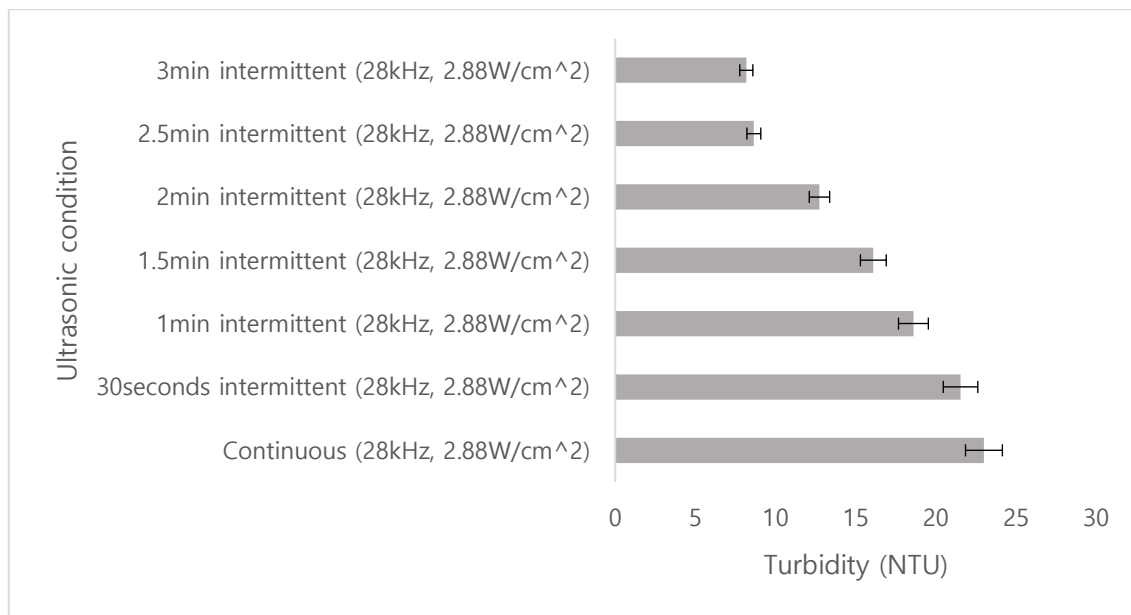
Figure 4.24 *– Comparison of turbidity of permeate solution at different ultrasonic frequency*

The result shows relatively higher turbidity of the permeate solution at the ultrasonic frequency of 28kHz compared to the one at 40kHz. This result follows the principle that stipulates that lower ultrasonic frequency produces larger cavitation bubbles and adsorbs greater number of accumulated particles on the membrane surface. Thus, a greater number of particles in the feed solution can pass through larger porous spaces, resulting in a higher turbidity of the permeate solution.

However, by comparing the results at the frequencies of 28kHz and 20kHz, the turbidity of the permeate solution was reduced even though much larger cavitation bubble would be produced by the ultrasound at a frequency of 20kHz. This can be explained again based on the stability of cavitation bubble. Larger cavitation bubbles produced by the ultrasonic frequency of 20kHz would be unstable and some would collapse before reaching the membrane surface. Therefore, relatively fewer number of cavitation bubbles could remain on the membrane surface. Hence, particles in feed solution would have less opportunity to pass through the smaller porous spaces of the cake layer and the membrane surface, resulting in lower turbidity of the permeate solution with the ultrasonic frequency of 20kHz.

<u>4.4.4 Time Interval of Intermittent Ultrasound at Optimal Condition</u>

It was analyzed and determined in **Section 4.3** that the optimal ultrasonic conditions that produced the highest amount of permeate are at 28kHz and 2.88 W/cm^2. In this section, turbidity test is implemented to observe if the high quality of the permeate solution could also be maintained with different time interval of the intermittent ultrasound at the optimal ultrasonic condition. The results obtained are presented in **Figure 4.25**.
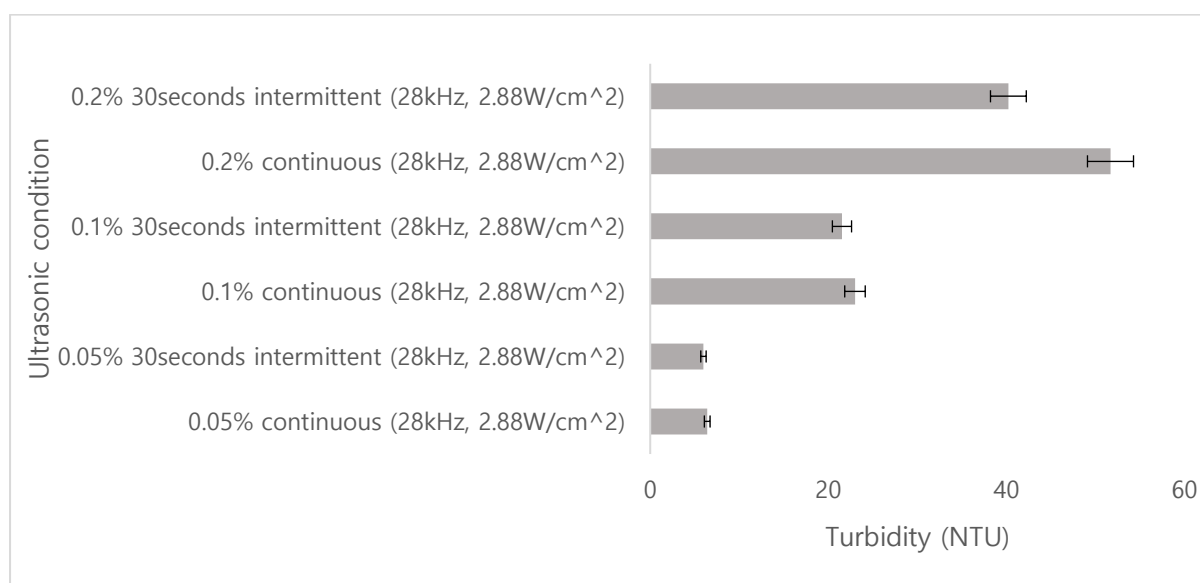

Figure 4.25 *– Comparison of turbidity of permeate solution among different time intervals of intermittent ultrasound at optimal ultrasonic condition (28kHz, 2.88 W/cm^2)*

The result indicates that the time interval of the intermittent ultrasound is inversely proportional to the turbidity of permeate solution. As the length of continuous deactivation time of the ultrasonic transducer increases, rate of increase in thickness of the cake layer would be accelerated rapidly; and hence, the passage for particles to move from the feed solution through the membrane would be interrupted significantly. For this reason, relatively lower turbidity of the permeate solution was obtained at longer time interval of the intermittent ultrasound.

4.4.5 Effect of Protein Concentration of the Feed Solution

The last analysis of the permeate turbidity is associated with the mass concentration of the protein in the feed solution. **Figure 4.26** shows the result in turbidity of the permeate solution for different feed solutions with 0.05%, 0.1%, and 0.2% weight of the protein with respect to the application of both continuous and intermittent ultrasound.

Figure 4.26 *– Comparison of turbidity of permeate solution between continuous and intermittent ultrasound with different mass concentration of protein in skim milk at optimal ultrasonic condition (28kHz, 2.88 W/cm^2)*

In general, higher turbidity of the permeate solution was obtained with continuous ultrasound, as compared to that for the intermittent ultrasound at any mass concentration of the protein in the feed solution. However, there is negligible turbidity difference between continuous and intermittent ultrasound with low mass concentration of the protein because the thickness of the cake layer was negligibly low; i.e. insignificant fouling. Therefore, the effect of ultrasound on the removal of fouling became less obvious and indistinguishable between intermittent and continuous ultrasound applications. The percentage changes of the turbidity of the permeate solution between continuous and intermittent ultrasound applications are presented in **Table 10.**

Table 10 *- Difference in turbidity of permeate solution between continuous and intermittent ultrasound with different mass concentrations of protein in feed solution*

Mass concentration of protein in skim milk (feed solution)	Ultrasonic condition	Turbidity of permeate solution (NTU)	Change in turbidity of permeate solution (%)
0.05%	Continuous	6.4	6.6
0.05%	30seconds intermittent	5.98	
0.10%	Continuous	23	10.7
0.10%	30seconds intermittent	20.54	
0.20%	Continuous	51.7	22.2
0.20%	30seconds intermittent	40.23	

As the table demonstrates, the turbidity of the permeate solution was reduced more with the application of the intermittent ultrasound at higher mass concentration of the feed solution. In other words, higher quality of the purification can be expected using intermittent ultrasound with highly concentrated feed solution.

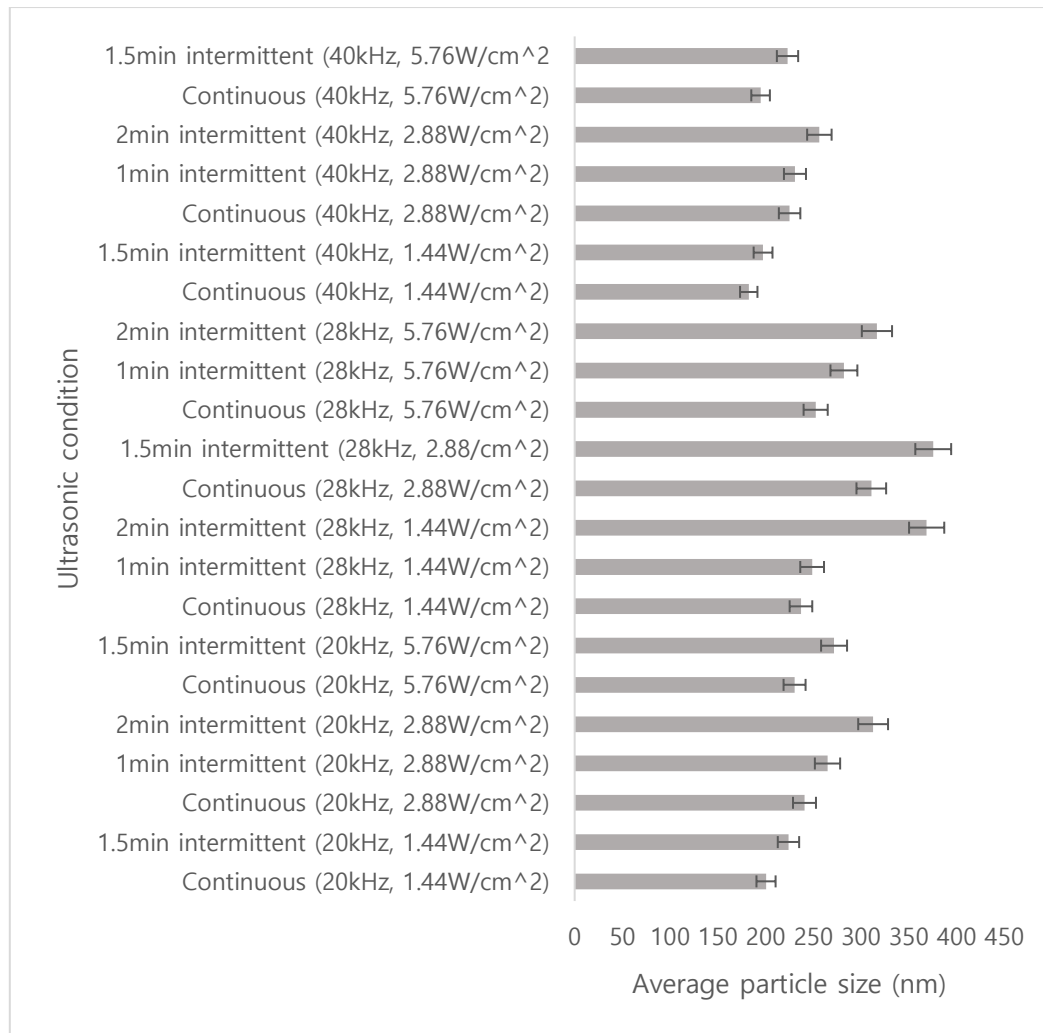## 4.5 Analysis of Average Particle Size in Permeate Solution

The last factor that was considered to examine the quality of the permeate solution after the filtration process in this study is the particle size distribution.

The average particle size in the retentate solution was checked to observe the possibility of the protein particles being broken by ultrasound. The size was measured as 674.9nm without ultrasound and 737.1nm with ultrasound (28kHz, $2.88\text{W}/cm^2$). It indicates that the protein particles were preserved from ultrasound due to the strong peptide bond among amino acid molecules as illustrated in **Section 3.5.2**.

4.5.1 Analysis of Intermittent Ultrasound

As the first step, the particle size distribution of the permeate solution is affected in terms of the change in the time interval of intermittent ultrasound, and **Figure 4.27** shows the result.
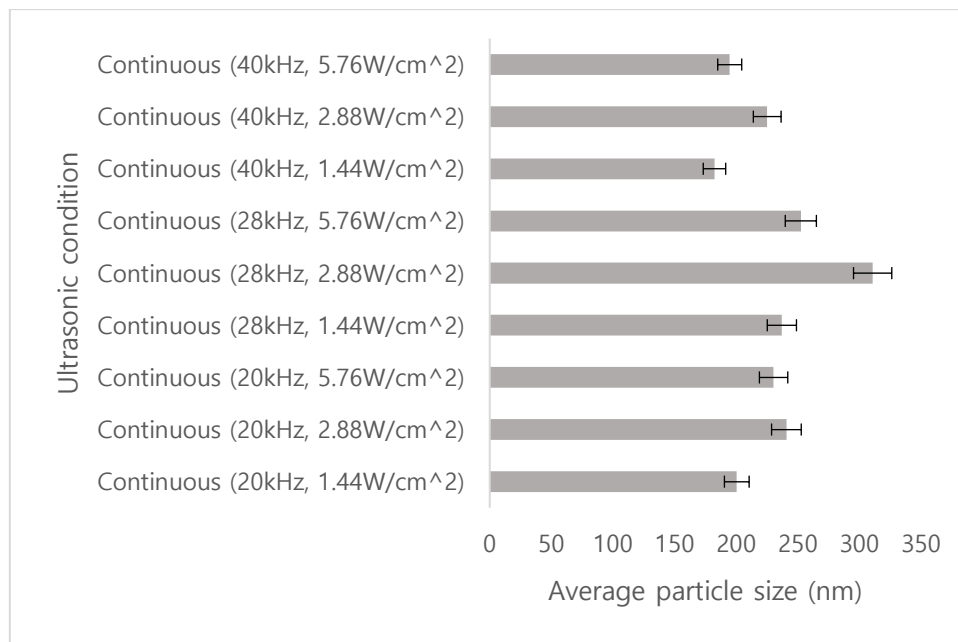
Figure 4.27 *- Average particle size in permeate solution at different condition of continuous and intermittent ultrasound*

Regardless of the ultrasonic frequency and the power intensity, **Figure 4.27** demonstrates that the intermittent ultrasound produced relatively larger particles in the permeate solution compared to the continuous ultrasound. The particle size in the permeate solution is critically affected by the size of the accumulated particle on the membrane surface while the thickness of the cake layer is not significantly related. The thickness of the cake layer affects more on the number of particles in the permeate solution rather than the particle size. With the application of the intermittent ultrasound, more large particles would accumulate on the membrane surface while the ultrasonic transducer was deactivated. Therefore, as **Figure 4.21** and **Figure 4.22** show, there are larger porous spaces among the accumulated large particles with intermittent ultrasound, and this phenomenon would allow larger particles to pass through the cake layer and the membrane. As a result, the permeate solution contains larger particles

with the application of the intermittent ultrasound.

4.5.2 Power Intensity of Ultrasound

Figure 4.28 presents the trend of solid particle size in the permeate solution at varied ultrasound power intensities.
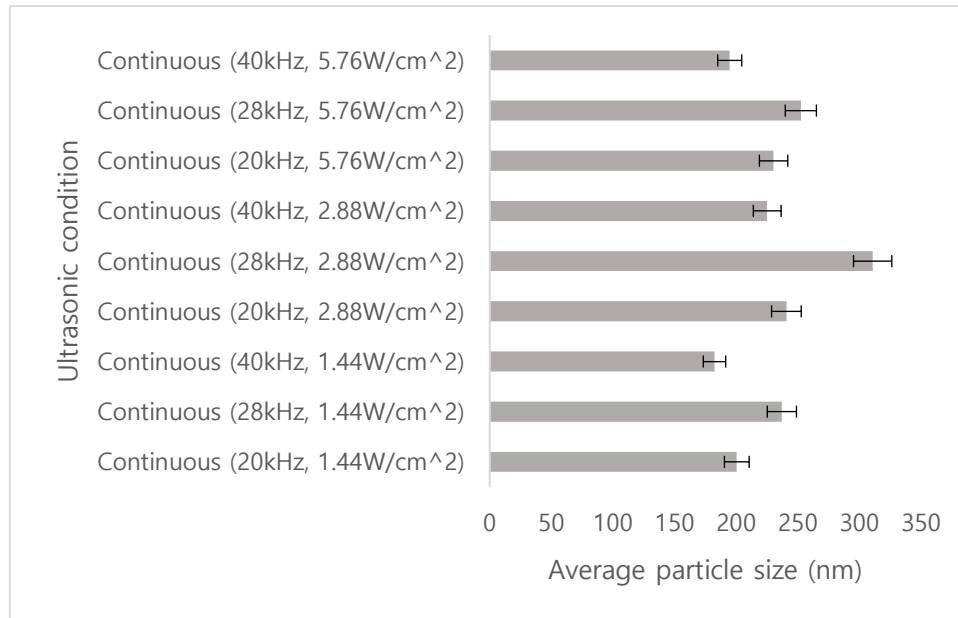

Figure 4.28 – Comparison of average particle size in permeate solution at different ultrasonic power intensity

The average particle size in the permeate solution has a direct relationship with the number of the cavitation bubbles remained on the membrane surface to remove the foulants. A greater number of cavitation bubbles was produced at the power intensity of $2.88\ \mathrm{W/cm^2}$ than at $1.44\ \mathrm{W/cm^2}$; and hence, there would be larger porous spaces in the cake layer allowing larger particle to pass through it, resulting in a larger average particle size in the permeate solution. However, because of the bubble destruction at the ultrasonic power intensity of $5.76\ \mathrm{W/cm^2}$, less foulant could be removed. This would result in relatively smaller porous space in the cake layer that would allow smaller particles in the feed solution to pass through the cake layer, and thus a lower average particle size in the permeate solution was observed.

The average particle size in the permeate solution was also affected by the magnitude of the ultrasonic frequency. **Figure 4.29** shows the detailed results below.
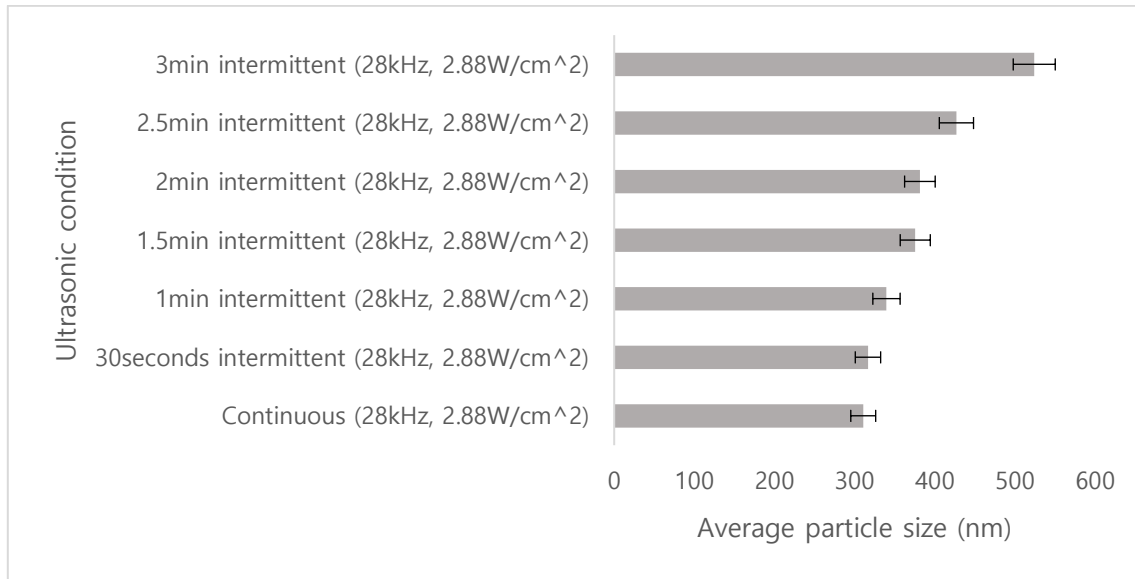

Figure 4.29 *- Comparison of average particle size in permeate solution at different ultrasonic frequency*

The average particle size in the permeate solution was highly related to the amount of permeate collected. According to **Figure 4.29**, Permeate solution contains the largest average particle size with the ultrasonic frequency of 28kHz. Lower ultrasonic frequency produces larger cavitation bubble, and more extensive surface area of the bubble can contribute to the removal of foulants. However, greatest amount of the permeate solution could be obtained with the ultrasonic frequency of 28kHz, since a smaller number of cavitation bubble is remained on the membrane surface due to the bubble destruction with unstable size at 20kHz. Similar pattern can be considered for average particle size in permeate solution. Because the cavitation bubble from 28kHz contributes more on adsorbing the accumulated particles, relatively larger porous space could be retained in the cake layer. As a result, relatively larger particles are allowed to pass through the membrane surface and this phenomenon induced larger average particle size distribution in the permeate solution.

4.5.4 Time Interval of Intermittent Ultrasound at Optimal Condition

By utilizing the optimal ultrasonic condition, 28kHz and 2.88 W/cm^2, change in average particle size distribution in the permeate solution with respect to the time interval length of the intermittent ultrasound is even analyzed, and **Figure 4.30** shows the result in detail.
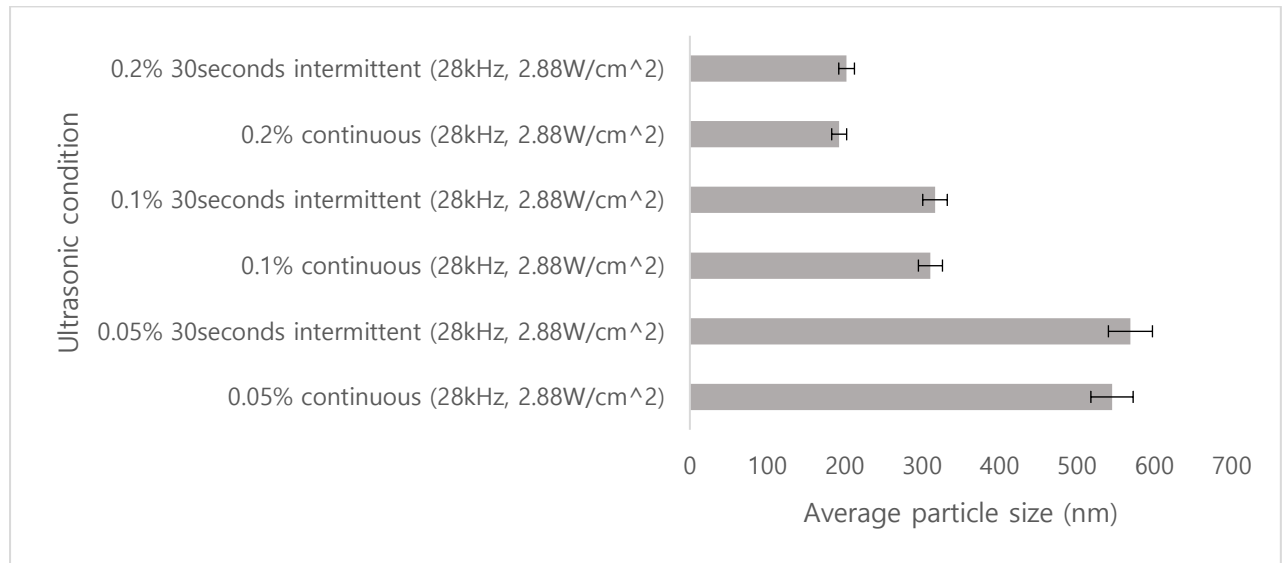

Figure 4.30 *– Comparison of average particle size in permeate solution among different time interval of intermittent ultrasound at optimal ultrasonic condition (28kHz, 2.88 W/cm^2)*

It was shown in **Section 4.5.1** that continuous ultrasound produced smaller average particle size in permeate solution compared to the one from the intermittent ultrasound. Moreover, **Figure 4.30** shows that the average particle size in the permeate solution increased with longer time interval of the intermittent ultrasound. A greater number of large particles would accumulate on the membrane surface during the period when the ultrasonic transducer was deactivated. Therefore, the level of particle accumulation on the membrane surface increased as the continuous deactivation period of the ultrasonic transducer was increased. As a result, larger average porous spaces were created in the cake layer to allow larger particle in the feed solution to pass through the membrane. Thus, the permeate solution contained relatively larger particles with the application of longer time interval length of the intermittent ultrasound.

4.5.5 Analysis in Concentration of Feed Solution

As the last analysis of the particle size distribution in the permeate solution, the concentration of the feed solution was considered in this section. **Figure 4.31** shows the results of the particle size in the permeate solution at various solid concentrations of the feed.

Figure 4.31 *– Comparison of average particle size in permeate solution between continuous and intermittent ultrasound with different mass concentration of protein in skim milk at optimal ultrasonic condition (28kHz, 2.88 W/cm²)*

As can be seen in **Figure 4.31**, the particle size in the permeate solution with intermittent ultrasound was slightly larger than that with continuous ultrasound at all solid concentrations of the feed solution used in the present study. In addition, the particle size in the permeate solution was larger at lower solid concentration of the feed solution. Much greater number of the particles would accumulate on the membrane surface with highly concentrated feed solution; and hence, the thickness of the cake layer would be increased. Thus, only small enough particle would be able to pass through the cake layer and the membrane. As a result, the permeate solution contains smaller average particle size with higher solid concentration of the feed solution.

Furthermore, the percentage difference of the average particle in the permeate solution between continuous and intermittent ultrasound was analyzed at each concentration of the feed solution. The results show that the difference of the average particle size in the permeate solution of the two modes of ultrasound applications is insignificant at all solid concentrations in the feed solution, as presented in **Table 11** below.

Table 11 - *Difference of average particle size in permeate solution between continuous and intermittent ultrasound with different mass concentration of protein in feed solution*

Mass concentration of protein in skim milk (feed solution)	Ultrasonic condition	Average particle size in permeate solution (nm)	Change in average particle size in permeate solution (%)
0.05%	Continuous	545.4	4.2
0.05%	30seconds intermittent	569.2	
0.10%	Continuous	310.8	1.9
0.10%	30seconds intermittent	316.7	
0.20%	Continuous	192.9	4.7
0.20%	30seconds intermittent	202.5	

4.6 Analysis of Scanning Electron Microscope

The SEM imaging (Scanning electron microscope) was used for visual analysis of the membrane surface before and after the filtration process in this study. The magnification levels of 200 times and 10000 times of the original size were used when the images of the membrane were taken. **Figure 4.32** shows the images of the membrane surface at 200 times magnification under different conditions.
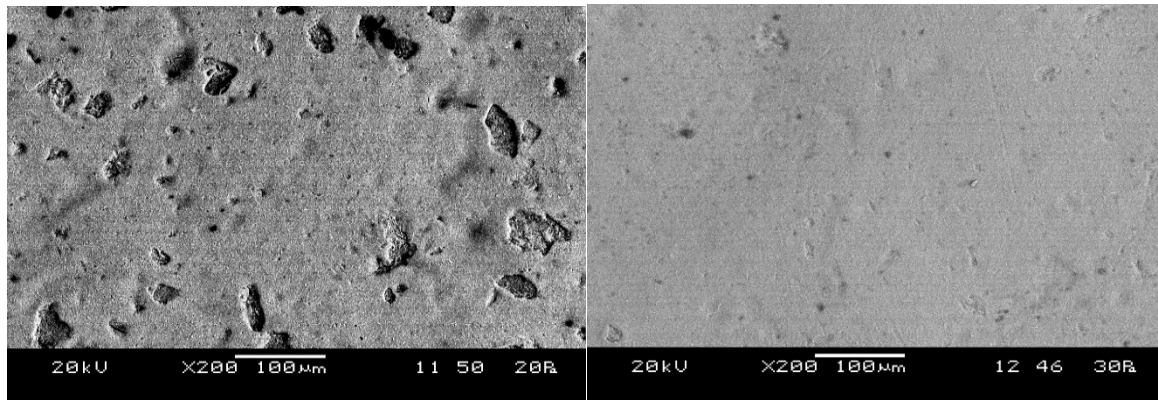
a) new membrane   b) without ultrasound (US)
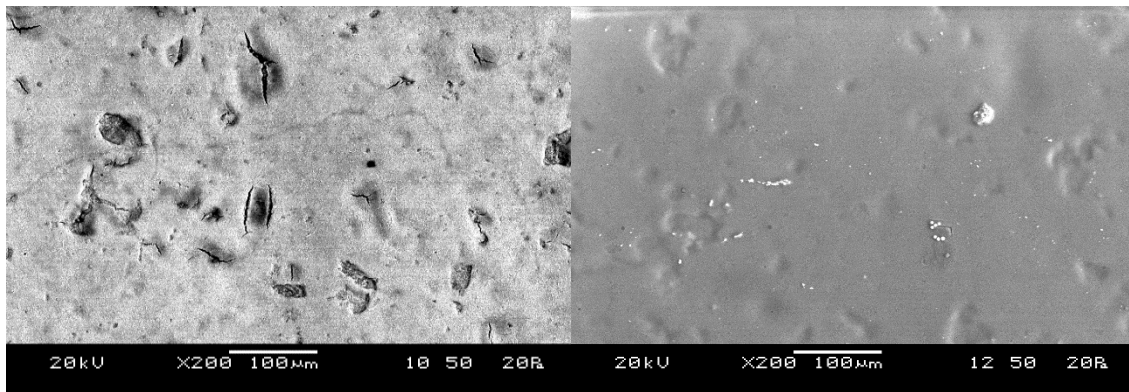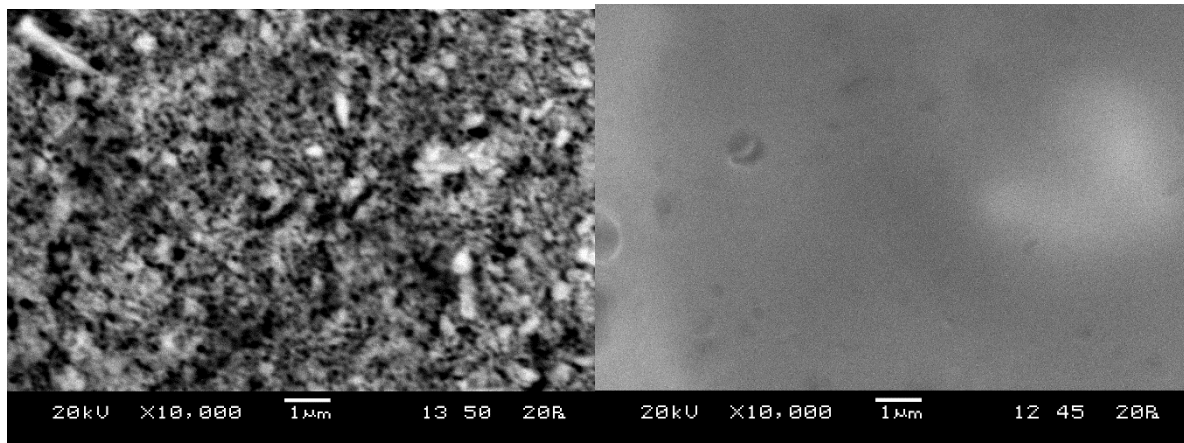

c) Continuous US 28kHz, 2.88 W/cm^2 d) 1.5min intermittent US 28kHz, 2.88 W/cm^2

Figure 4.32 - SEM images of the ceramic membrane surface with 200 times magnification at different conditions. a) before the filtration process b) after the filtration process without ultrasound c) after the filtration process with continuous ultrasound d) after the filtration process with intermittent ultrasound

The clearest porous spaces are displayed on the new membrane surface in **Figure 4.32a** while they are completely covered by a smooth and continuous layer of accumulated particles after the filtration process without ultrasound, as shown in **Figure 3.2b**. However, the porous spaces could be seen for the membrane with the application of continuous ultrasound in **Figure 4.32c**. For the case with intermittent ultrasound, the shape of the porous spaces could still be partially viewed on the membrane surface, indicating that although the membrane surface was covered by a layer of deposited particles, it appears to be thinner than that for the case without the application of ultrasound.
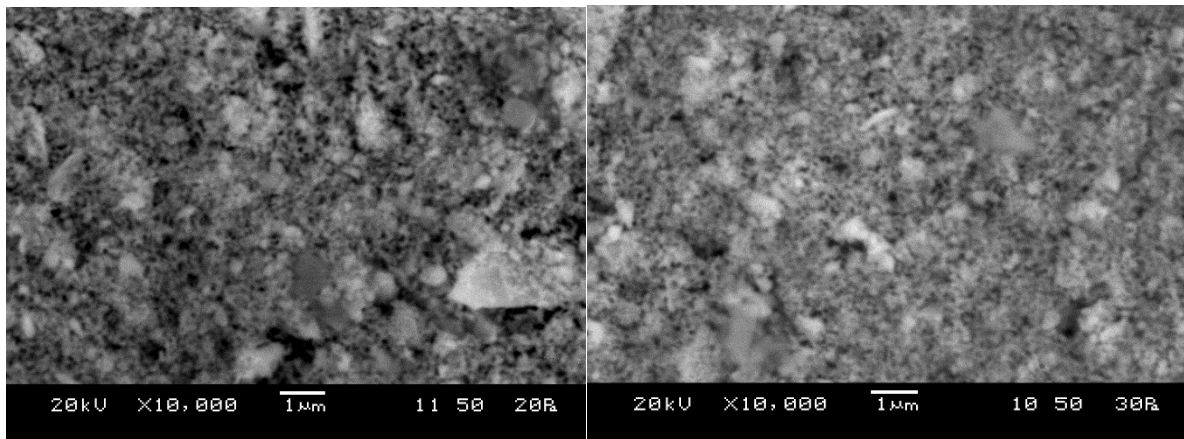
Figure 4.33 shows the images of the same set of membrane at 10000 times

magnification as to observe the porous spaces on the membrane in more detail.

a) New membrane   b) Without ultrasound (US)

c) Continuous US 28kHz, 2.88 W/cm^2 d) 1.5min intermittent US 28kHz, 2.88 W/cm^2

Figure 4.33 - SEM images of the ceramic membrane surface with 10000 times magnification at different conditions. a) before the filtration process b) after the filtration process without ultrasound c) after the filtration process with continuous ultrasound d) after the filtration process with intermittent ultrasound

Porous spaces can be clearly seen again on the new membrane surface in **Figure 4.33a.** On the other hand, the pores were completely fouled after the filtration process without the application of ultrasound, as can be seen in **Figure 4.33b**. However, the pores were partially remained after the filtration with the continuous and intermittent ultrasound as the **Figure 4.33a and b** show. Overall, SEM images, along with the results of the obtained permeate amount presented in the previous sections, support the conclusion that the application of ultrasound effectively contributed to overcome the fouling problem during the membrane separation process.

Chapter 5: Conclusion

In conclusion, the application of ultrasound successfully contributed to remove the foulants on the membrane surface to alleviate membrane fouling in this study. The ultrasonic frequencies (20kHz, 28kHz, and 40kHz), ultrasonic power intensities (1.44 W/cm^2, 2.88 W/cm^2, and 5.76 W/cm^2), and the time interval of the intermittent ultrasound (1min, 1.5min, and 2min) were the parameters used in the experiments. The effect of the feed concentration was additionally analyzed at the optimal ultrasonic condition. The Box-Behnken method was used for the experimental design and statistical analyses.

Overall, the optimal ultrasonic condition was found at the frequency of 28kHz and the power intensity of 2.88 W/cm^2. A direct relationship between the magnitude of the ultrasonic power intensity and the production rate of the permeate solution was observed. Based on the principle of cavitation bubble generation by ultrasound, higher ultrasonic power intensity should provide higher production rate of the cavitation bubble. Thus, it should contribute more to remove the accumulated particle. This was observed to be valid for the power intensity lower than 5.76 W/cm^2. However, at 5.76 W/cm^2, the amount of the permeate solution was lower than that at 2.88 W/cm^2 due to unstable cavitation bubbles resulting in bubble collapse before reaching the membrane surface. In addition, although the anti-proportional relationship between the magnitude of the ultrasonic frequency and the size of the cavitation bubble was already proved in reported literature, relatively less amount of the permeate solution was collected at 20kHz, compared to the one at 28kHz in this study. This can be attributed to the large and unstable cavitation bubbles generated at 20kHz.

With respect to the optimal ultrasonic conditions of 28kHz and 2.88 W/cm^2, analysis of the effect of the time interval of the intermittent ultrasound on the filtration performance showed that much more permeate solution could be collected by reducing the length of the time interval. Also, higher fouling control efficiency of intermittent ultrasound was obtained at the lower solid concentration of the feed solution.

Cumulative mass and turbidity of the permeate solution had a proportional relationship at any ultrasonic condition. Not only the solvent but also the solid particles in feed solution could have more opportunity to pass through the membrane by reducing the

resistance of the cake layer.

The largest particle size was detected in the permeate solution at the optimal ultrasonic conditions of 28kHz and 2.88 $\mathrm{W/cm^2}$. However, the particle size in the permeate solution was critically affected by the size of the accumulated particle on the membrane surface. More large particles accumulated on the membrane surface while the ultrasonic transducer was deactivated. As a result, the permeate solution contained larger particles with the application of the intermittent ultrasound compared to the case with the continuous ultrasound.

Lastly, SEM images supported the conclusion that the application of ultrasound effectively contributed to overcome the fouling problem during the membrane separation process.

Chapter 6: Recommendations

Although the objective of the present study was successfully achieved, some recommendations are suggested to improve the practicality of the ultrasonic application during membrane filtration process in industrial applications.

- In practice, many types of membranes are applied depending on the purpose of the separation process in industries, such as microfiltration, nanofiltration, ultrafiltration, and reverse osmosis. Each type of these membranes is distinguished by the range of pore sizes. In fact, the experiment was performed based on only one single pore size, 0.14micron, to analyze the effect of the ultrasonic application in this project. Change in degree of fouling is expected with respect to the membrane pore size, since smaller porous spaces would increase the rate of particle accumulation, inducing the thicker cake layer with higher resistance. Thus, it is recommended to examine multiple membrane pore sizes rather than a single size to consider diverse applications.

- Secondly, this study considered only the ceramic membrane with the flat surface. However, the most popular designs of the membrane apparatus in industries are spiral wound and hollow-fine fibre due to their high economic efficiency. Those membrane modules are tubular rather than flat. For this reason, it is recommended to consider testing with those modules.

- Thirdly, the size of the ceramic membrane used in this project was tiny with the diameter of 4.7cm. For this reason, the membrane surface tended to be completely fouled in a short period. Thus, a large membrane surface is preferred so to delay the fouling time and augment the effect of ultrasound on fouling remediation.

- Lastly, membrane separation technology can be applied to various types of feed solution. In practice, each type of feed solution has different physical and chemical properties, such as thermal stability, chemical stability, and hydrophobic or hydrophilic properties. Not only the concentration of feed solution but also these properties are expected to affect the degree of fouling during the separation process. In addition to that, the response of the ultrasonic application would be different. Therefore, it is suggested to test with diverse type of feed solution instead of relying on one single solution.
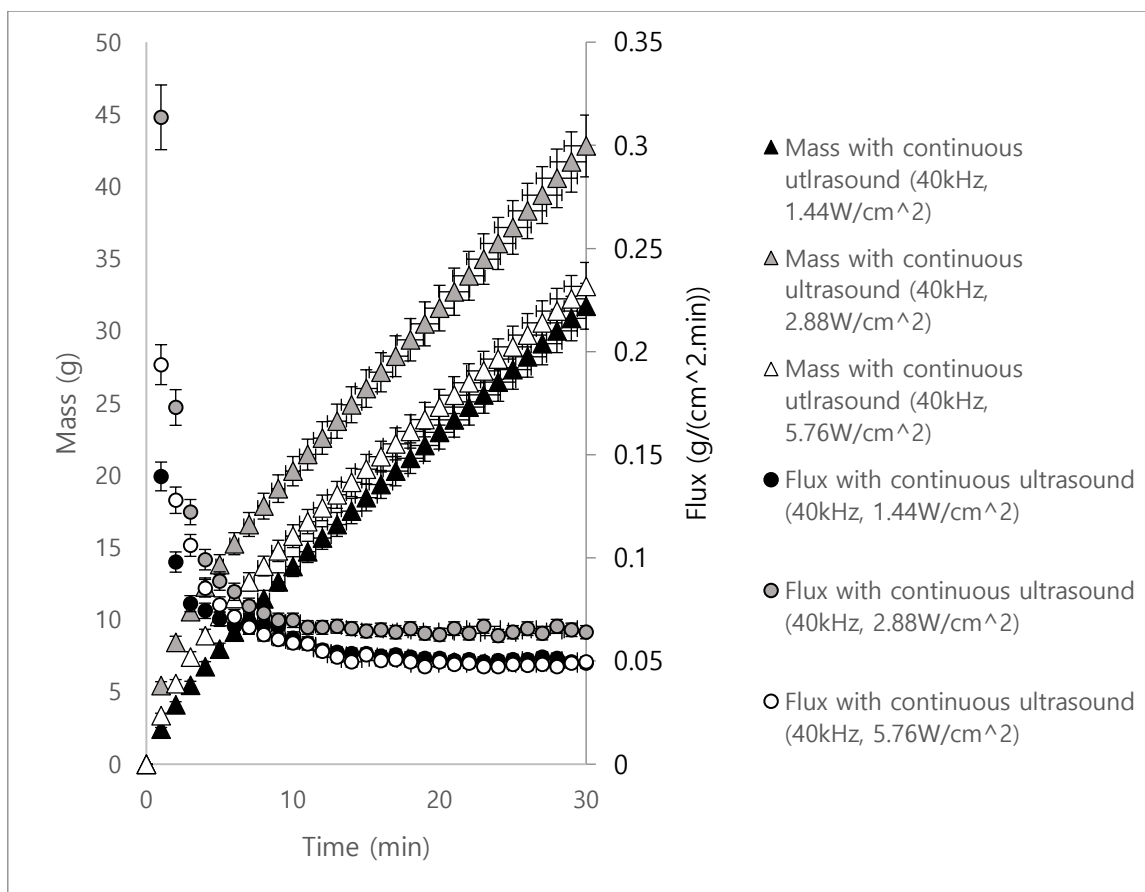
Appendices

Appendix A Graph of cumulative mass and change in flux of permeate solution
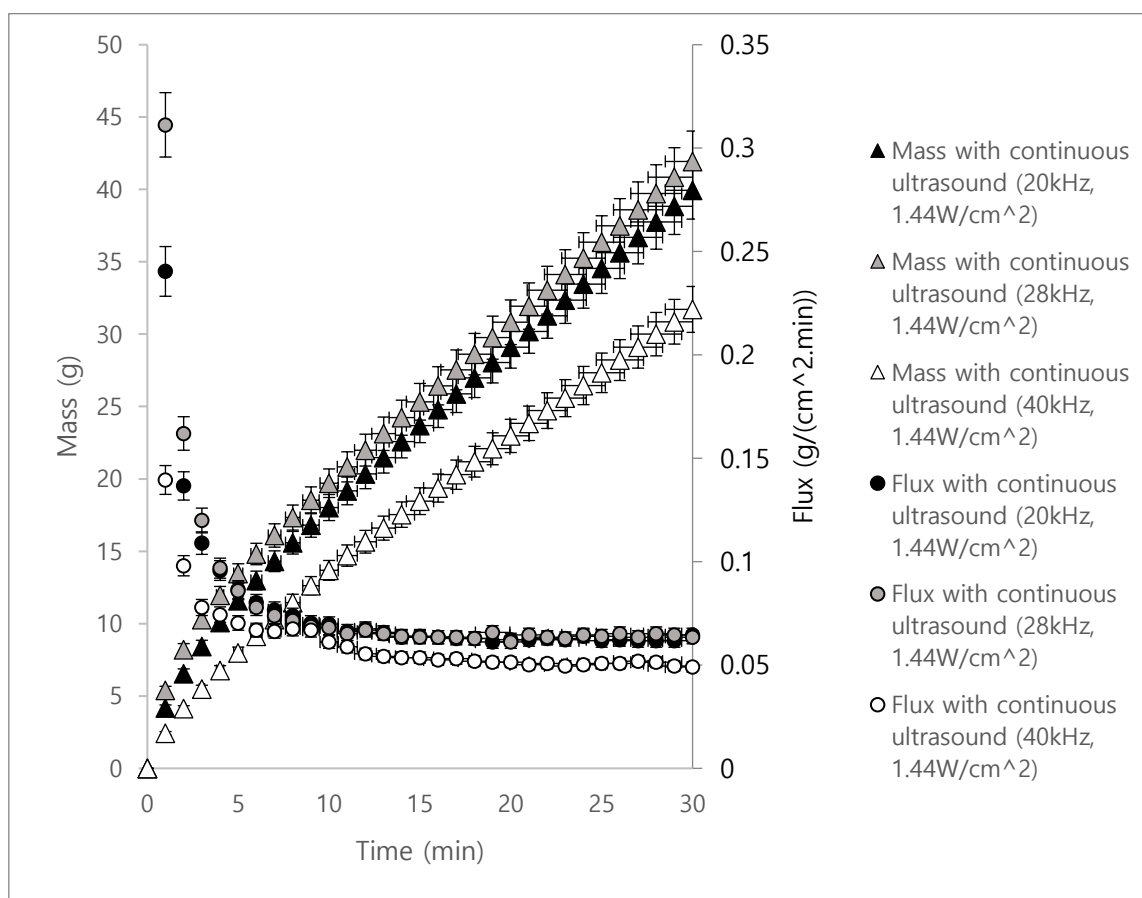
Analysis in ultrasonic power intensity
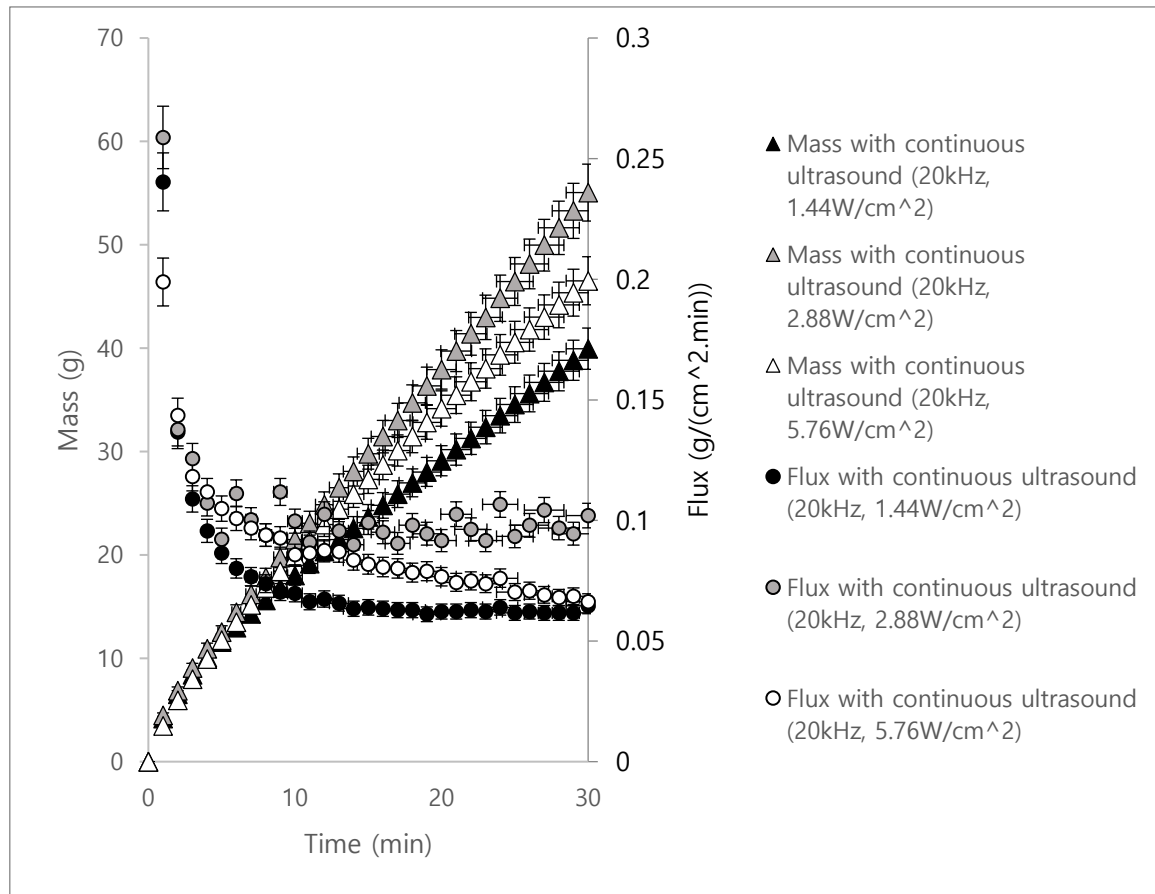
Figure A_1 *- Cumulative mass and change in flux of permeate solution at ultrasonic frequency of 20kHz*
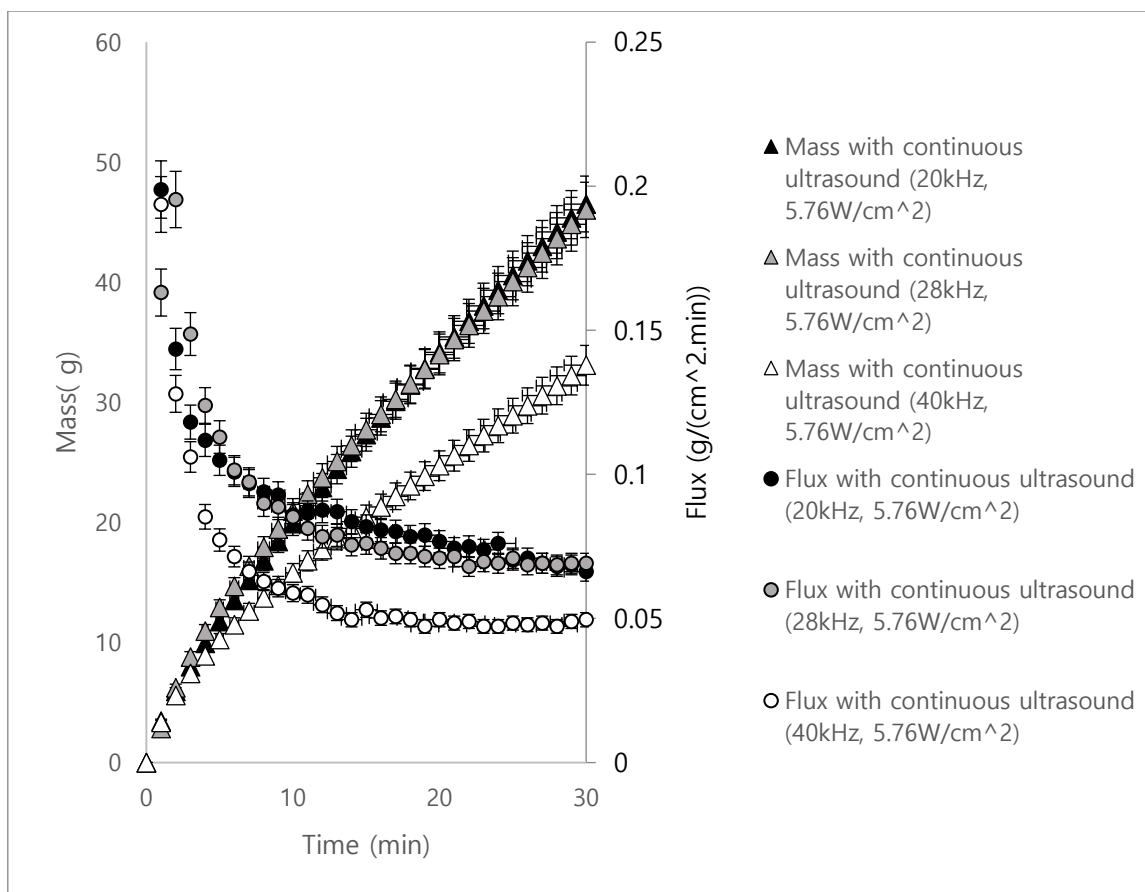
Figure A_2 *- Cumulative mass and change in flux of permeate solution at ultrasonic frequency of 40kHz*
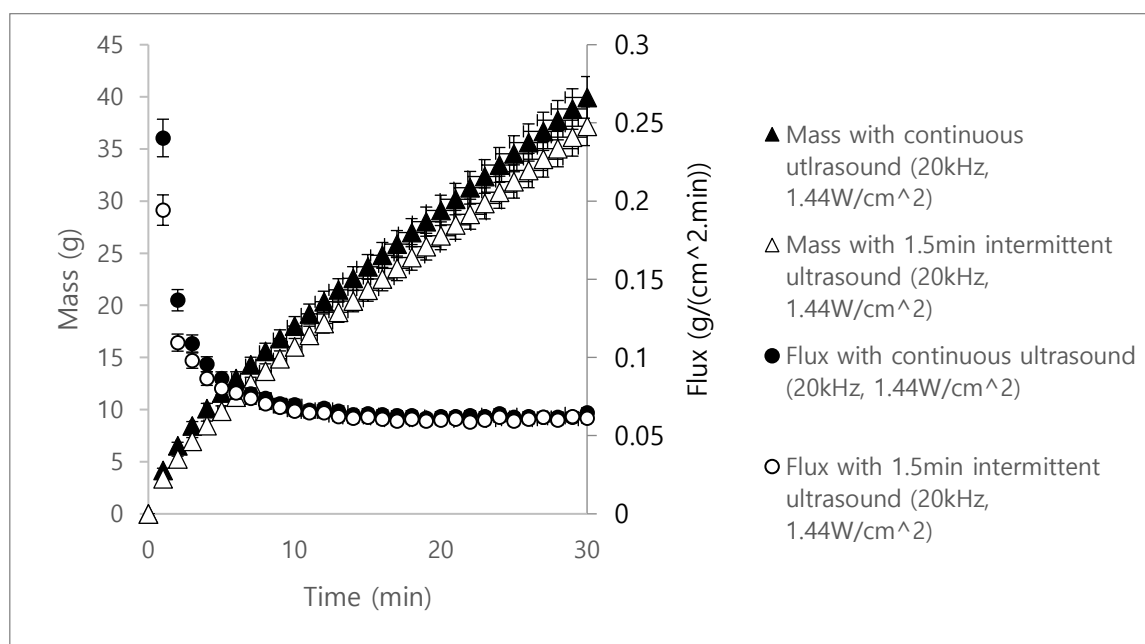
Analysis in ultrasonic frequency

Figure A_3 - *Cumulative mass and change in flux of permeate solution at ultrasonic power intensity of* $1.44 W/cm^2$

Figure A_4 *- Cumulative mass and change in flux of permeate solution at ultrasonic power intensity of $5.76\,W/cm^2$*

Figure A_5 - *Cumulative mass and change in flux of permeate solution at ultrasonic frequency of 20kHz and power intensity of $1.44\,W/cm^2$*
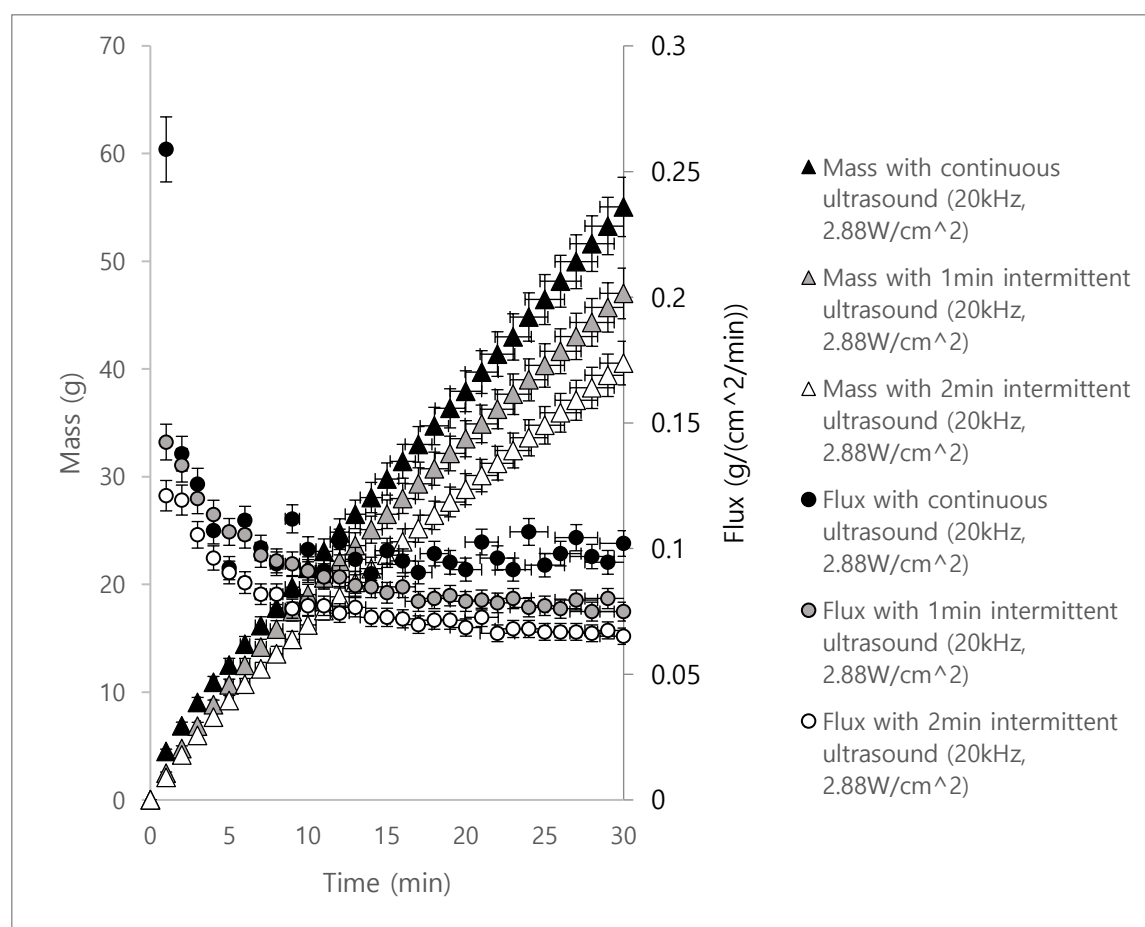
Figure A_6 - *Cumulative mass and change in flux of permeate solution at ultrasonic frequency of 20kHz and power intensity of* $2.88\,W/cm^2$
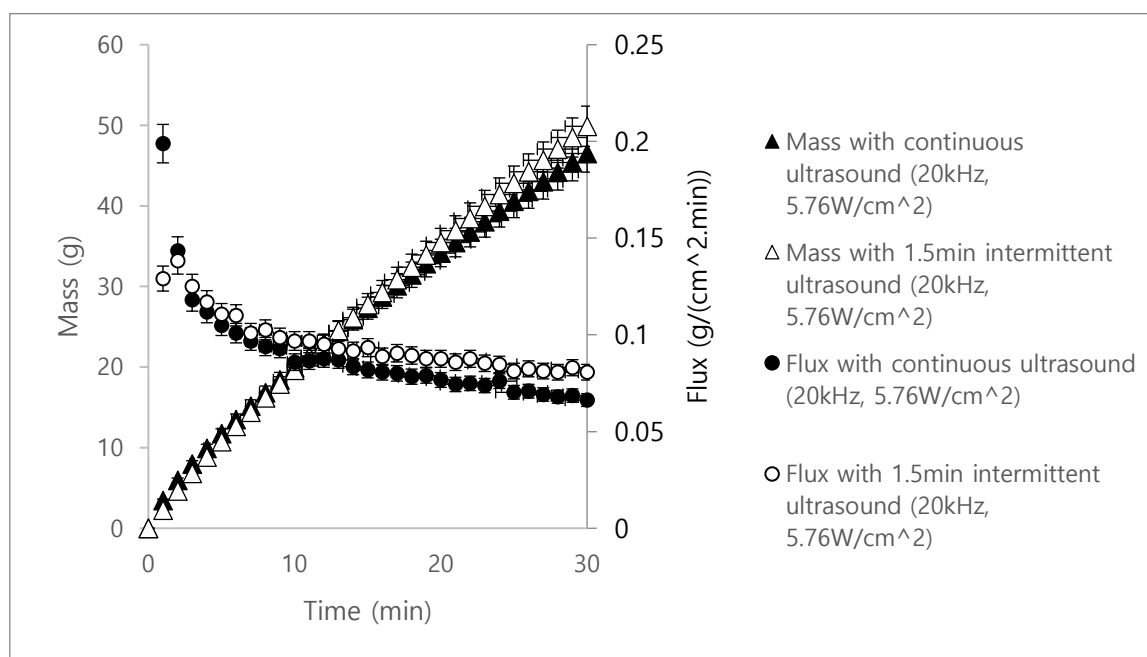
Figure A_7 - *Cumulative mass and change in flux of permeate solution at ultrasonic frequency of 20kHz and power intensity of* $5.76\,W/cm^2$
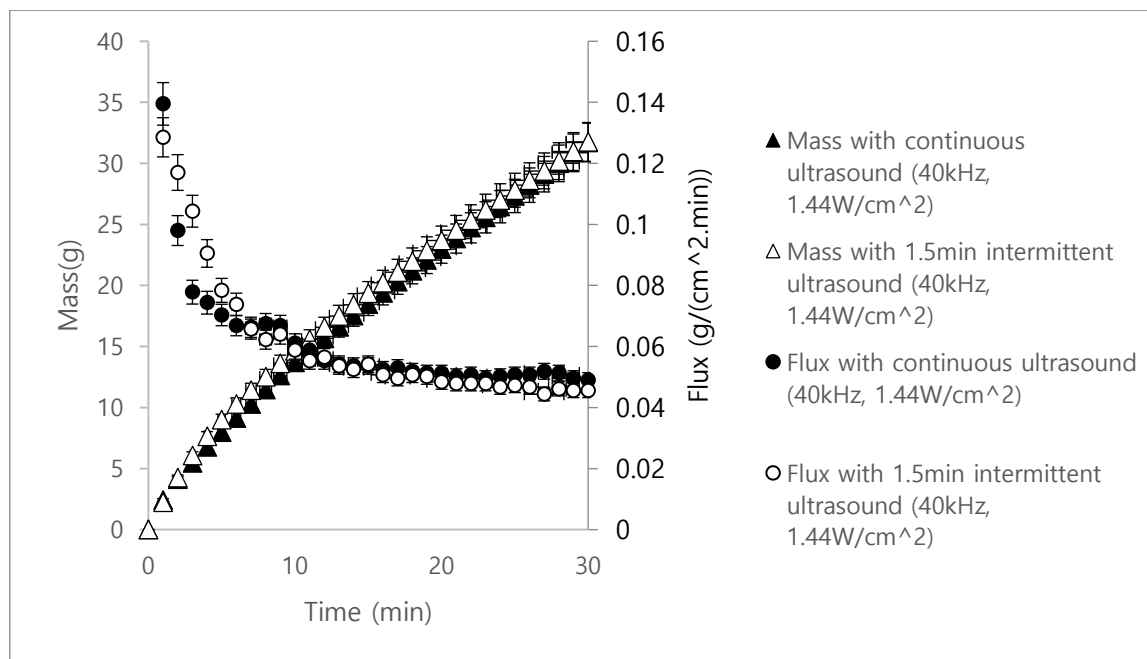
Figure A_8 - *Cumulative mass and change in flux of permeate solution at ultrasonic frequency of 40kHz and power intensity of* $1.44\,W/cm^2$
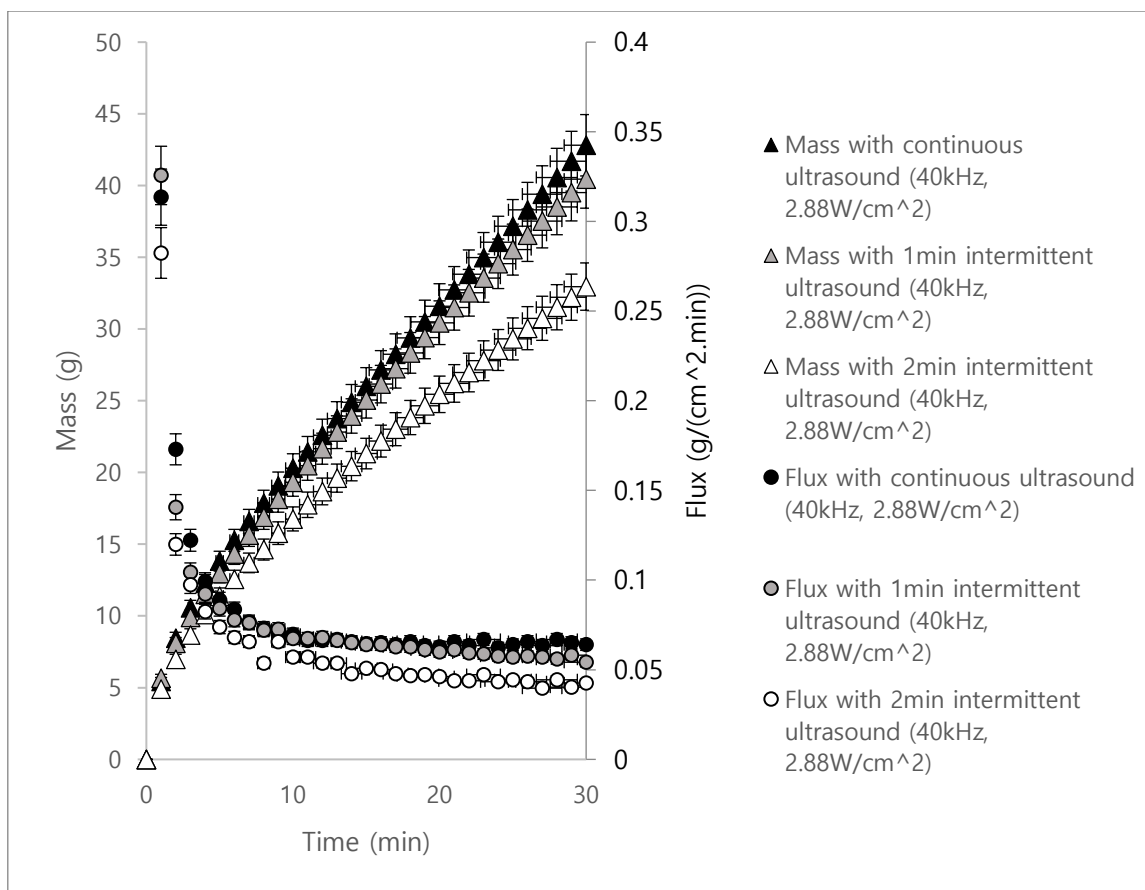
Figure A_9 - *Cumulative mass and change in flux of permeate solution at ultrasonic frequency of 40kHz and power intensity of* $2.88\,W\,/cm^2$
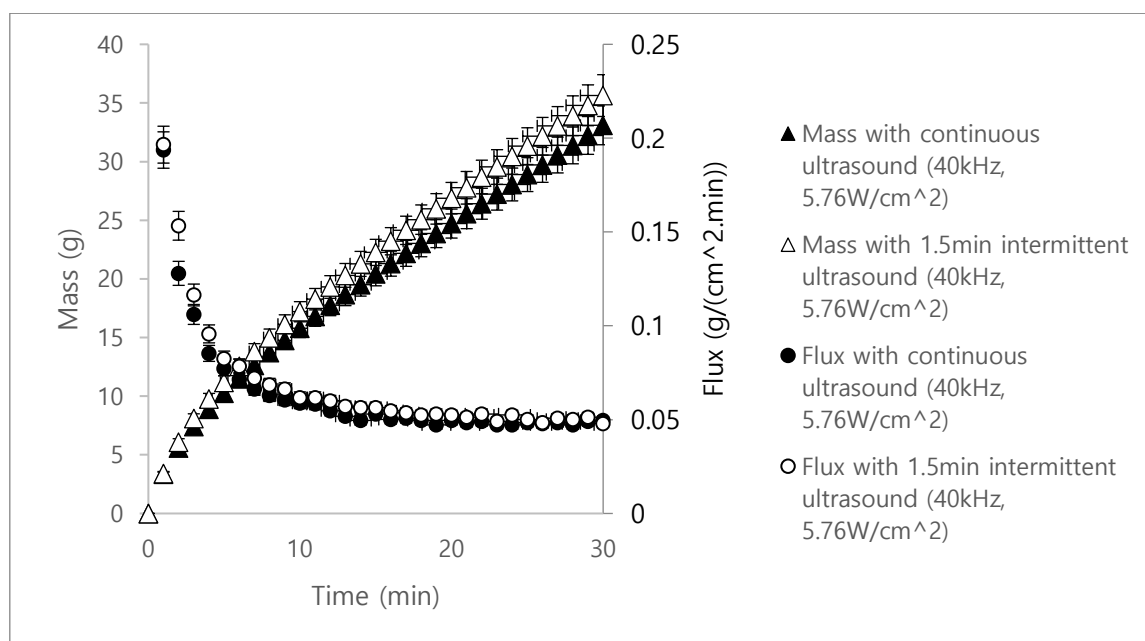
Figure A_10 - *Cumulative mass and change in flux of permeate solution at ultrasonic frequency of 40kHz and power intensity of* $5.76\,W\,/cm^2$

Appendix B List of average particle size in permeate solution

<u>Ultrasonic conditions in Box-Behnken design</u>

Ultrasonic condition	Average particle size (nm)
Continuous (20kHz, 1.44 W/cm^2)	200.5
1.5min intermittent (20kHz, 1.44 W/cm^2)	224
Continuous (20kHz, 2.88 W/cm^2)	240.8
1min intermittent (20kHz, 2.88 W/cm^2)	264.9
2min intermittent (20kHz, 2.88 W/cm^2)	312.7
Continuous (20kHz, 5.76 W/cm^2)	230.4
1.5min intermittent (20kHz, 5.76 W/cm^2)	271.8
Continuous (28kHz, 1.44 W/cm^2)	237.1
1min intermittent (28kHz, 1.44 W/cm^2)	248.8
2min intermittent (28kHz, 1.44 W/cm^2)	368.8
Continuous (28kHz, 2.88 W/cm^2)	310.8
1.5min intermittent (28kHz, 2.88 W/cm^2)	375.7
Continuous (28kHz, 5.76 W/cm^2)	252.5
1min intermittent (28kHz, 5.76 W/cm^2)	282.1
2min intermittent (28kHz, 5.76 W/cm^2)	320.3
Continuous (40kHz, 1.44 W/cm^2)	182.4
1.5min intermittent (40kHz, 1.44 W/cm^2)	197.4
Continuous (40kHz, 2.88 W/cm^2)	225.2
1min intermittent (40kHz, 2.88 W/cm^2)	230.8
2min intermittent (40kHz, 2.88 W/cm^2)	256.4
Continuous (40kHz, 5.76 W/cm^2)	194.8
1.5min intermittent (40kHz, 5.76 W/cm^2)	223

<u>Time intervals of intermittent ultrasound at optimal ultrasonic condition (28kHz, 2.88 W/cm^2)</u>

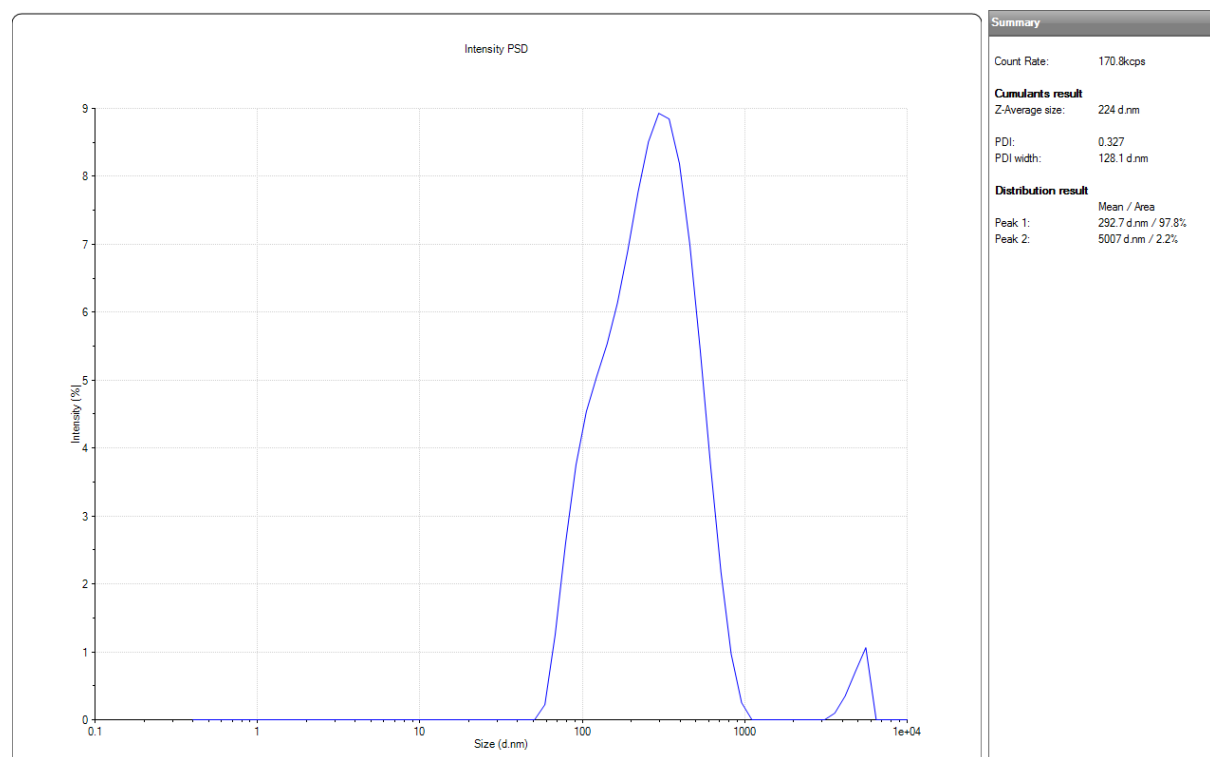| Ultrasonic condition	Average particle size (nm)
Continuous (28kHz, 2.88 W/cm^2)	310.8
30seconds intermittent (28kHz, 2.88 W/cm^2)	316.7
1min intermittent (28kHz, 2.88 W/cm^2)	339.8
1.5min intermittent (28kHz, 2.88 W/cm^2)	375.7
2min intermittent (28kHz, 2.88 W/cm^2)	381.5
2.5min intermittent (28kHz, 2.88 W/cm^2)	427.1
3min intermittent (28kHz, 2.88 W/cm^2)	524.2

Mass concentrations of protein in skim milk

Ultrasonic condition	Average particle size (nm)
0.05% continuous (28kHz, 2.88 W/cm^2)	545.4
0.05% 30seconds intermittent (28kHz, 2.88 W/cm^2)	569.2
0.1% continuous (28kHz, 2.88 W/cm^2)	310.8
0.1% 30seconds intermittent (28kHz, 2.88 W/cm^2)	316.7
0.2% continuous (28kHz, 2.88 W/cm^2)	192.9
0.2% 30seconds intermittent (28kHz, 2.88 W/cm^2)	202.5

Appendix C Graphs of particle size distribution in permeate solution
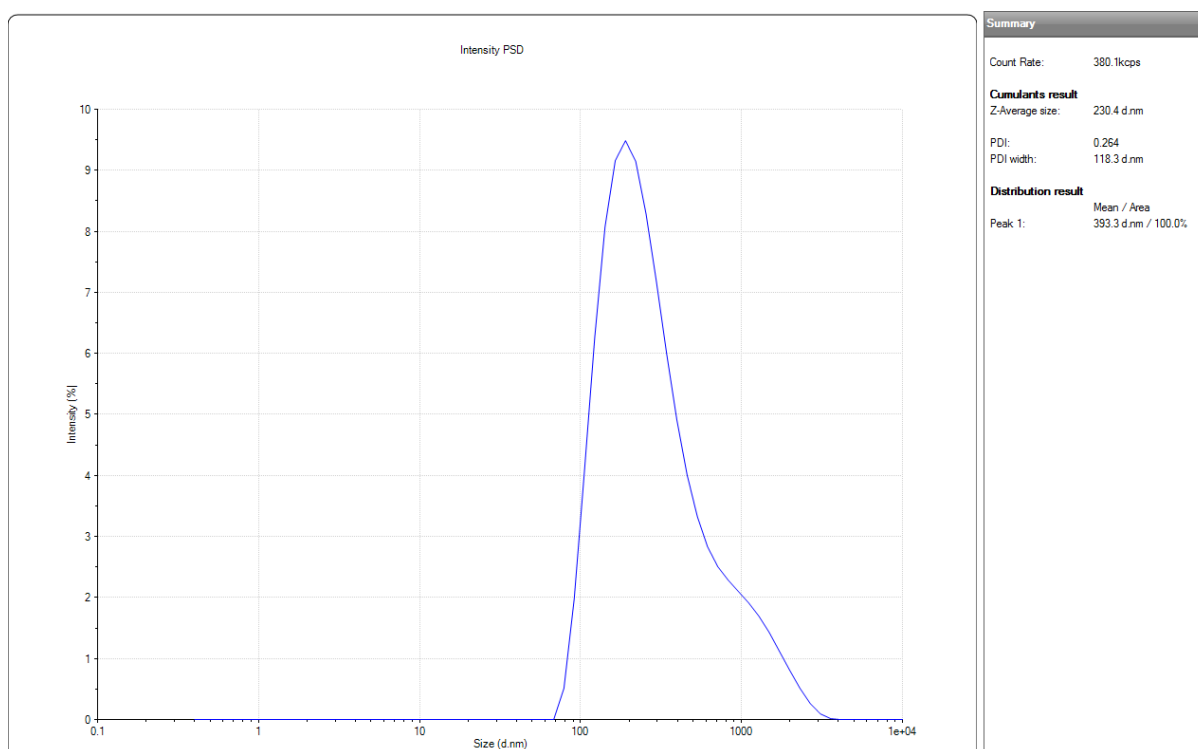
<u>Ultrasonic conditions in Box-Behnken design</u>
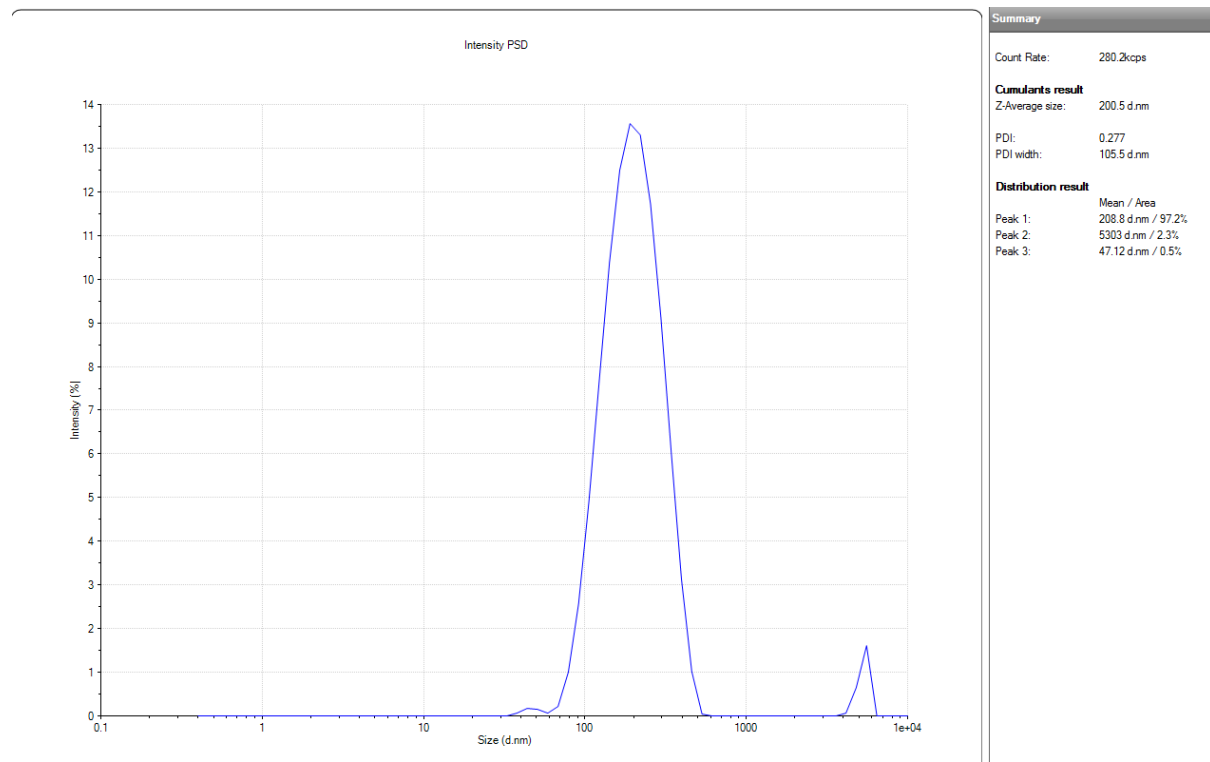
Figure C_1 *- Particle size distribution in permeate solution with continuous ultrasonic condition of 20kHz in frequency and $1.44 \, W/cm^2$ in power intensity*
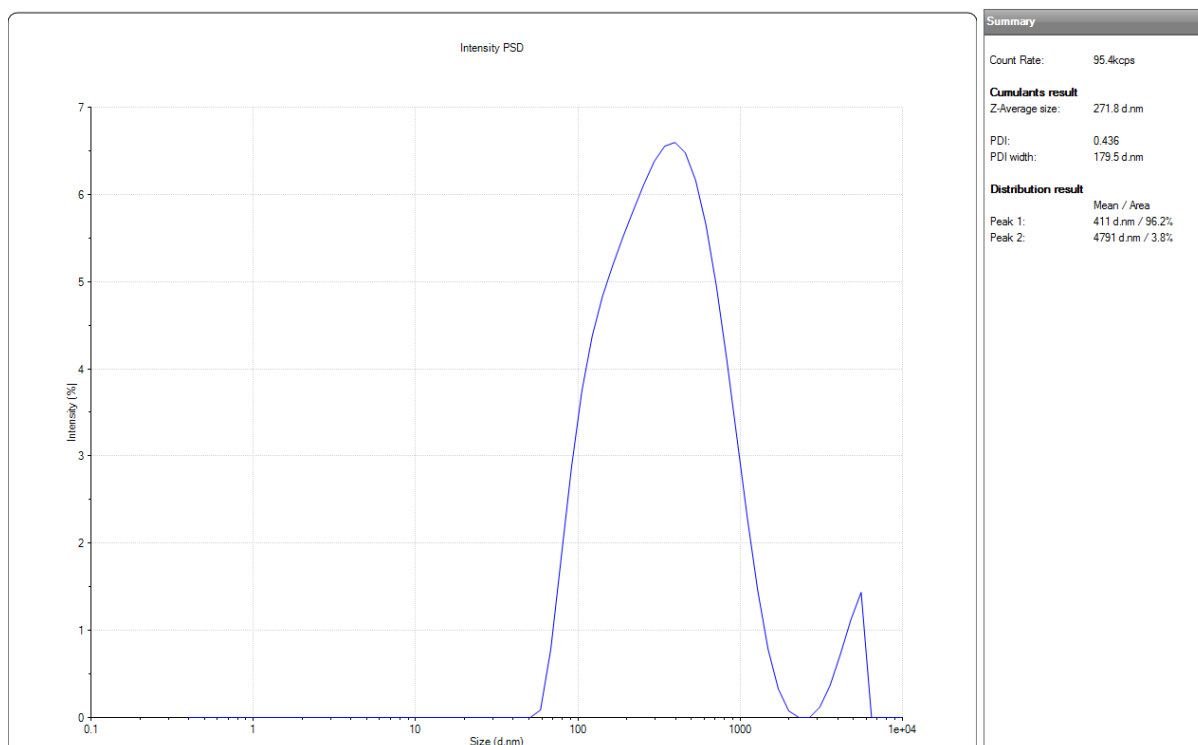
Figure C_2 - *Particle size distribution in permeate solution with intermittent ultrasonic condition of 20kHz in frequency, $1.44\,W/cm^2$ in power intensity, and 1.5minutes in time interval*

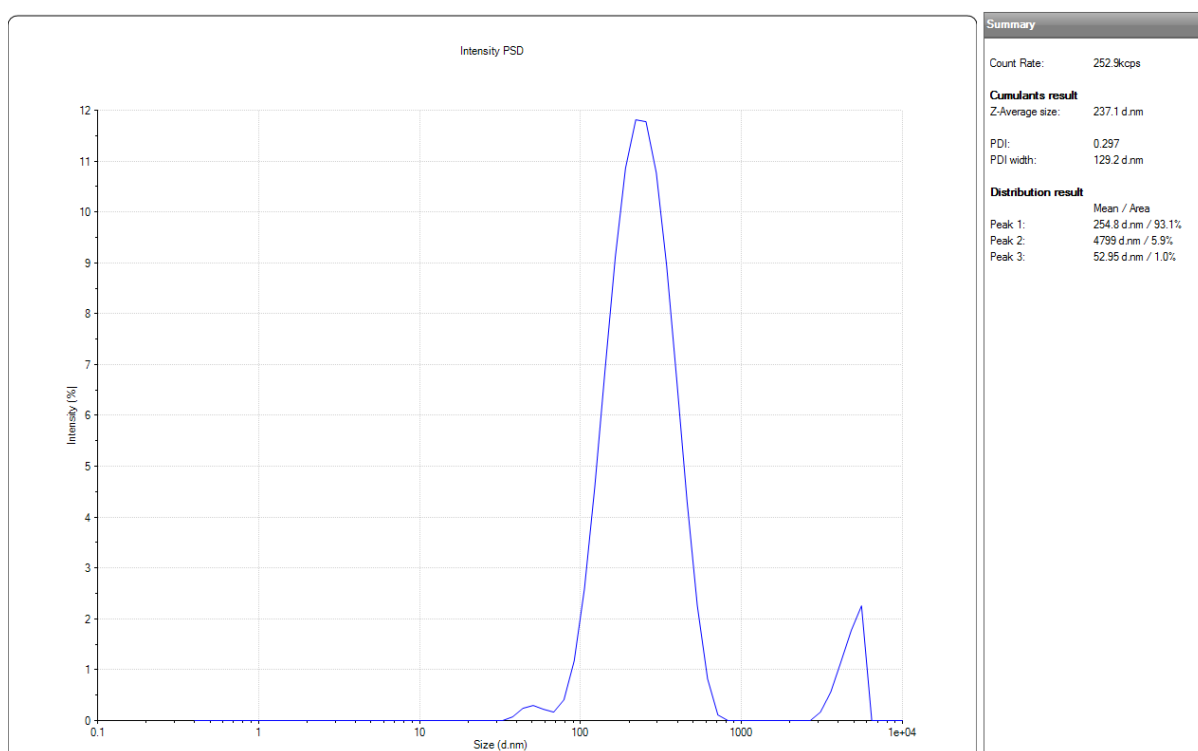Intensity PSD

Summary	
Count Rate:	439.8kcps
Cumulants result	
Z-Average size:	240.8 d.nm
PDI:	0.249
PDI width:	120.1 d.nm
Distribution result	
	Mean / Area
Peak 1:	284.1 d.nm / 97.5%
Peak 2:	5010 d.nm / 2.5%
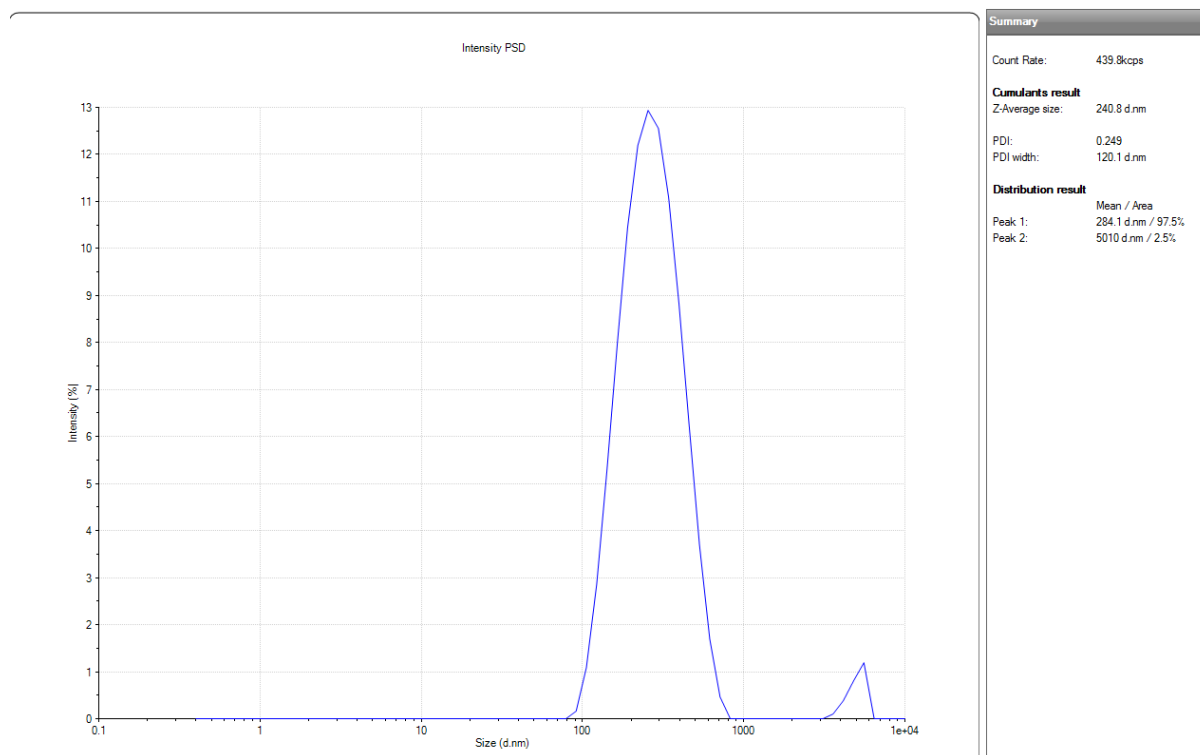
Figure C_3 - *Particle size distribution in permeate solution with continuous ultrasonic condition of 20kHz in frequency and $2.88\,W/cm^2$ in power intensity*
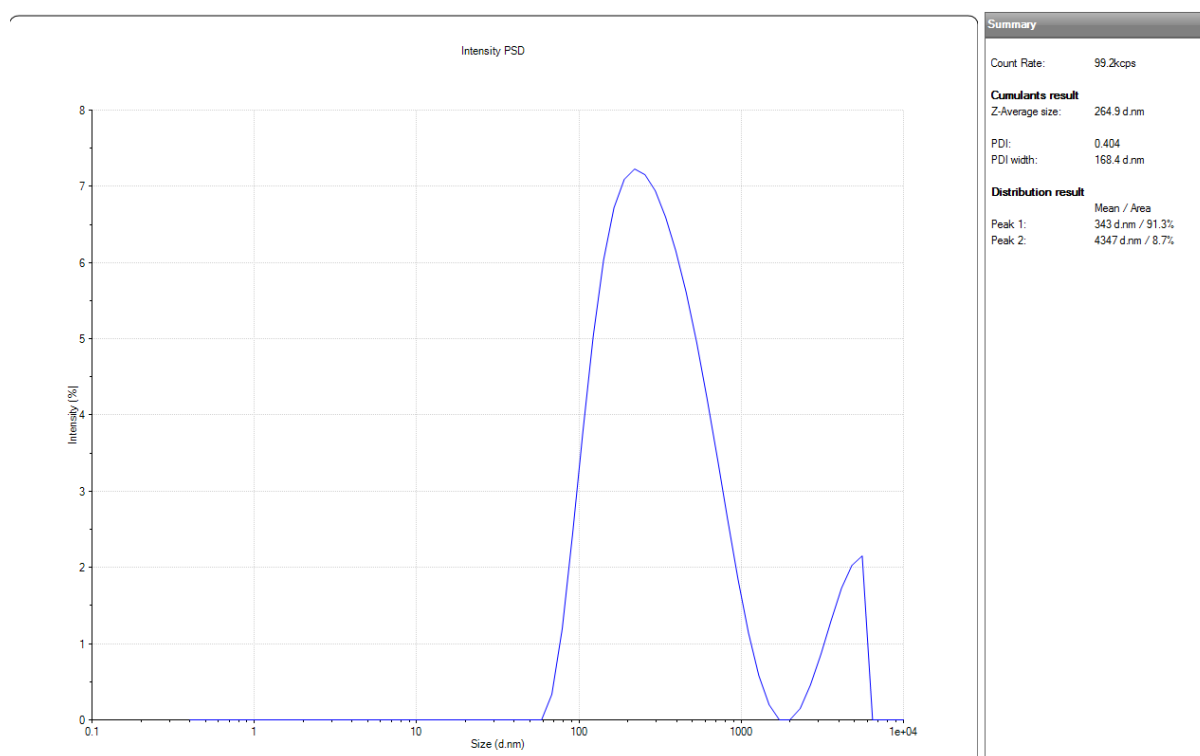
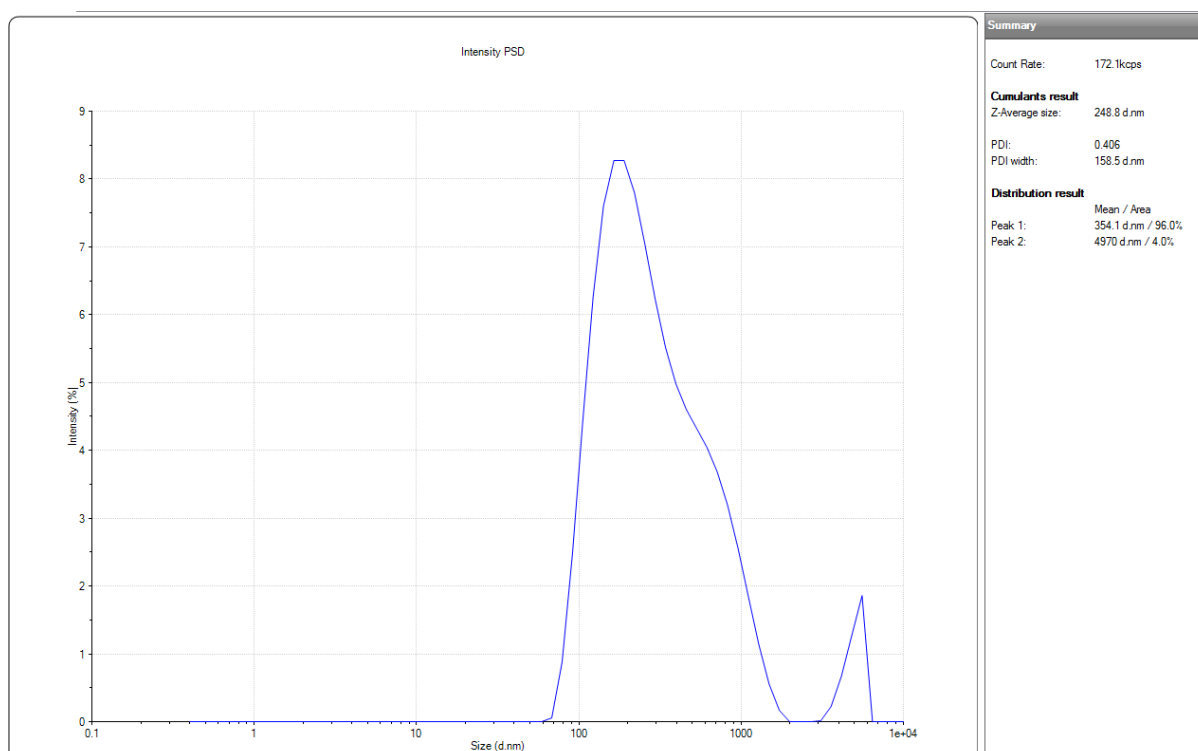**Figure C_4** - *Particle size distribution in permeate solution with intermittent ultrasonic condition of 20kHz in frequency, $2.88\,W/cm^2$ in power intensity, and 1minute in time interval*
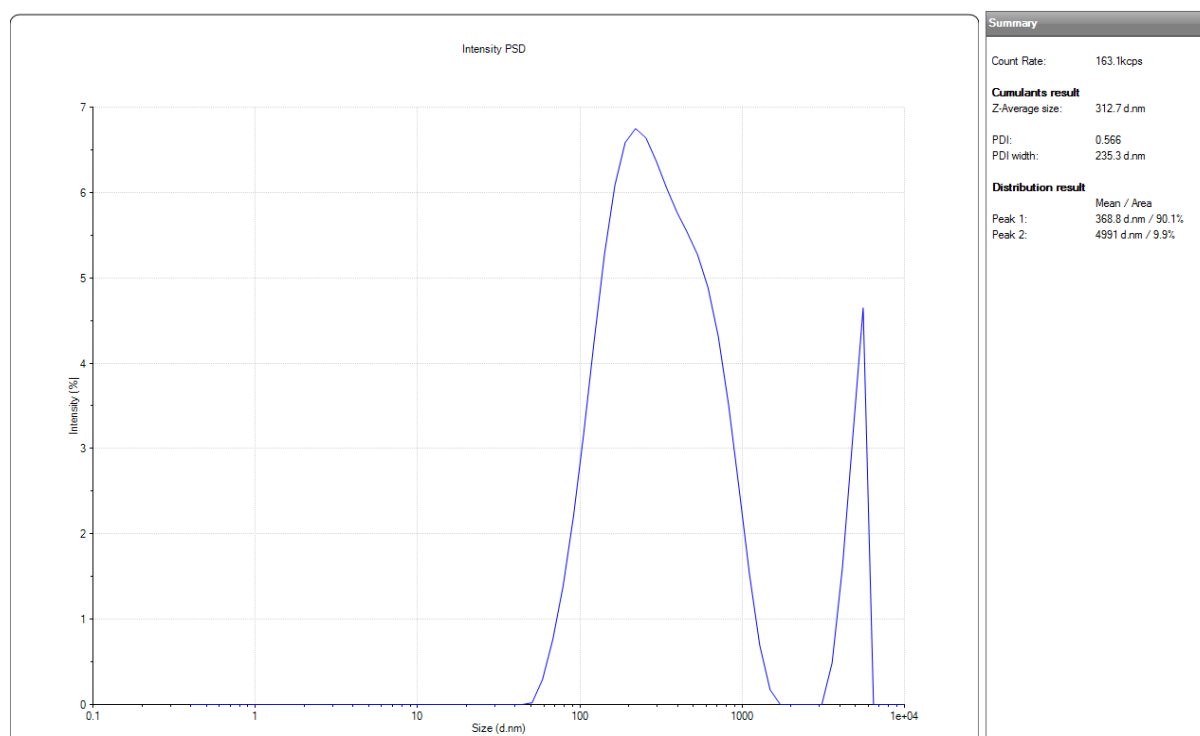
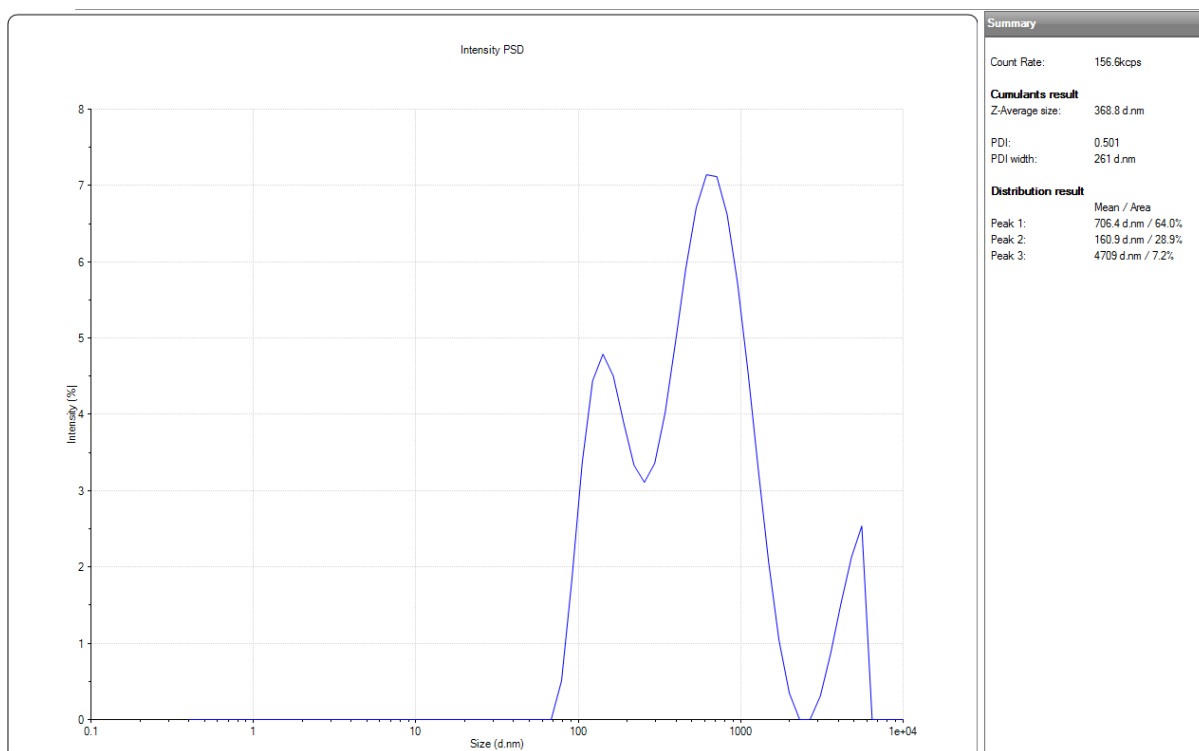**Figure C_5** - *Particle size distribution in permeate solution with intermittent ultrasonic condition of 20kHz in frequency, $2.88\,W/cm^2$ in power intensity, and 2minutes in time interval*

Figure C_6 - *Particle size distribution in permeate solution with continuous ultrasonic condition of 20kHz in frequency and 5.76 W /cm² in power intensity*

Figure C_7 - *Particle size distribution in permeate solution with intermittent ultrasonic condition of 20kHz in frequency, 5.76 W /cm² in power intensity, and 1.5minutes in time interval*
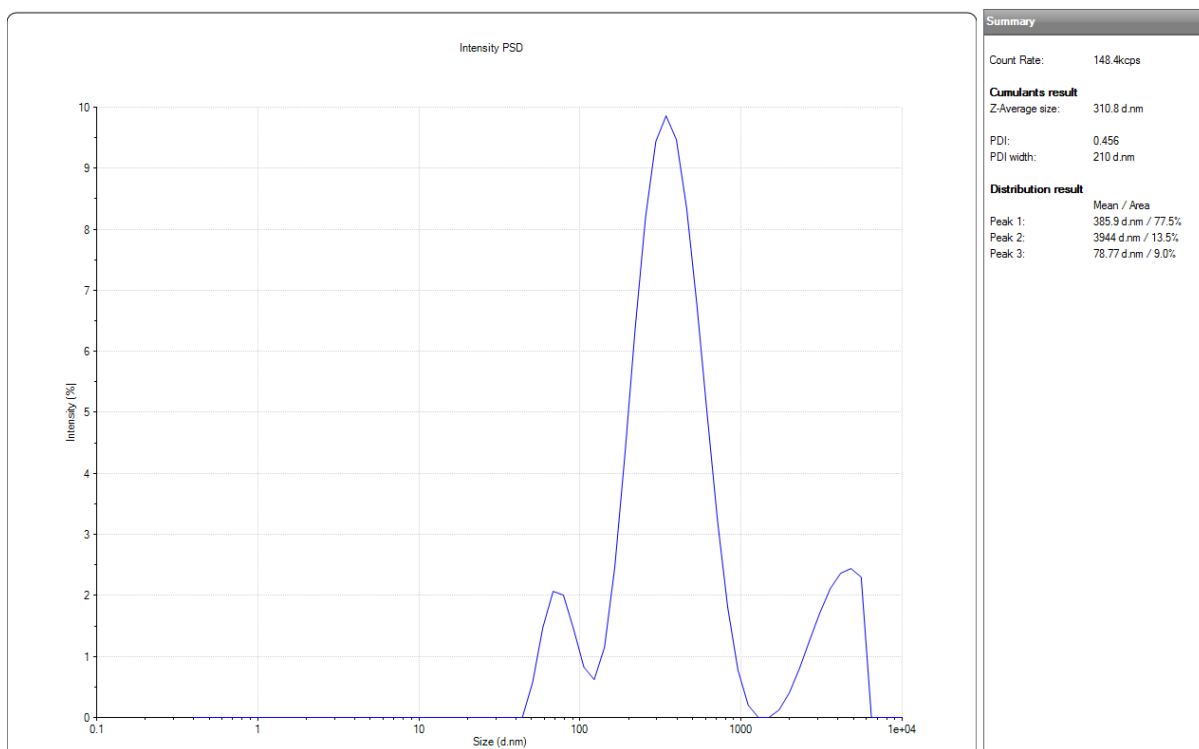
Figure C_8 - *Particle size distribution in permeate solution with continuous ultrasonic condition of 28kHz in frequency and $1.44\,W/cm^2$ in power intensity*

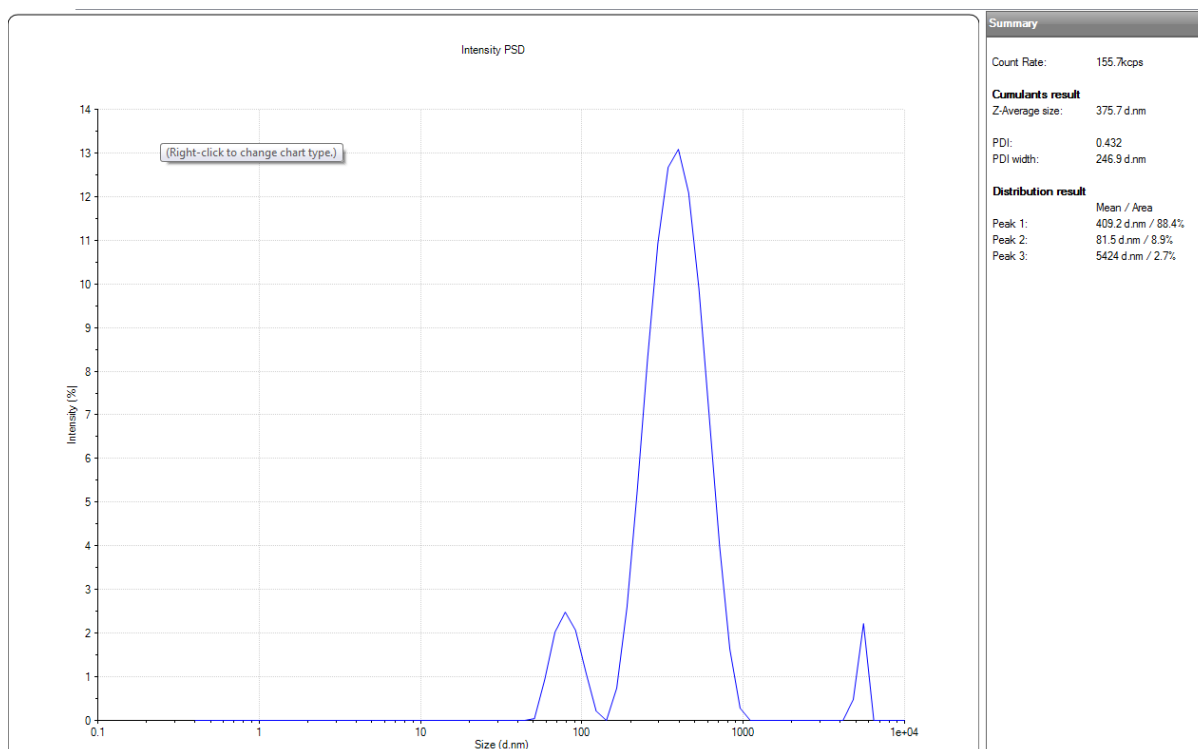**Figure C_9** - *Particle size distribution in permeate solution with intermittent ultrasonic condition of 28kHz in frequency, $1.44\,W/cm^2$ in power intensity, and 1minute in time interval*
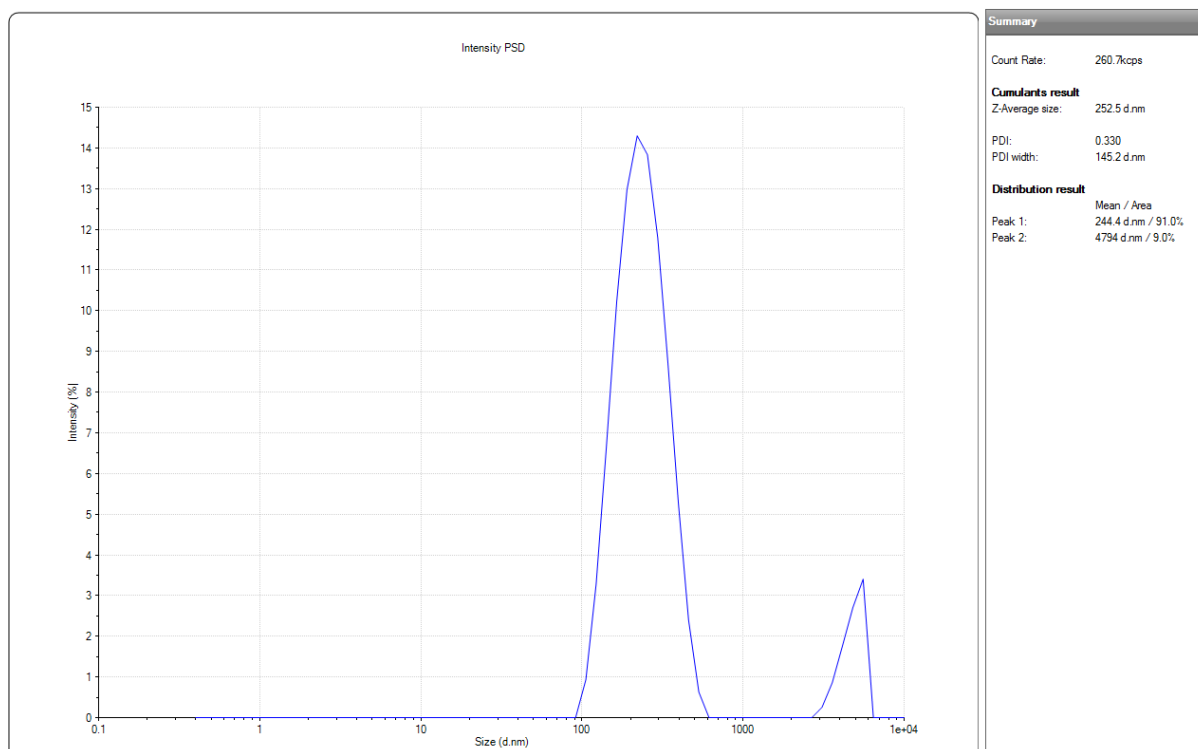
Figure C_10 - *Particle size distribution in permeate solution with intermittent ultrasonic condition of 28kHz in frequency, $1.44\,W/cm^2$ in power intensity, and 2minutes in time interval*

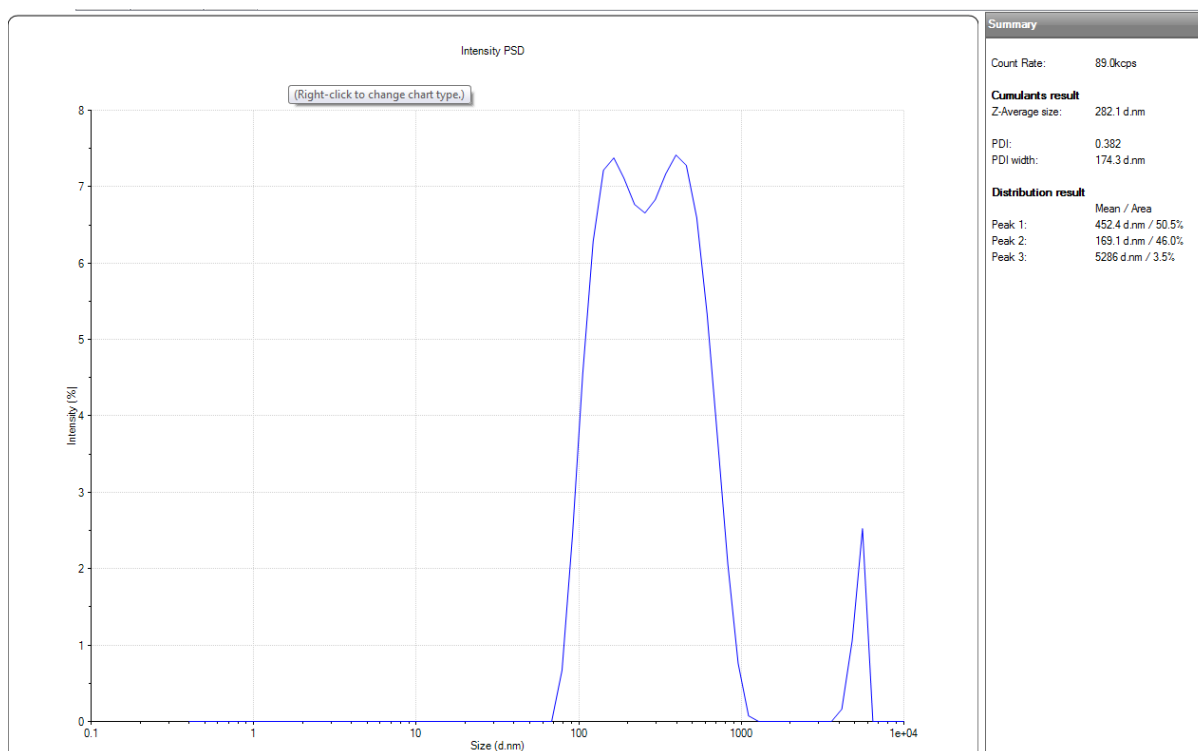**Figure C_11** - *Particle size distribution in permeate solution with continuous ultrasonic condition of 28kHz in frequency and $2.88\,W/cm^2$ in power intensity*
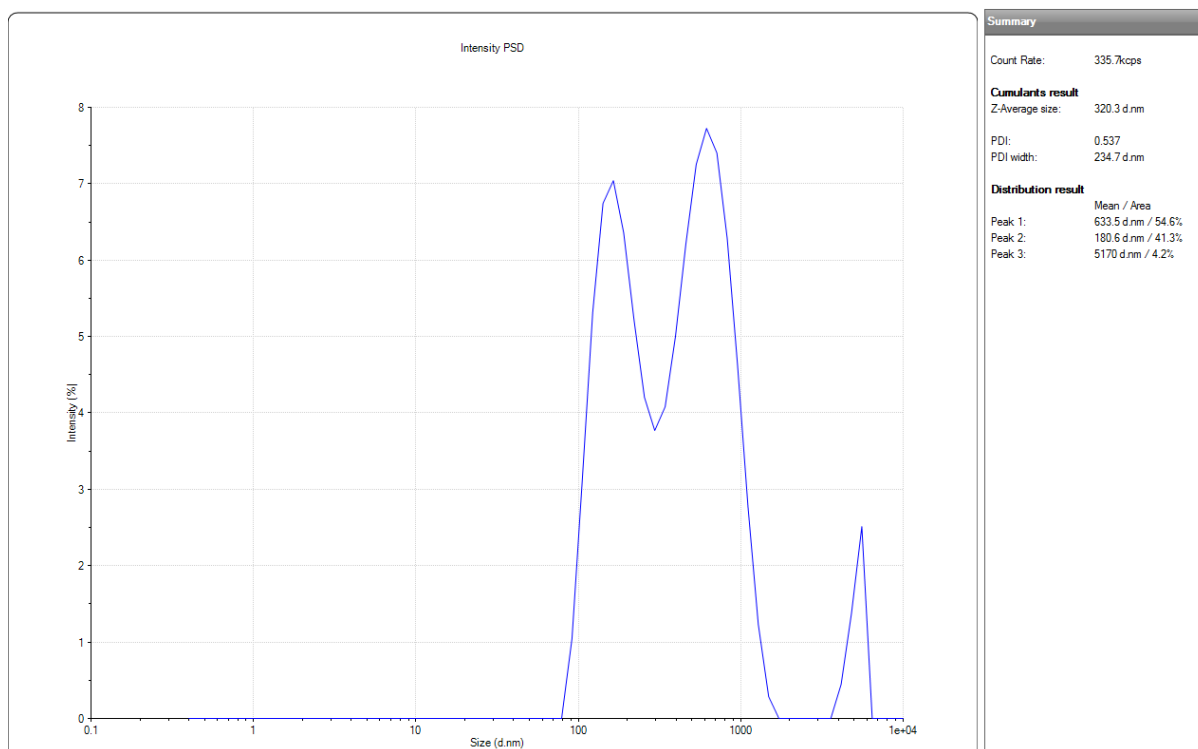
Figure C_12 - *Particle size distribution in permeate solution with intermittent ultrasonic condition of 28kHz in frequency, 2.88 W/cm² in power intensity, and 1.5minutes in time interval*
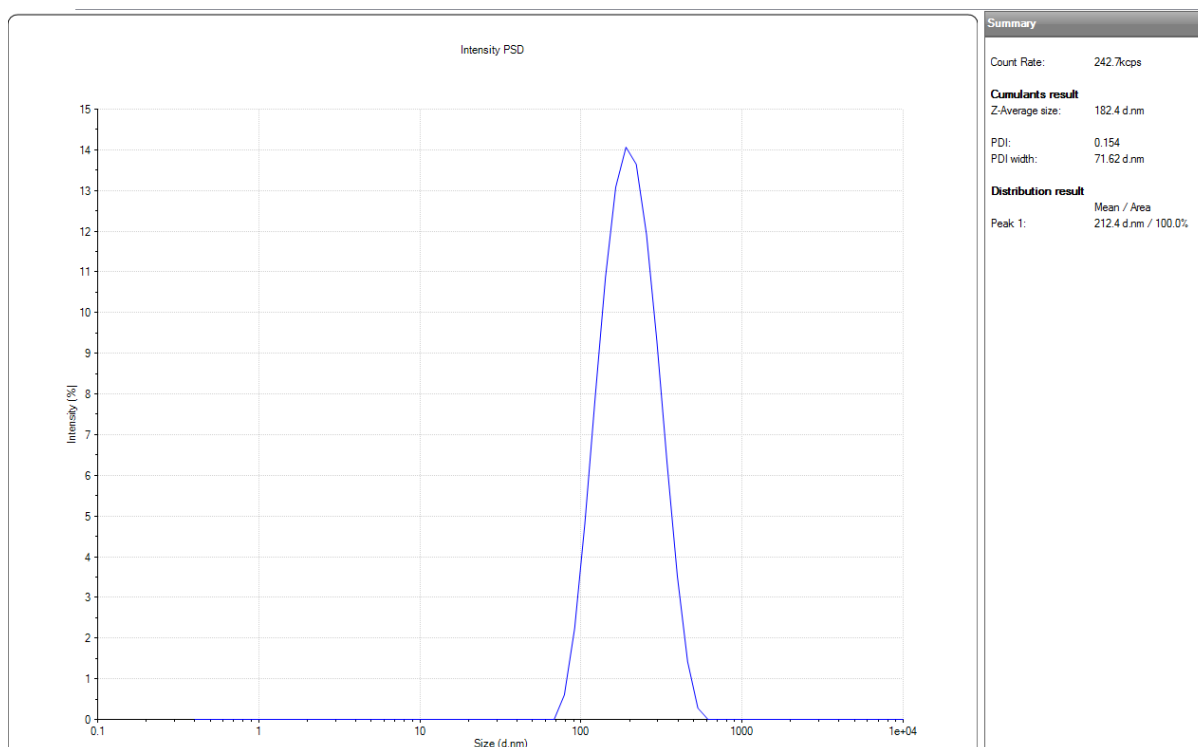

Figure C_13 - *Particle size distribution in permeate solution with continuous ultrasonic condition of 28kHz in frequency and 5.76 W/cm² in power intensity*

Figure C_14 *- Particle size distribution in permeate solution with intermittent ultrasonic condition of 28kHz in frequency, $5.76\,W/cm^2$ in power intensity, and 1minute in time interval*

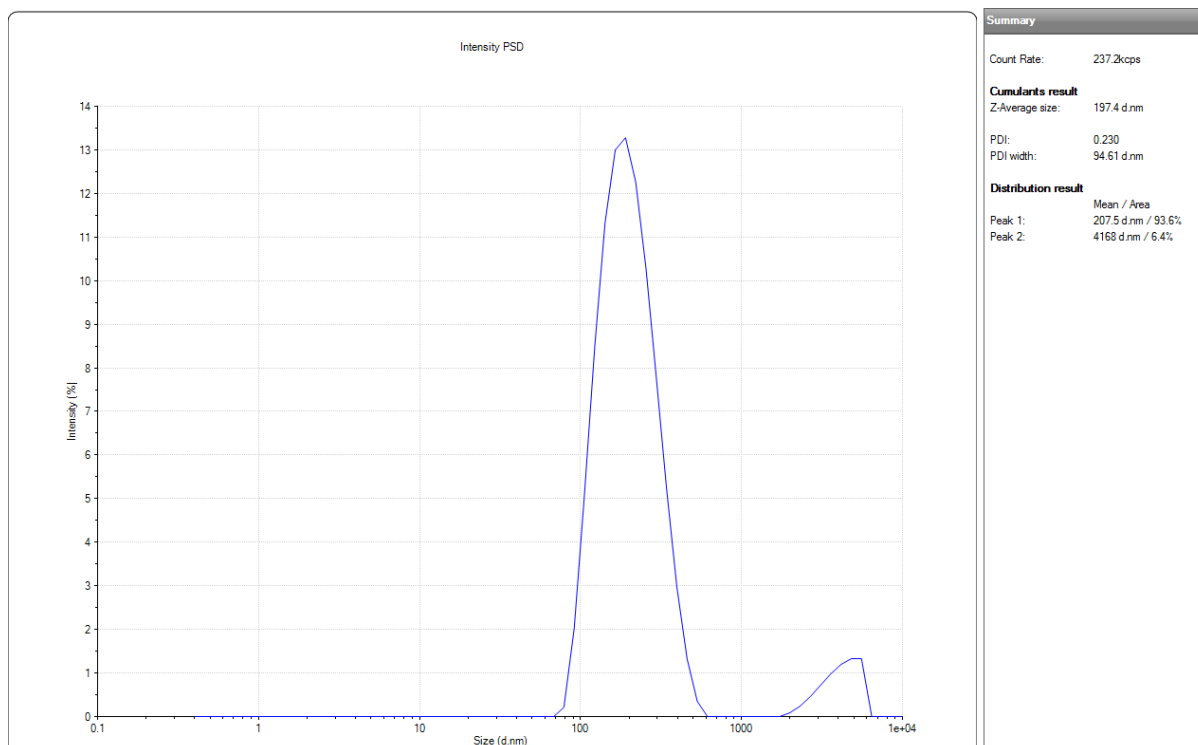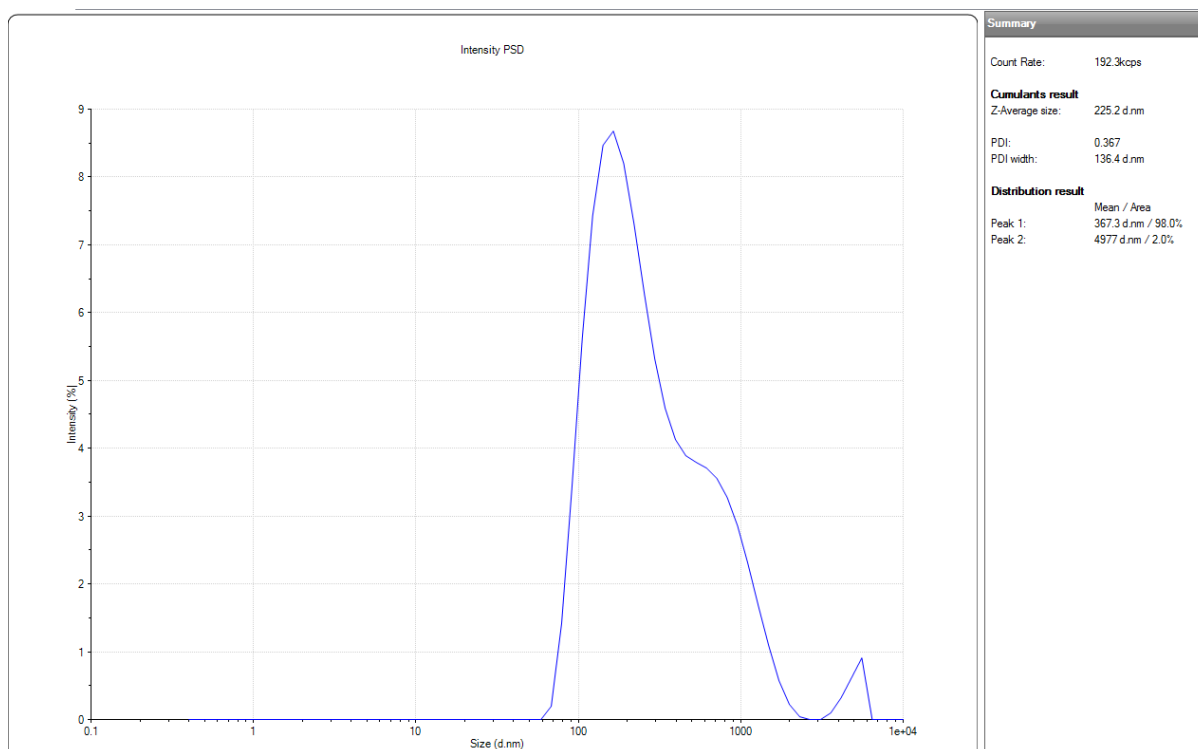***Figure C_15*** *- Particle size distribution in permeate solution with intermittent ultrasonic condition of 28kHz in frequency, $5.76\,W/cm^2$ in power intensity, and 2minutes in time interval*

Figure C_16 - *Particle size distribution in permeate solution with continuous ultrasonic condition of 40kHz in frequency and 1.44 W/cm^2 in power intensity*

Figure C_17 - *Particle size distribution in permeate solution with intermittent ultrasonic condition of 40kHz in frequency, 1.44 W/cm^2 in power intensity, and 1.5minutes in time interval*
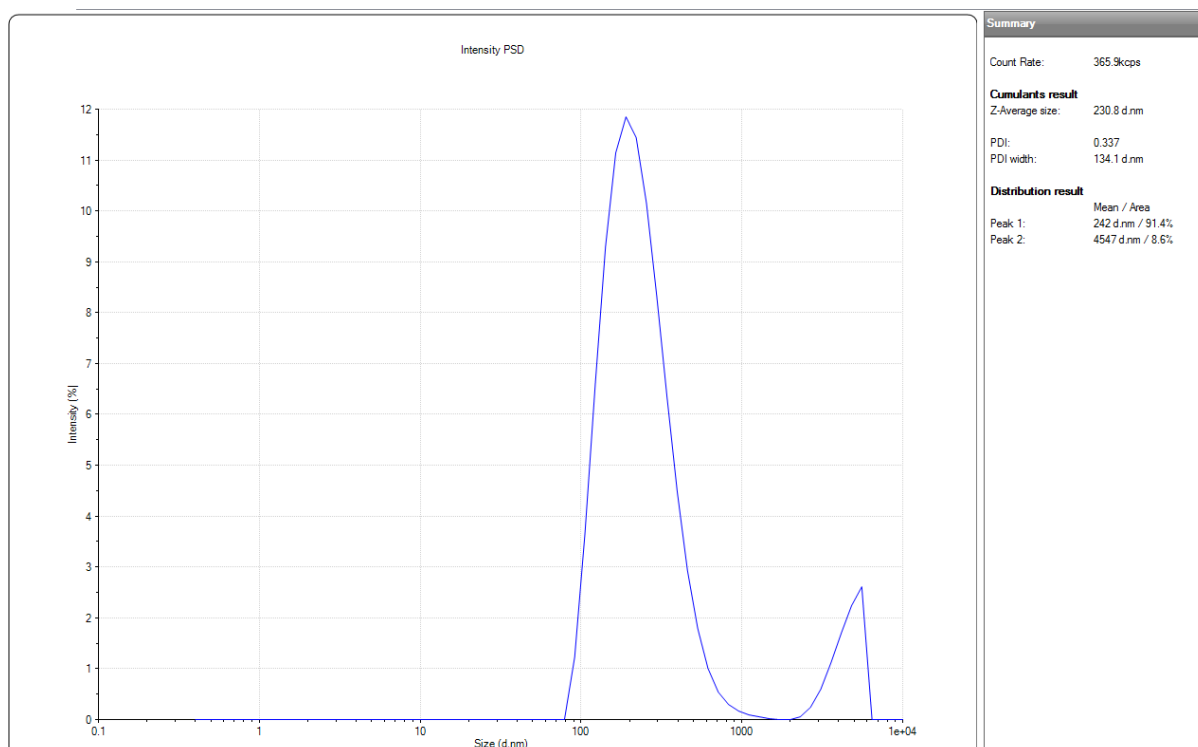
Figure C_18 - *Particle size distribution in permeate solution with continuous ultrasonic condition of 40kHz in frequency and 2.88 W /cm² in power intensity*

Figure C_19 - *Particle size distribution in permeate solution with intermittent ultrasonic condition of 40kHz in frequency, 2.88 W /cm² in power intensity, and 1minute in time interval*

Figure C_20 *- Particle size distribution in permeate solution with intermittent ultrasonic condition of 40kHz in frequency, 2.88 W/cm² in power intensity, and 2minutes in time interval*

Figure C_21 *- Particle size distribution in permeate solution with continuous ultrasonic condition of 40kHz in frequency and 5.76 W/cm² in power intensity*
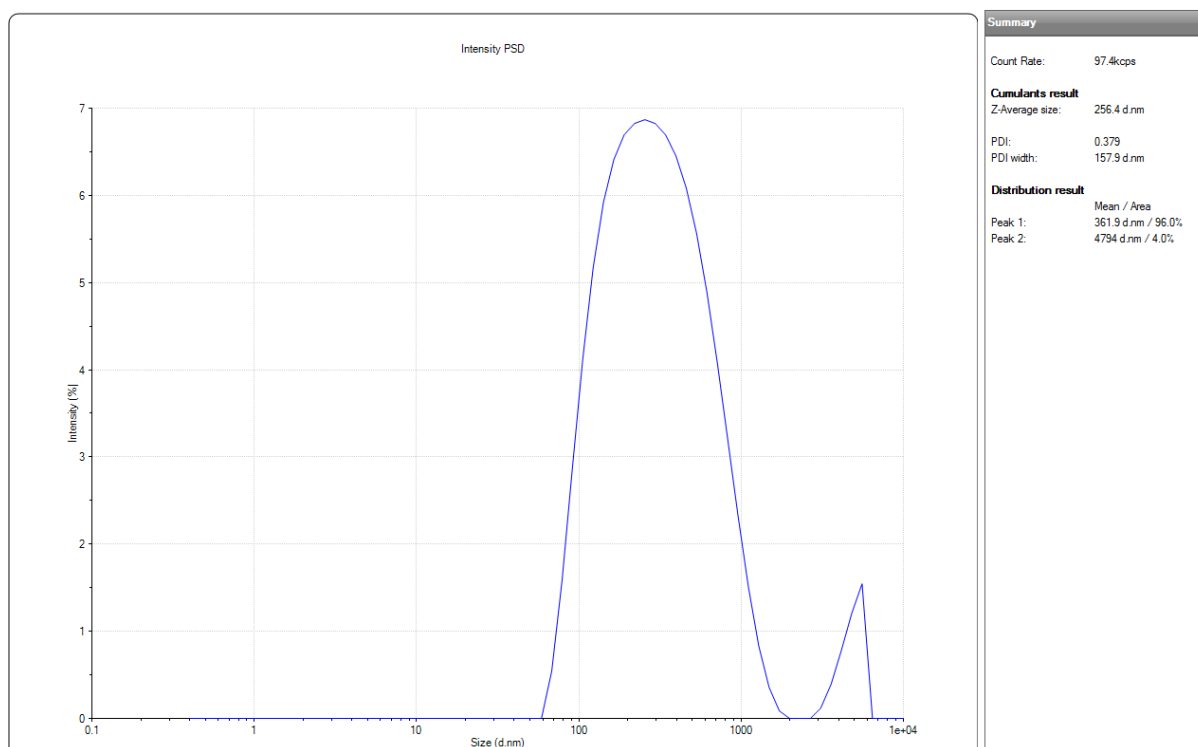
Figure C_22 *- Particle size distribution in permeate solution with intermittent ultrasonic condition of 40kHz in frequency, $5.76 \, W/cm^2$ in power intensity, and 1.5minutes in time interval*
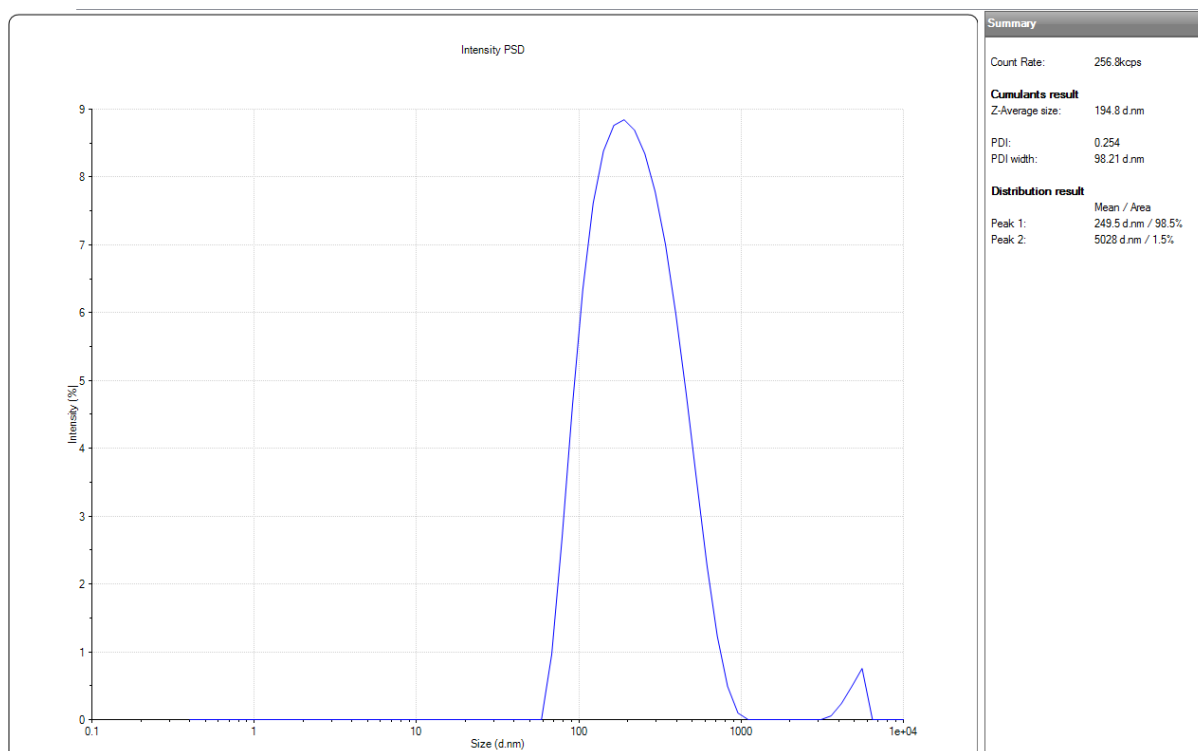
Figure C_23 *- Particle size distribution in permeate solution with intermittent ultrasonic condition of 28kHz in frequency, $2.88 \, W/cm^2$ in power intensity, and 30seconds in time interval*

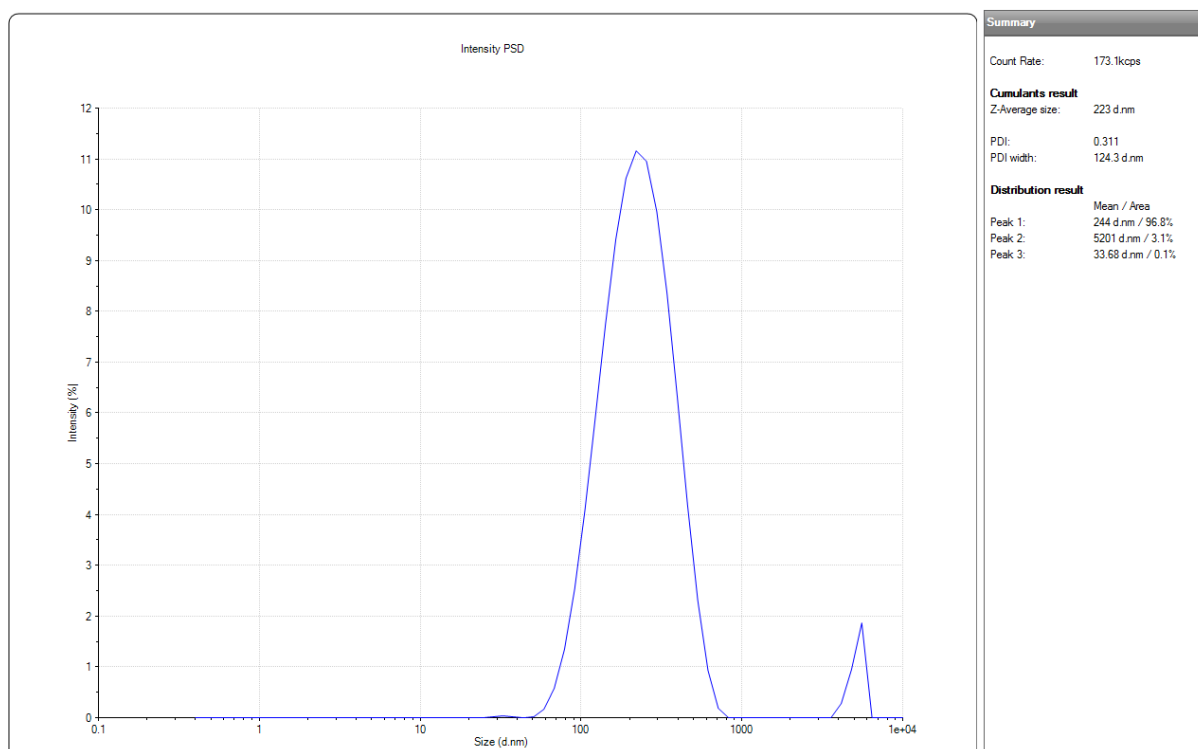**Figure C_25** - *Particle size distribution in permeate solution with intermittent ultrasonic condition of 28kHz in frequency, $2.88\,W/cm^2$ in power intensity, and 2minutes in time interval*

Figure C_26 *- Particle size distribution in permeate solution with intermittent ultrasonic condition of 28kHz in frequency, 2.88 W / cm² in power intensity, and 2.5minutes in time interval*
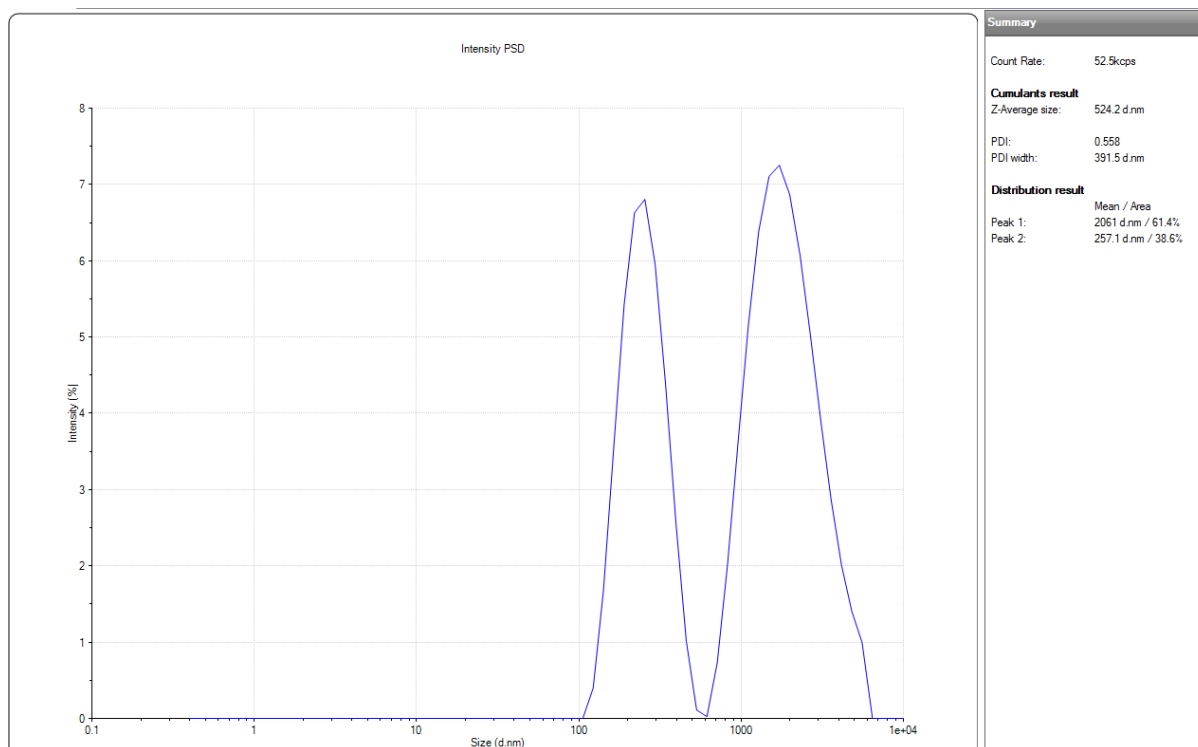
Figure C_27 *- Particle size distribution in permeate solution with intermittent ultrasonic condition of 28kHz in frequency, 2.88 W / cm² in power intensity, and 3minutes in time interval*

117

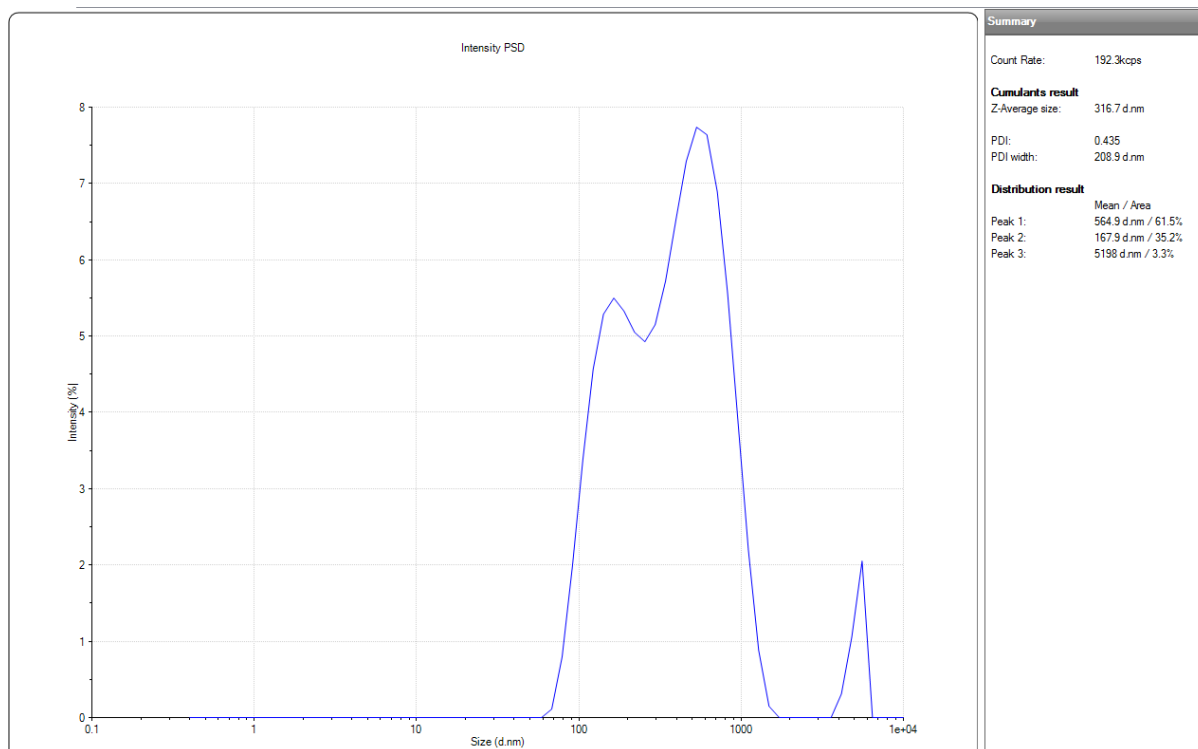Mass concentrations of protein in skim milk
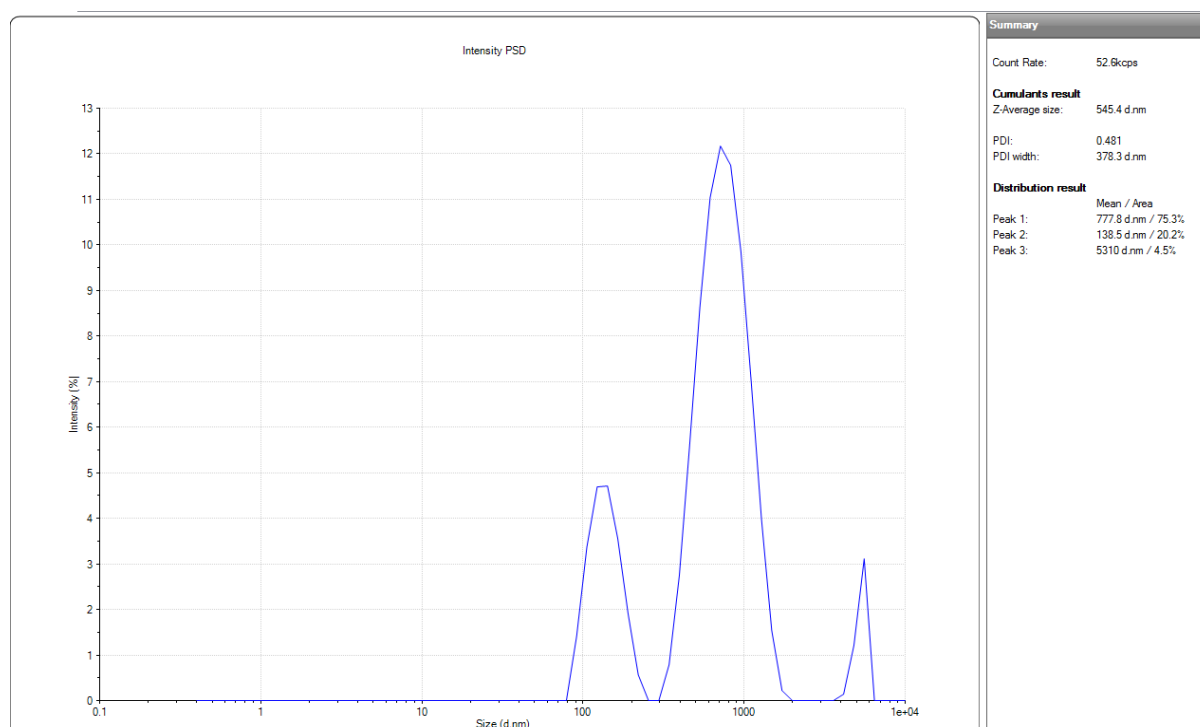
Figure C_28 *- Particle size distribution in permeate solution with continuous ultrasonic condition of 28kHz in frequency, 2.88 W/cm² in power intensity and with 0.05% mass concentration of protein in skim milk*
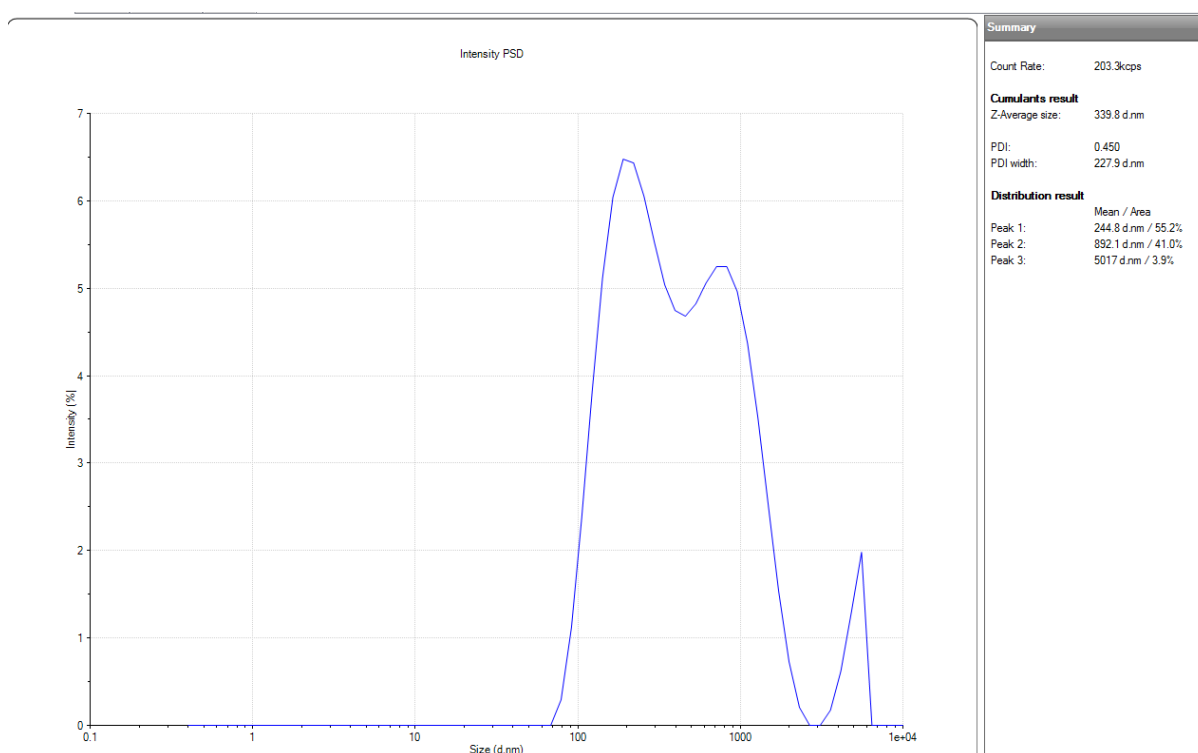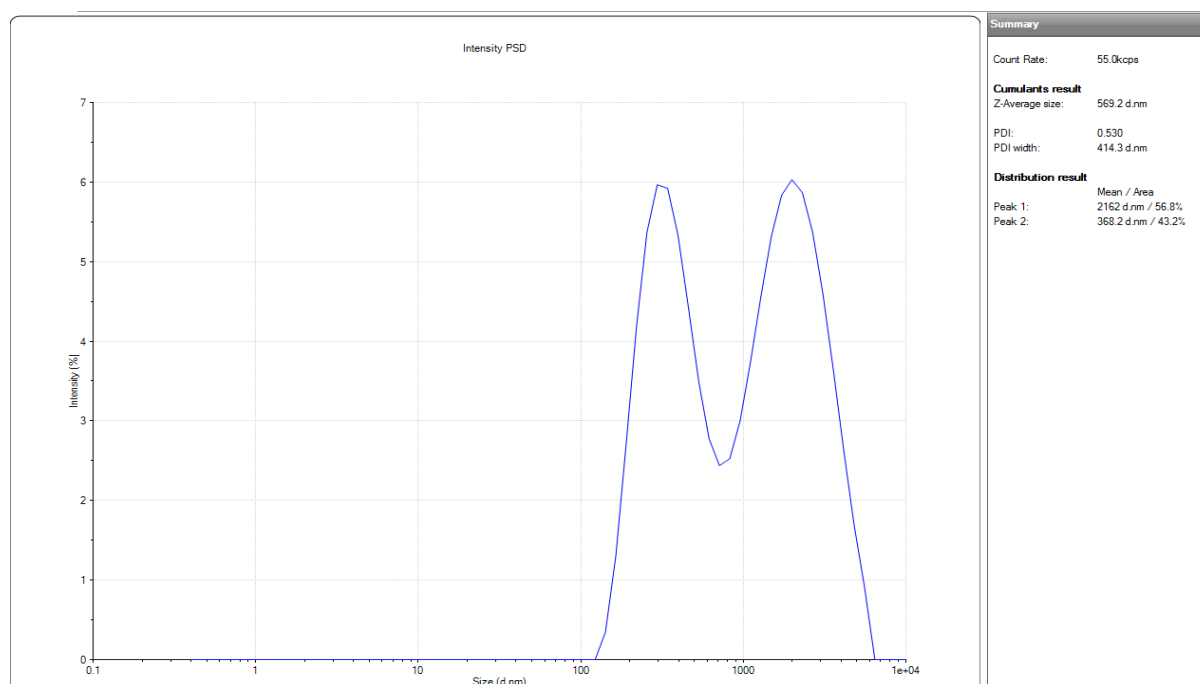

Figure C_29 *- Particle size distribution in permeate solution with intermittent ultrasonic condition of 28kHz in frequency, 2.88 W/cm² in power intensity, and 30seconds in time interval with 0.05% mass concentration of protein in skim milk*
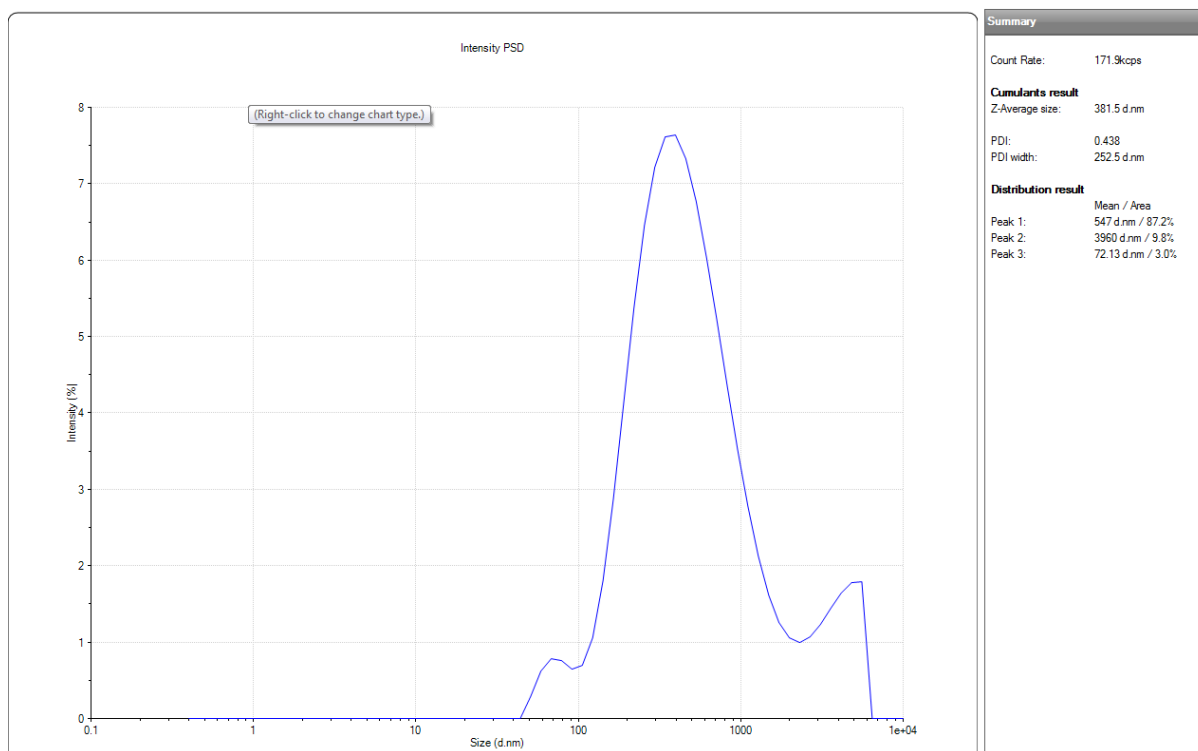
Figure C_30 - *Particle size distribution in permeate solution with continuous ultrasonic condition of 28kHz in frequency, $2.88\,W/cm^2$ in power intensity and with 0.2% mass concentration of protein in skim milk*
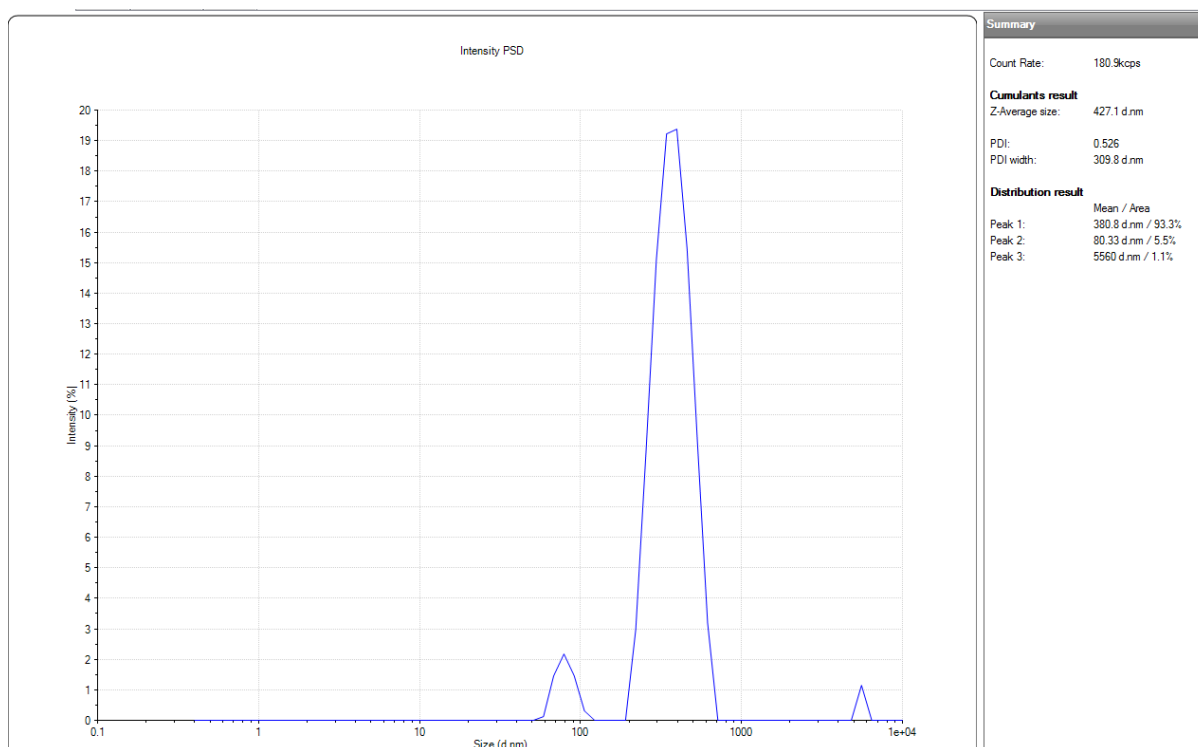

Figure C_31 - *Particle size distribution in permeate solution with intermittent ultrasonic condition of 28kHz in frequency, $2.88\,W/cm^2$ in power intensity, and 30seconds in time interval with 0.2% mass concentration of protein in skim milk*
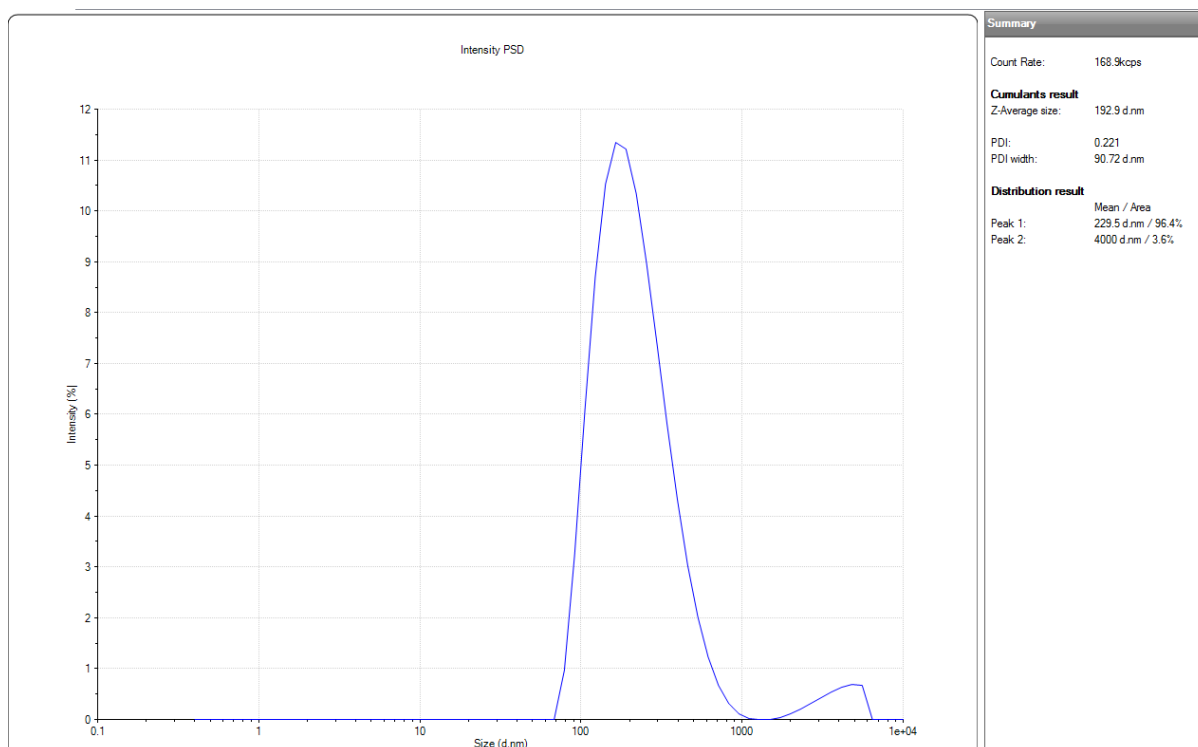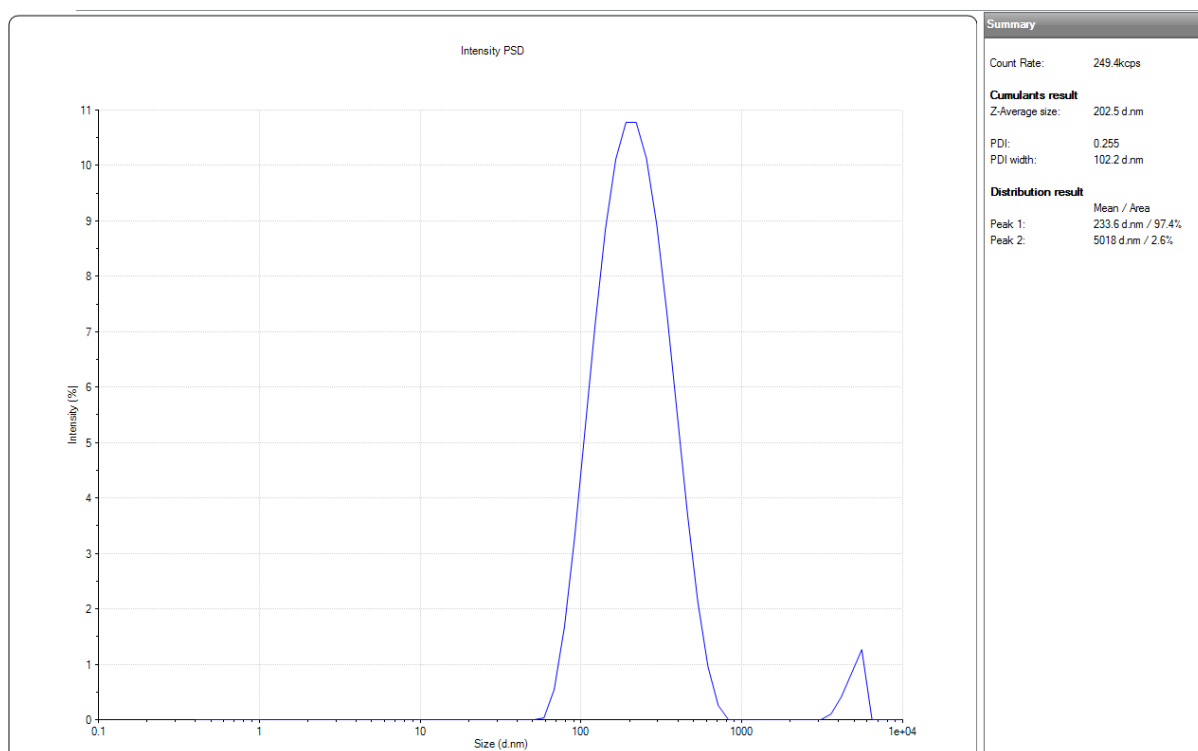
Appendix D List of turbidity of permeate solution

Ultrasonic conditions in Box-Behnken design

Ultrasonic condition	Turbidity (NTU)
Continuous (20kHz, 1.44 W/cm^2)	10.52
1.5min intermittent (20kHz, 1.44 W/cm^2)	7.91
Continuous (20kHz, 2.88 W/cm^2)	20.65
1min intermittent (20kHz, 2.88 W/cm^2)	16.4
2min intermittent (20kHz, 2.88 W/cm^2)	12.33
Continuous (20kHz, 5.76 W/cm^2)	15.92
1.5min intermittent (20kHz, 5.76 W/cm^2)	17.21
Continuous (28kHz, 1.44 W/cm^2)	12.6
1min intermittent (28kHz, 1.44 W/cm^2)	12.3
2min intermittent (28kHz, 1.44 W/cm^2)	8.81
Continuous (28kHz, 2.88 W/cm^2)	23
1.5min intermittent (28kHz, 2.88 W/cm^2)	16.1
Continuous (28kHz, 5.76 W/cm^2)	15.6
1min intermittent (28KkHz, 5.76 W/cm^2)	20.8
2min intermittent (28kHz, 5.76 W/cm^2)	18.6
Continuous (40kHz, 1.44 W/cm^2)	6.27
1.5min intermittent (40kHz, 1.44 W/cm^2)	6.31
Continuous (40kHz, 2.88 W/cm^2)	13.9
1min intermittent (40kHz, 2.88 W/cm^2)	11.7
2min intermittent (40kHz, 2.88 W/cm^2)	7.41
Continuous (40kHz, 5.76 W/cm^2)	7.78
1.5min intermittent (40kHz, 5.76 W/cm^2)	8.26

Time intervals of intermittent ultrasound at optimal ultrasonic condition (28kH, 2.88 W/cm^2)

Ultrasonic condition	Turbidity (NTU)
Continuous (28kHz, 2.88 W/cm^2)	23
30seconds intermittent (28kHz, 2.88 W/cm^2)	21.54
1min intermittent (28kHz, 2.88 W/cm^2)	18.6
1.5min intermittent (28kHz, 2.88 W/cm^2)	16.1
2min intermittent (28kHz, 2.88 W/cm^2)	12.74
2.5min intermittent (28kHz, 2.88 W/cm^2)	8.65
3min intermittent (28kHz, 2.88 W/cm^2)	8.18

Mass concentrations of protein in skim milk

Ultrasonic condition	Turbidity (NTU)
0.05% continuous (28kHz, 2.88 W/cm^2)	6.4
0.05% 30seconds intermittent (28kHz, 2.88 W/cm^2)	5.98
0.1% continuous (28kHz, 2.88 W/cm^2)	23
0.1% 30seconds intermittent (28kHz, 2.88 W/cm^2)	21.54
0.2% continuous (28kHz, 2.88 W/cm^2)	51.7
0.2% 30seconds intermittent (28kHz, 2.88 W/cm^2)	40.23

Appendix E Standard Deviation for Reproductivity of Experimental Data

$$\bar{x} = \frac{\sum_{i=1}^{n} x_i}{n}$$

$$\bar{x} = \frac{46.61g + 45.67g + 44.33g}{3} = 45.54g$$

Then, the standard deviation is calculated as,

$$\sigma = \sqrt{\frac{\sum_{i=1}^{n}(x_i - \bar{x})^2}{n}}$$

$$\sigma = \sqrt{\frac{(46.61g - 45.54g)^2 + (45.67g - 45.54g)^2 + (44.33g - 45.54g)^2}{3}} = 0.94g$$

References

[1] M.K. Tolba, O.A. El-Kholy, The world environment, Chapman and Hall, (1992) 1972-1992

[2] UN Educ. Sci. Cult. Organ. (UNESCO). The United Nations World Water Development Report 3: Water in a Changing World. Paris/New York: UNESCO/Berghahn Books. (2009)

[3] R.P. Schwarzenbach, B.I. Escher, K. Fenner, T.B. Hofstetter, C.A. Johnson, U. V. Gunten, B. Wehrli, The challenge of micropollutants in aquatic systems. Science. 313 (2006) 1072-1077

[4] R.P. Schwarzenbach, T. Egli, T.B. Hofstetter, U. Gunten, B. Wehrli, Global water pollution and human health. Annual Review of Environment and Resources. 35 (2010) 109-136

[5] Rajindar, Singh, Membrane technology and engineering for water purification. 2nd edition. Butterworth-Heinemann. (2014)

[6] W. Gao, H. Liang, J. Ma, M. Han, Z. Chen, Z. Han, G. Li, Membrane fouling control in ultrafiltration technology for drinking water production: A review. Desalination. 272 (2011) 1-8

[7] J.M. Laine, D. Vial, Pierre Moulart, Status after 10 years of operation – overview of UF technology today. Desalination. 131 (2000) 17-25

[8] Z. Domany, I. Galambos, G. Vatai, E. B. Molnar, Humic substances removal from drinking water by membrane filtration. Desalination. 145 (2002) 333-337

[9] L. Fiksdal, T. Leiknes, The effect of coagulation with MF/UF membrane filtration for the removal of virus in drinking water. J. Membr. Sci. 279 (2006) 364-371

[10] I. Galambos, G. vatai, E. B. Molnar, Membrane screening for humic substances removal. Desalination. 162 (2004) 111-116

[11] R. H. Peiris, Cynthia Halle, H. Budman, C. Moresoli, S. Peldszus, P. M. Huck, R. L. Legge, Identifying fouling events in a membrane-based drinking water treatment process using principal component analysis of fluorescence excitation-emission matrices. Water Res. 44 (2010) 185-194

[12] B. Tansel, J. Sager, T. Rector, J. Garland, R. F. Strayer, L. Levine, M. Roberts, M. Hummerick, J. Bauer, Significance of hydrated radius and hydration shells on ionic permeability during nanofiltration in dead end and cross flow modes. Separation and Purification Technology. 51 (2006) 40-47

[13] H.K. Lonsdale, The growth of membrane technology. J. Membr. Sci. 10 (1982) 81–181

[14] Y. Maeda, D.R. Paul, Effect of antiplasticization on selectivity and productivity of gas separation membranes. J. Membr. Sci. 30 (1987) 1-9

[15] S. Loeb, The Loeb–Sourirajan membrane: how it came about. ACS Symp. Ser. 153 (1981) 1–9.

[16] R.J. Petersen, Composite reverse osmosis and nanofiltration membranes. J.Membr. Sci. 83 (1993) 81–150.

[17] R. W. Baker, Membrane technology and applications. 2nd edition. John Willey&Sons, Ltd. (2004)

[18] M.C. Porter, Ultrafiltration, in Handbook of Industrial Membrane Technology, M.C. Porter (ed.), Noyes Publication, Park Ridge, NJ, (1990) 136-259

[19] J.L. Acero, F.J. Benitez, F.J. Real, C. Garcia, Removal of phenyl-urea herbicides in natural waters by UF membranes: Permeate flux, analysis of resistances and rejection coefficients. Separation and Purification Technology. 65 (2009) 322-330

[20] P. Pradanos, J.I. Arribas, A. Hernandez, Mass transfer coefficient and retention of PEGs in low pressure cross-flow ultrafiltration through asymmetric membranes. J. Membr. Sci. 99 (1995) 1-20

[21] R. W. Baker and H. Strathmann, Ultrafiltration of Macromolecular Solutions with High-Flux Membranes. J. Appl. Polym. Sci. 14 (1970) 1197-1214

[22] W. Gao, H. Liang., J. Ma, M. Han, Z. Chen, Z. Han, G. Li, Membrane fouling control in ultrafiltration technology for drinking water production: A review. Desalination. 272 (2011) 1-8

[23] C. Psoch, S. Schiewer, Direct filtration of natural and simulated river water with air sparging and sponge ball application for fouling control. Desalination. 197 (2006) 190-204

[24] B.R. Breslau, A.J. Testa, B.A. Milnes and G. Medjanis, Advances in Hollow Fiber Ultrafiltration Technology, in Ultrafiltration Membranes and Applications, A.R. Cooper (ed.), Plenum Press, New York, NY, (1980) 109-128

[25] M. Miyamoto, S. Ueyama, N. Hinomoto, T. Saitoh, S. Maekawa, J. Hirotsuji, Degreasing of solid surfaces by microbubble cleaning. Jpn. J. Appl. Phys. 46 (2007) 1236-1243

[26] L.-B. Chu, X.-H Xing, A.-F. Yu, X.-L. Sun, B. Jurcik, Enhanced treatment of practical textile wastewater by microbubble ozonation, Process Saf. Environ. Protect. 86 (2008) 389-393

[27] K. Terasaka, A. Hirabayashi, T. Nishino, S. Fujioka, D. Kobayashi, Development of microbubble aerator for waste water treatment using aerobic activated sludge. Chem. Eng. Sci. 66(14) (2011) 3172-3179

[28] M. Takahashi, K. Chiba, P. Li, Free-radical generation from collapsing microbubbles in the absence of a dynamic stimulus. J. Phys. Chem. B 111 (2007) 1343-1347

[29] T. Watabi, K. Matsuyama, T. Takahashi, H. Matsuyama, Use of microbubbles to reduce membrane fouling during water filtration. Desalination and Water Treatment. 57 (2016) 3820-3826

[30] S. Dicker, M. Mleczko, G. Schmitz, S.P. Wrenn, Size distribution of microbubbles as a function of shell composition. Ultrasonics. 53 (2013) 1363-1367

[31] H.M. Kyllonen, P. Pirkonen, M. Nystrom, Membrane filtration enhanced by ultrasound: a review. Desalination. 181 (2005) 319-335

[32] T.G. Leighton, The Acoustic Bubble. Academic Press San Diego, (1994)

[33] L.A. Crum, Comments on the evolving field of sonochemistry by a cavitation physicist. Ultrasonics Sonochemistry. 2 (1995) S147

[34] K.S. Suslick, Ultrasound Its Chemical, Physical, and Biological Effects. VCH Publishers, Inc., New York, (1988)

[35] H. Li, A.G. Fane, H.G.L. Coster, S. Vigneswaran, Direct observation of particle deposition on the membrane surface during crossflow microfiltration. Journal of Membrane Science. 149 (1998) 83

[36] Canadian Ministry of Health and Welfare, Guidelines for the safe use of Ultrasound: Part II – Industrial and Commercial Applications, Canadian Communications Group Publishing (1991)

[37] T. G. Leighton, The principles of cavitation. Ultrasound in Food Processing, Thompson Science, (1998) 151-182. Retrieved from

http://books.google.com/books?hl=en&lr=&id=eyCB2vJQA9cC&oi=fnd&pg=PA151&dq=the+principles +of+cavitation&ots=RJ0NOVgCLz&sig=Bs9895CIRCVGIj2CIuDgWzhungA%5Cnhttp://books.google.c om/books?hl=en&lr=&id=eyCB2vJQA9cC&oi=fnd&pg=PA151&dq=9+The+principles+of+cavita

[38] D. Ensminger, Ultrasonic: Fundamentals. Tech-nology and Applications, 2nd ed., Marcel Dekker, New York, (1988)

[39] W. Yu, N. Graham, T. Liu, Effect of intermittent ultrasound on controlling membrane fouling with coagulation pre-treatment: Significance of the nature of adsorbed organic matter. J. Membr. Sci. 535 (2017) 167-177

[40] Y. Gao, D. Chen, L.K. Weavers, H. W. Walker, Ultrasonic control of UF membrane fouling by natural waters: Effects of calcium pH, and fractionated natural organic matter. J. Membr. Sci. 401-402 (2012) 232-240

[41] M.O. Lamminen, H.W. Walker, L.K. Weavers, Mechanisms and factors influencing the ultrasonic cleaning of particle-fouled ceramic membranes. J. Membr. Sci. 237 (2004) 213-223

[42] S. Kertesz, I. Kovacs, C. Hodur, G. Keszthelyi-Szabo, G. Vereb, Z. Laszlo, Ultrasound membrane hybrid processes for dairy wastewater treatment: pilot-scale analysis. Desalination and Water Treatment. 57 (2016) 23335-23342

[43] W. Yu, N. Graham, Y. Yang, Z. Zhou, L.C. Campos, Effect of sludge retention on UF membrane fouling: The significance of sludge crystallization and EPS increase. Water Research. 83 (2015) 319-328

[44] K.K. Latt, T. Kobayashi, Ultrasound-membrane hybrid processes for enhancement of filtration properties. Ultrasonics Sonochemistry. 13 (2006) 321-328

[45] S.L.C. Ferreira, R.E. Bruns, H.S. Ferreira, G.D. Matos, J.M. David, G.C. Brandao, E.G.P. da Silva, L.A. Portugal, P.S. dos Reis, A.S. Souza, W.N.L. dos Santos, Box-Behnken design: An alternative for the optimization of analytical methods. Analytica Chimica Acta. 597 (2007) 179-186

[46] J. Prakash Maran, S. Manikandan, K. Thrugnanasambandham, C. Vigna Nivetha, R. Dinesh, Box-Behnken design based statistical modeling for ultrasound-assisted extraction of corn silk polysaccharide. Carbohydrate Polymers. 92 (2013) 604-611

[47] Z. Ye, W. Wang, Q. Yuan, H. Ye, Y. Sun, H. Zhang, Box-Behnken design for extraction optimization, characterization and in vitro antioxidant activity of Cicer arietinum L. hull polysaccharides. Carbohydrate Polymers. 147 (2016) 354-364

[48] G. Bylund, Dairy processing handbook. Tetra Pak Processing Systems. 1995

[49] X. Li, J. Choo, P. Syong, Y. Zhang, Sodium stannate promoted double bond cleavage of oleic acid by hydrogen peroxide over a heterogeneous WO_3 catalyst. Green Chem. 20 (2018) 3619-3624

[50] V. Rioux, Fatty acid acylation of proteins: specific roles for palmitic, myristic and caprylic acids. EDP Sciences. 23(3) (2016) D304

[51] I. Avan, C. Dennis hall, A.R. Katritzky, Peptidomimetics via modifications of amino acids and peptide bonds. Chem. Soc. Rev. 43 (2014) 3575-3594

[52] H. Li, Y. Hsu, Z. Zhang, N. Dharsana, Y. Ye, V. Chen, The influence of milk components on the performance of ultrafiltration/diafiltration of concentrated skim milk. Separation Science and Technology. 52 (2017) 381-391

[53] H. Guo, S. Zhao, X. Wu, H. Qi, Fabrication and characterization of TiO_2/ZrO_2 ceramic membranes for nanofiltration. Microporous and Mesoporous Materials. 260 (2018) 125-131

[54] T.V. Gestel, C. Vandecasteele, A. Buekenhoudt, C. Dotremont, J. Luyten, B.V. de Bruggen, G. Maes, Corrosion properties of alumina and titania NF membranes. J. Membr. Sci. 214 (2003) 21-29

[55] J. Schaep, C. Vandecasteele, B. Peeters, J. Luyten, C. Dotremont, D. Roles, Characteristics and retention properties of a mesoporous $\gamma-Al_2O_3$ membrane for nanofiltration. J. Membr. Sci. 163 (1999) 229-237

[56] T. Kuzniatsova, M.L. Mottern, K. Shqau, D. Yu, H. Verweij, Micro-structural optimization of supported γ-alumina membranes. J. Membr. Sci. 316 (2008) 80-88

[57] H. Grib, M. Persin, C. Gavach, D.L. Piron, J. Sandeaux, N. Mameri, Amino acid retention with alumina γ nanofiltration membrane. J. Membr. Sci. 172 (2000) 9-17

[58] P. Puhlifurb, A. Voigt, R. Weber, M. Morbe, Microporous TiO_2 membranes with a cut off <500 Da. J. Membr. Sci. 174 (2000) 123-133

[59] T.V. Gestel, C. Vandecasteele, A. Buekenhoudt, C. Dotremont, J. Luyten, R. Leysen, B.V. der Bruggen, G. Maes, Salt retention in nanofiltration with multilayer ceramic TiO_2 membranes. J. Membr. Sci. 209 (2002) 379-389

[60] J. Sekulic, J.E. ten Elshof, D.H.A. Blank, A microporous titania membrane for nanofiltration and pervaporation. Advanced Materials. 16 (2004) 1546-1550

[61] T. Tsuru, D. Hironaka, T. Yoshioka, M. Asaeda, Effect of divalent cations on permeate volume flux through porous titania membranes. Desalination. 147 (2002) 213-216

[62] T.V. Gestel, C. Vandecasteele, A. Buekenhoudt, C. Dotremont, J. Luyten, R. Leysen, B.V. der Bruggen, G. Maes, Alumina and titania multilayer membranes for nanofiltration: preparation, characterization and chemical stability. J. Membr. Sci. 207 (2002) 73-89

[63] T.V. Gestel, H. Kruidhof, D.H.A. Blank, H.J.M. Bouwmeester, ZrO_2 and TiO_2 membranes for nanofiltration and pervaporation: Part 1. Preparation and characterization of a corrosion-resistant ZrO_2 nanofiltration membrane with a MWCO<300. J. Membr. Sci. 284 (2006) 128-136

[64] T.V. Gestel, D. Sebold, H. Kruidhof, H.J.M. Bouwmeester, ZrO_2 and TiO_2 membranes for nanofiltration and pervaporation: Part 2. Development of ZrO_2 and TiO_2 top layers for pervaporation. J. Membr. Sci. 318 (2008) 413-421

[65] H. Qi, G. Zhu, L. Li, N. Xu, Fabrication of a sol-gel derived microporous zirconia membrane for nanofiltration. J. Sol-Gel Science and Technology. 62 (2012) 208-216

[66] U. Aust, S. Benfer, M. Dietze, A. Rost, G. Tomandl, Development of microporous ceramic membranes in the system TiO2/ZrO2. J. Membr. Sci. 281 (2006) 463-471